1 2 9 0

UNIVERSIDADE Ð
COIMBRA

Margarida Gonçalves Santos

BIOMATERIALS FOR PET DIAGNOSIS

Dissertação no âmbito do Mestrado em Engenharia Biomédica orientada pelo Professor Doutor Abílio José Fraga do Nascimento Sobral e pela Doutora Mafalda Sofia Laranjo Cândido apresentada ao Departamento de Física da Faculdade de Ciências e Tecnologia da Universidade de Coimbra.

Outubro de 2021

Faculdade de Ciências e Tecnologia
da Universidade de Coimbra

Biomaterials for PET Diagnosis

Margarida Gonçalves Santos

Dissertação de Mestrado na área científica da Engenharia Biomédica orientada pelo Professor
Doutor Abílio José Fraga do Nascimento Sobral e pela Doutora Mafalda Sofia Laranjo Cândido e
apresentada ao Departamento de Física da Faculdade de Ciências e Tecnologia da Universidade
de Coimbra.

Coimbra, 2021

1 2 9 0

UNIVERSIDADE Ð
COIMBRA

This work was developed in collaboration with:

Faculty of Medicine of the University of Coimbra

Faculty of Sciences and Technology of the University of Coimbra

Agradecimentos

Em primeiro lugar, deixo um agradecimento especial aos meus orientadores, Doutor Abílio Sobral e Doutora Mafalda Laranjo, por todo o apoio e ajuda ao longo deste último ano. Ao Doutor Abílio queria realçar que sem todas as correções e paciência em ouvir e esclarecer todas as minhas dúvidas, este projeto nunca poderia ter avançado. À Doutora Mafalda, um enorme obrigada pela atenção e grande humanidade com que me ajudou a resolver os diversos problemas nesta jornada.

Agradeço aos meus pais, Graça e Juan, por todo o apoio, amor, compreensão, carinho e enorme esforço que fizeram para me ajudar a ingressar, e também a terminar esta fase tão importante para mim como para eles. À minha tia, Nancy, não poderia deixar de agradecer todo o apoio moral e amizade. À minha professora de Judo, Elisabete, deixo também a minha gratidão, uma vez que foi um dos pilares desde o início. Ao Pedro gostava de agradecer toda a paciência, dedicação, carinho e incansável positivismo que me fez animar nos momentos mais difíceis. À minha amiga de longa data, Liliana, que mesmo longe foi um apoio indispensável e que sempre me colocou um enorme sorriso no rosto. À Maria relembro os momentos vividos, e deixo uma palavra de gratidão pela vizinha de parede amigável e divertida, pelos conselhos e pelo esforço enorme por fazer-me sair de casa mesmo nos dias mais difíceis. Obrigada à Sandra, ao Joaquim e à Margarida pelo amor e pelo acolhimento a que sempre se predispuseram, sem dúvida foram uma parte crucial quando a família próxima estava longe. Deixo também um agradecimento especial à Srª. Conceição, ao Srº. Gilberto e toda a família da Maria pelo carinho com que me receberam em vossa casa inúmeras vezes, e pelo apoio e ânimo.

À Juliana por todos os conselhos dados, por todos os telefonemas atendidos, por toda a paciência, dedicação e amizade além de toda a partilha de conhecimento e informação. À Chrislaura que com uma mão extraordinária para a cozinha animou sempre os dias, e que com a sua alegria e predisposição em ajudar se revelou uma boa amiga. À Andreia, deixo um enorme obrigada pela alegria e por ter tornado as tardes de laboratório mais divertidas. Ao Leonardo, obrigada pela ajuda e pelo facto de ter-se demonstrado sempre prestável.

À Professora Doutora Filomena Botelho, um muito obrigada por ter disponibilizado as condições e me ter permitido a realização do trabalho laboratorial no instituto de Biofísica. À Gabriela, uma amiga inesperada, obrigada pela ajuda e pelo positivismo constante, de certeza que esta jornada se tornou muito mais fácil com a tua amizade. À Lúcia, agradeço o facto de teres sido sempre tão prestável, pela tua ajuda e pelas palavras amigas. À professora Margarida, à professora Salomé, ao Teixo o meu muito obrigada pela vossa ajuda nos ensaios de Hemólise, uma vez que foram cruciais para que estes fossem realizados. Obrigada, também à Beatriz pela ajuda incansável com aquela linha celular tão matreira, e por todos os conselhos. Não menos importantes, deixo uma palavra de carinho a todas as pessoas do Instituto de Biofísica com as quais partilhei estes últimos 7 meses e que sempre me acolheram de braços abertos e estiveram sempre predispostos a ajudar.

Sem o apoio e dedicação de todas estas pessoas, nunca teria sido possível completar esta fase. De coração cheio, deixo a todos o meu mais sincero obrigada.

«No fundo, há que reconhecer que a história não é apenas seletiva, é também discriminatória, só colhe da vida o que lhe interessa como material socialmente tido por histórico e despreza todo o resto, precisamente onde talvez poderia ser encontrada a verdadeira explicação dos factos, das coisas, da (...) realidade.»

José Saramago, em *A Viagem do Elefante*

Abstract

Lung cancer is a pathology with a high prevalence worldwide, and it generally has a bad prognosis since it is detected in later stages. Aside from the requirement for a faster diagnosis, it is also critical to develop additional techniques or methodologies that can be complementary or improve the PET scan with FDG, which is already an advanced diagnostic tool.

BODIPYs are small aromatic compounds with interesting spectroscopic, photophysical, and chemical properties. These last characteristics are best defined by the great structural and substitutive flexibility of the fluorophores. BODIPYs have been investigated for use in a wide range of applications, including brain and cardiac perfusion imaging, due in part to their excellent photochemical stability.

PET systems employ radiopharmaceuticals with Fluorine-18 to detect a variety of diseases, being cancer one of the most studied with this methodology. Fluorine-18 has been widely used due to its unique characteristics and ability to label small biomolecules as well as more complex structures. Therefore, if the unique characteristics of BODIPYs can be associated with those of the ^{18}F radioisotope, we may have a very valuable tool for PET-based lung cancer diagnosis.

To that end, BODIPYs with Fluorine-19 or alkoxy groups linked to the boron atom were synthesized, characterized by NMR, absorption and emission spectroscopy, and mass spectrometry. Some structural motifs were also evaluated, such as the planarity of the boron atom in relation to the plane of the pyrrole rings, along with the angles of the boron substituents, that may influence the radiolabelling process. Lastly, cytotoxicity and compound uptake by two lung cancer cell lines were assessed through *in vitro* studies such as MTT, SRB, haemolysis, and cellular uptake assays.

From the results obtained, it was possible to confirm that the BODIPYs obtained were the ones initially expected and that two of the six compounds, BODIPYs 3 and 6, showed low cytotoxic effects on metabolic activity and viability. Even so, BODIPY 3 showed slightly better results than BODIPY 6, with greater uptake and less release of haemoglobin.

In summary, BODIPYs 3 and 6 appear to be good candidates for investigating the ^{18}F insertion into the structure of the compound. It is worth noting that both compounds include alkoxy groups associated with the boron atom, which was one of the properties we intended to look into in the future to improve the radiolabelling kinetics.

Keywords: Lung Cancer, BODIPY, Characterization, Biocompatibility, PET.

Resumo

O cancro de pulmão é uma doença com grande prevalência a nível mundial e geralmente com um prognóstico relativamente pobre, uma vez que é detetado em fases tardias. Além da necessidade de um diagnóstico em estadios não tão avançados, é também fundamental o desenvolvimento de outras técnicas ou metodologias que possam complementar ou melhorar o exame PET com FDG, que por si só já é uma das técnicas de diagnóstico mais avançadas.

Os BODIPYs são compostos aromáticos com propriedades espectroscópicas, fotofísicas e químicas interessantes. Estas características são mais bem definidas pela grande flexibilidade estrutural e substitutiva destes fluoróforos. Além disso, os BODIPYs têm sido investigados para uma ampla gama de aplicações, incluindo para a obtenção de imagens de perfusão cerebral e cardíaca, devido em parte à sua excelente estabilidade fotoquímica.

Os sistemas PET usam radiofármacos com Flúor-18 para detetar uma grande variedade de doenças, sendo o cancro uma das mais estudadas com esta metodologia. O Flúor-18 tem sido amplamente utilizado devido às suas características únicas e à capacidade de marcar pequenas biomoléculas, bem como estruturas mais complexas. Posto isto, se as características exclusivas dos BODIPYs puderem ser associadas às do radioisótopo ^{18}F, podemos ter uma ferramenta muito valiosa para o diagnóstico PET do cancro de pulmão.

Para esse fim, BODIPYs com Flúor-19 ou grupos alcóxidos associados ao átomo de boro, foram sintetizados, caracterizados por espectroscopia de RMN, de absorção e emissão e espectrometria de massa. Alguns motivos estruturais também foram avaliados, como a planaridade do boro em relação ao plano dos anéis pirrólicos, bem como os ângulos dos substituintes do boro que podem influenciar a velocidade do processo de radiomarcação. Por fim, a citotoxicidade e a incorporação do composto por duas linhas de células do cancro de pulmão também foram avaliadas por meio de estudos *in vitro*, tais como os ensaios de MTT, SRB, hemólise e incorporação celular.

Pelos dados obtidos, foi possível confirmar que os BODIPYs obtidos foram os inicialmente pretendidos, com os BODIPYs 3 e 6 a apresentarem menor citotoxicidade para a atividade metabólica e para a viabilidade celular. Ainda assim, o BODIPY 3 apresentou resultados ligeiramente melhores, com maior captação por ambas as linhas celulares em estudo e provocando menor libertação de hemoglobina.

Em suma, os BODIPYs 3 e 6 parecem ser bons candidatos para serem investigados quanto à incorporação do ^{18}F nas suas estruturas. De realçar que ambos os compostos incluem grupos alcóxidos associados ao átomo de boro, que era uma das propriedades que pretendíamos estudar no futuro para melhorar a velocidade de radiomarcação.

Palavras-chave: Cancro do Pulmão, BODIPY, Caraterização, Biocompatibilidade, PET.

Figures

Schemes

Tables

Abbreviations and Symbols

β⁺: Positrons

β⁻: Electrons

¹⁸F-F₂: Fluorine gas labelled with ¹⁸F

¹⁸F-ALF-NOTA-PRGD₂: ¹⁸F-Alfatide

¹⁸F-FDG: Fluorodeoxyglucose labelled with ¹⁸F

¹⁸F-FET: O-(2-[¹⁸F]-fluoroethyl)-L-tyrosine

¹⁸F-FAMT: L-[3-¹⁸F] (¹⁸F)-Fluorothymidine

¹⁸F-FETNIM: [¹⁸F]-Fluoro Erythro Nitro Imidazole

¹⁸F-NaF: ¹⁸F-sodium fluoride

¹⁸F-MISO: [¹⁸F]-fluoromisonidazole

¹⁸[O]H₂O: Water labeled with ¹⁸O

⁶⁰Cu-ASTM: ⁶⁰Cu-4-(N)-methylthiosemicarbazone

⁶⁴Cu-DOTA-RGD: [⁶⁴Cu]-(1,4,7,10-tetraazacyclododecaneN,N',N'',N'''-tetraacetic acid) - (arginine-glycine-aspartic acid)

⁶⁸Ga-RGD₂: ⁶⁸Ga dimerized-RGD

Å: Amstrong

ALK: Anaplastic lymphoma kinase

ALK-EML4: Fusion of *ALK* and *EML4*

Aza-BODIPY: Aza-4,4-Difluoro-4-bora-3a,4a-diaza-s-indacene

BF₃.Et₂O: Boron trifluoride diethyl etherate

BODIPY: 4,4-Difluoro-4-bora-3a,4a-diaza-s-indacene

BRAF: Proto-oncogene B-Raf or v-Raf murine sarcoma viral oncogene homolog B

CDKN2A: Cyclin-dependent kinase inhibitor 2A

CI: Confidence interval

COPD: Chronic Obstructive Pulmonary Disease

D-¹⁸F-FMT: D-(¹⁸F)-Fluoro-Methyl-Tyrosine

DC: Dendritic Cell

DDQ: 2,3-dichloro-5,6-dicyano-1,4-benzoquinone

DMAP: 4-dimethylaminopyridine

DMSO: Dimethyl sulfoxide

DNA: Deoxyribonucleic acid

DMEM: Dulbecco's Modified Eagle Medium

EasyPET: Easy Positron Emission Tomography

EGFR: Epidermal Growth Factor Receptor

EML4: Echinoderm Microtubule-associated Protein-like 4

ES-SCLC: Extensive-Stage of Small Cell Lung Cancer

FAP: Fibroblast Activation Protein

FAPIs: FAP-specific inhibitor (FAPI)

FBS: Fetal Bovine Serum

FDG: Fluorodeoxyglucose

FHIT: Fragile Histidine Triad Protein

HER2: Human Epidermal Growth Factor Receptor 2

KRAS: Kirsten Rat Sarcoma viral oncogene homolog

LAT1: Large Amino Acid Transporter 1

LS-SCLC: Limited-Stage of Small Cell Lung Cancer

MT-MMP1: Membrane-type matrix metalloproteinase-1

MTT: 3-(4,5-dimethylthiazol-2-yl)-2,5-diphenyltetrazolium bromide

NIR: Near-Infrared

NIR-II: Second Near-Infrared

NMR: Nuclear Magnetic Resonance

NSCLC: Non-Small Cell Lung Cancer

OTf: Trifluoromethanesulfonate

*PIK3CA***:** Phosphatidylinositol-4,5-bisphosphate 3-kinase, catalytic subunit alpha

*p16***:** p16^{INK4a}, cyclin-dependent kinase inhibitor 2A

TP53: Tumour protein p53

PACMA31: Protein Disulfide Isomerase Inhibitor III

PARP1: Poly [ADP-ribose] Polymerase 1

PARPi-FL: a Fluorescent PARP1 Inhibitor

PBS: Phosphate Buffered Saline

PDT: Photodynamic Therapy

PET: Positron Emission Tomography

PET/CT: Positron Emission Tomography/Computed Tomography

pH: - log [H$^+$]

*PTEN***:** Phosphatase and Tensin Homolog

*RASSF1A***:** Ras Association Domain Family 1 Isoform A

Rb: Retinoblastoma protein

*Rb1***:** Gene Name Abbreviated RB or RB1

RGD: Tripeptide Arg-Gly-Asp

*ROS1***:** ROS proto-oncogene 1, receptor tyrosine kinase

RNA: Ribonucleic Acid

SA: Specific Activity

SCLC: Small Cell Lung Cancer

SD: Standard Deviation

S$_N$2: Bimolecular Nucleophilic Substitution

S$_N$Ar: Nucleophilic Aromatic Substitution

SPECT: Single-photon Emission Computed Tomography

SRB: Sulforhodamine B

SUV: Standard Uptake Value

T$_{1/2}$: Half-life

TFA: Trifluoroacetic acid

TKI: Tyrosine Kinase Inhibitors

TMSOTf: Trimethylsilyl triaflate

TLC: Thin Layer Chromatography

*VEGF***:** Vascular Endothelial Growth Factor

WHO: World Health Organization

*Val600Glu***:** BRAF V600E mutation

Structures

1.   2,8-diethyl-5,5-difluoro-1,3,7,9-tetramethyl-10-(perfluorophenyl)-5H-dipyrrolo[1,2-c:2',1'-f][1,3,2]diazaborinin-4-ium-5-uide
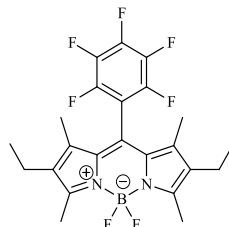
= BODIPY 1

2.   2,8-diethyl-5,5-difluoro-1,3,7,9-tetramethyl-10-phenyl-5H-dipyrrolo[1,2-c:2',1'-f][1,3,2]diazaborinin-4-ium-5-uide
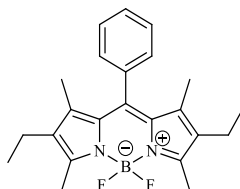
= BODIPY 2

3.   2,8-diethyl-1,3,7,9-tetramethyl-10-(perfluorophenyl)-5,5-diphenoxy-5H-dipyrrolo[1,2-c:2',1'-f][1,3,2]diazaborinin-4-ium-5-uide
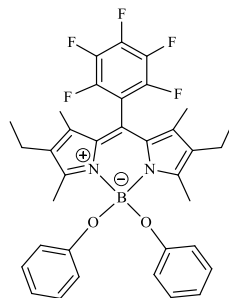
= BODIPY 3

4.   2,8-diethyl-1,3,7,9-tetramethyl-5,5-diphenoxy-10-phenyl-5H-dipyrrolo[1,2-c:2',1'-f][1,3,2]diazaborinin-4-ium-5-uide
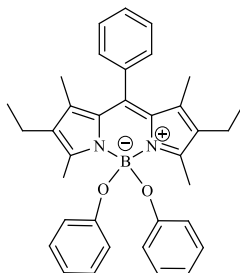
= BODIPY 4

5.   **2',8'-diethyl-1',3',7',9'-tetramethyl-10'-(perfluorophenyl)spiro[benzo[d][1,3,2]dioxaborole-2,5'-dipyrrolo[1,2-c:2',1'-f][1,3,2]diazaborinin]-4'-ium-12-uide**
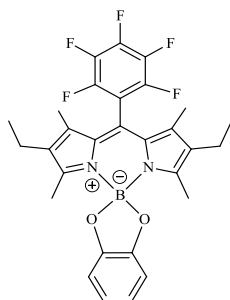
= BODIPY 5

6.   **2',8'-diethyl-1',3',7',9'-tetramethyl-10'-phenylspiro[benzo[d][1,3,2]dioxaborole-2,5'-dipyrrolo[1,2-c:2',1'-f][1,3,2]diazaborinin]-4'-ium-12-uide**

= BODIPY 6

Index

Introduction

1 - Introduction

The knowledge of how the body works and how it is structured in health and disease is important not only for diagnosing disorders and injuries but also for planning therapies[1]. Prevent premature death or disability, restore well-being or at least structural and functional capacity, or even provide some comfort to the patient are some of the other roles of medicine.

Medical imaging is paramount for visualizing and monitoring the biological processes of the body. This area is dedicated to the acquisition of anatomical/structural and physiological/functional images of the patient's organs or tissues, which can help in the correlation of imaging findings with pathological conditions and with the detection and diagnosis of human diseases and injuries[1].

However, in most cases, diagnosis occurs at a stage where disease treatment is not always effective[1]. The expansion of medical imaging from organ or tissue levels to cellular or molecular levels can result in a better understanding of the molecular and genetic infrastructure underlying human body processes[1]. Tracers with useful physical and optical properties are used to visualize and follow biological processes in the body. When tracers are associated with biological molecules, they tend to accumulate in certain organs or tissues, providing images and tracking of those structures.

New tracers based on 4,4-Difluoro-4-bora-3a,4a-diaza-s-indacene, BODIPY, have been studied for therapy and cancer diagnostics, due to their excellent optoelectronic properties and easy functionalization[2–4]. Some of the BODIPYs that are under study appear to have had good results and could turn out to be great tools for the healthcare industry.

1.1 Lung Cancer

Lung cancer starts in the lungs, two spongy organs in the chest with the primary function of exchanging oxygen and carbon dioxide, whose general anatomy is summarized in figure 1. Although advances in detection and therapy have improved the disease prognosis over time, lung cancer may still be lethal.
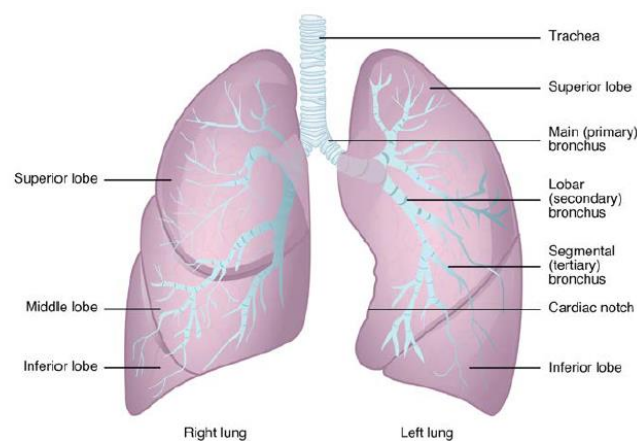
Figure 1 - Lung anatomy schematized in simple terms, adapted from[5].

Lung cancer is generally divided into two broad categories: Small Cell Lung Cancer (SCLC) and Non-Small Cell Lung Cancer (NSCLC). The most prevalent type of lung cancer is non-small cell lung cancer (NSCLC), with Adenocarcinomas being one of the most predominant subtype[6].

Smoking is the leading cause of SCLC, which develops from neuroendocrine-cell precursors. Despite the fact that SCLC subtypes are not clinically useful in deciding which therapy to apply, the discovery that mixed tumours containing elements of SCLC, Adenocarcinoma, or Squamous Cell Carcinoma promoted the idea that the main forms of lung cancer are closely related, possibly arising from a common stem cell[7].

Another type of cancer associated with the pathology is a second primary cancer. A second primary cancer is a form of lung cancer that occurs in people who have already had another cancer[8]. Patients with lung cancer are at significant risk of acquiring a second primary cancer, however, determining whether the new tumour is a second primary cancer or metastasis of the original can be challenging[8].

Lung cancer can also cause brain metastases, which is a substantial source of illness and mortality[8]. The prevalence of brain metastases is greater in patients with Adenocarcinoma and Large Cell Carcinoma than in patients with Squamous Cell Carcinoma, among the various histologies of NSCLC[8].

1.1.1 Epidemiology

Cancer is one of the most prevalent disease in the world, and the number of new cases has been growing over the years. In 2020, 19.29 million individuals worldwide were diagnosed with cancer, and 9.96 million died as a result of it[9]. Lung cancer is the second most often diagnosed cancer (11.4 % of all cases) and the main cause of cancer mortality (18 % of all deaths), as presented in figure 2[9]. In Portugal, lung cancer was the leading cause of death in 2020, as demonstrated by figure 3.
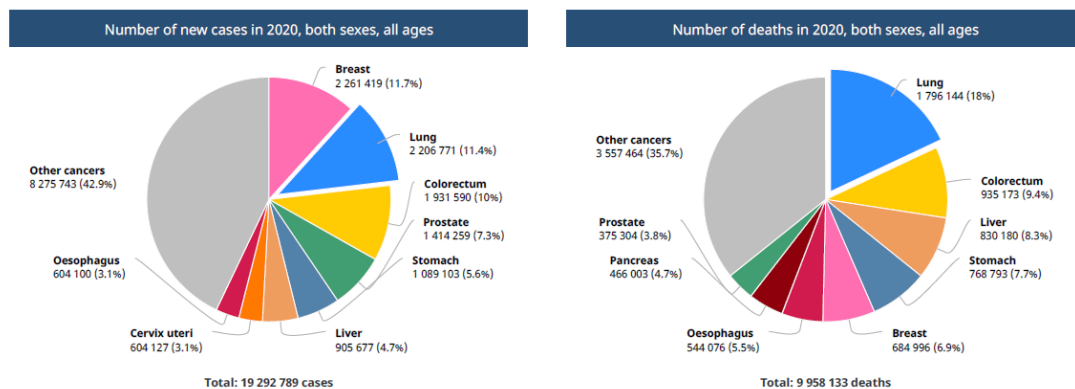
Figure 2 - Cases and fatalities of cancer types for both men and women in 2020, adapted from[9].

Lung cancer has gained significant numbers over the last century mostly due to the increase in tobacco use. In 1920, there was a widespread belief that tobacco use was a major cause of lung cancer, and in 1950, multiple case reports were published that confirmed the link between smoking and lung cancer[7]. The majority of lung cancers are caused by smoking, and unfortunately the consumption continues to be prevalent in almost all regions of the globe, as illustrated in figure 4[10,11].
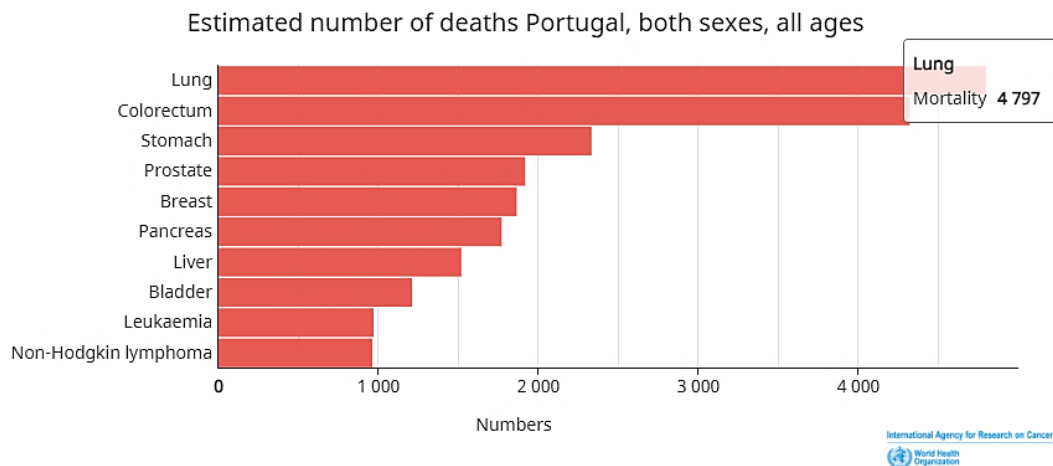
Figure 3 - Estimated number of deaths in Portugal, for both sexes and all ages (2020), adapted from[12].

Generally speaking, lung cancer is more frequent in men and has a greater incidence with increasing age[10,11,13]. Recent evidence, however, has revealed a changing pattern in lung cancer rates, with a greater incidence in young individuals and non-smoking women, particularly in Asia and nations with Asian emigrants[10]. Moreover, lung cancer and Chronic Obstructive Pulmonary Disease (COPD) appear to be correlated[7].
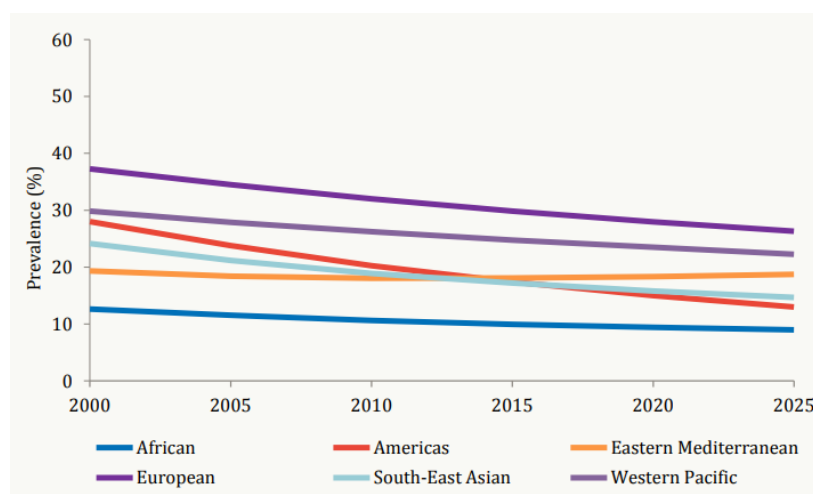
Figure 4 - Between 2000 and 2025, adjusted and projected smoking prevalence rates normalized by age among individuals aged 15 and above, for both genders, by WHO region, adapted from[11].

1.1.2 Risk Factors

When it comes to a disease with such a high global incidence, risk factors are important to consider since they influence disease susceptibility, treatment results, and survival rates. A person's vulnerability to lung cancer might be influenced by environmental or regional variables, genetics, ethnicity, and age, as well as pollution and air quality, exposure to radon or ionising radiation, education or profession, and socioeconomic level[7,8,10,13,14].

As mentioned earlier, smoking is the most frequent cause of SCLC, with smoking duration being the greatest predictor of lung cancer risk among smokers[7,15]. Even so, a family history of lung cancer can be a significant risk factor, since it is possible that hereditary predisposition plays a role in developing nicotine addiction[7]. Additionally, cigars, cigarettes and pipes have also been shown to have a carcinogenic impact, with an exposure-response association with lung cancer risk[15].

Genetic risk factors such as the ones related to the chromosomal regions *5p15, 15q25-26, 6q21, 6q23-25,* and *3q28* have been associated with an increased risk of lung cancer[14]. The *5p15* region encodes *telomerase reverse transcriptase* (*TERT*), implicated in cell replication, that has been connected to the development of Adenocarcinomas in smokers and non-smokers[14–16]. Both nicotine dependency and lung cancer risk are connected to mutations in the *15q25-26* chromosomal locus[14]. G-protein signalling is regulated by chromosome locus *6p21*, and mutations in this region provide a significantly greater risk to never-smokers[14]. A gene on chromosome *6q23–25* has been correlated to lung cancer susceptibility in families where numerous individuals have been diagnosed with lung or head and neck cancer[7]. Some genetic variations in the *3q28* area have also been linked to the incidence of the pathology, particularly Adenocarcinoma in non-smoking Asian women[15,17].

Older age is also a risk factor, in part due to DNA damage over time and telomere shortening, which leads to greater susceptibility to cancer[14]. The development of the pathology is also influenced by air quality. Outdoor pollution can be linked to the presence of different substances in the atmosphere, while indoor pollution is generally associated with the use of coal and biomass fuels for heating or cooking[14,15].

Exposure to ionising radiation can also increase the risk of lung cancer, being mainly reported in atomic bomb survivors and in patients treated with radiotherapy[15]. Furthermore, underground miners who have been exposed to radioactive radon and its decay products, as well as residential radon from soil, are factors that contribute to the higher risk of developing lung cancer[14,15].

Educational level are typically connected to socioeconomic variables such as work possibilities and income, which may have consequences for the previously stated risk factors[14].

1.1.3 Aetiology

Taking into account all the risk factors mentioned above, lung cancer can originate from different factors and types of exposure. However, occupational exposures play a key

part in lung cancer aetiology, affecting workers in a variety of sectors and occupations[15]. Asbestos, silica, radon, heavy metals, and polycyclic aromatic hydrocarbons have been identified as the most significant occupational lung carcinogens[15].

Additionally, the regulatory circuits that control normal cell growth and homeostasis are found defective in cancer cells[8]. A normal cell should turn into a malignant one in a few steps, with genetic and epigenetic alterations leading to invasive cancer via clonal growth, in more advanced stages leading to metastases and in some cases resistance to therapy[8]. Genome and epigenome alterations can cause inactivation of tumour suppressor genes like *RB1*, TP*53*, *CDKN2A*, *FHIT*, *RASSF1A*, and *PTEN*, and other mutations, amplifications or rearrangements described in table 1[6,8,14,16].

Table 1 - Some changes in proto-oncogenes in some subtypes of lung cancer.

Alterations	Types of Cancer	Notes	References
***EGFR* mutations**	NSCLC	The *EGFR* protein is critical for proper cell proliferation, apoptosis, and other biological activities. The prevalence of *EGFR* mutations varies with histotype, ethnicity, and other demographic or pathological factors.	6,8,16,18
***HER2* Overexpression and Amplification**	NSCLC - Adenocarcinoma, and rare in Lung Squamous Cell Carcinoma	*HER2* can directly modulate *EGFR* signalling and therefore activate important signalling pathways. Amplifications in *HER2* in men and ex-smokers, and mutations in females and never smokers have been found.	6
***ALK* rearrangement (*ALK-EML4*), inversions or translocations**	NSCLC	*ALK* gene encodes a transmembrane protein that belongs to the insulin receptor family, with the most common translocated partner gene in NSCLC being *EML4*. Such alterations are more prevalent in younger patients and never or light smokers.	6,8,16,18
***KRAS* mutations**	NSCLC - Adenocarcinomas and in some other types	*KRAS* is a proto-oncogene that acts as a molecular on/off switch regulator to cell proliferation, maturation, and differentiation. *KRAS* mutations are a prevalent occurrence in lung cancer, particularly in smokers of non-Asian ethnicity.	6,14,16
***BRAF* mutations**	NSCLC - Adenocarcinomas	Once activated, the *BRAF* protein plays an important role in regulating a signalling pathway, which ultimately induces cell growth, mobility, and survival. The *Val600Glu* mutation is reported in half of the patients with *BRAF*-mutated lung adenocarcinomas. *BRAF* mutations can occur in smokers and non-smokers.	6,16,18
***ROS1* fusions and rearrangements**	NSCLC - Adenocarcinoma and advanced stages	It seems that *ROS1* is able to directly couple extracellular adhesion-mediated events to intracellular signalling mediated by tyrosine phosphorylation. *ROS1* fusions are more prevalent in adenocarcinomas than in other NSCLC histologies, and *ROS1* rearrangements are significantly more frequent in advanced NSCLC clinical stages.	6,16
***PIK3CA* mutations and amplifications**	NSCLC SCLC	In recent years, they have been linked to carcinogenesis and disease development due to the great number of signalling pathways they influence.	6,19

1.1.4 Presentation

Personalized medicine has made significant progress over the past decade in diagnosing and treating tumours with specific histological and genetic characteristics specific to each patient, and this is just one reason why histological categorization, diagnosis, and proper staging is so important[20].

Lung tumours are classified by the *World Health Organization* (WHO) into histological types and subtypes. Epithelial tumours, mesenchymal tumours, lymphohistiocytic tumours, tumours of ectopic origin, and metastatic tumours are the primary divisions of the categorization[20].

1.1.4.1 Signs and Symptoms

Some symptoms that may indicate lung cancer for smokers are the lack of appetite or thrombocytosis[10]. Cough that does not go away, coughing up blood, shortness of breath, chest discomfort or infections (bronchitis or pneumonia), hoarseness, weight loss, bone pain, tiredness, and headache are some of the symptoms that can also be associated with different types of lung cancer. Nonetheless, because some patients have comorbidities, symptom presentation is frequently intricate, and there is generally no clear manifestation[10].

Many people do not have any non-respiratory symptoms. Only half of the patients exhibit the initial isolated symptom, and haemoptysis, even though being the most predictive sign, occurs in just 20 % of patients[10]. Therefore, it is of paramount importance to diagnose the disease as soon as possible, even if the revealed symptoms are not a clear manifestation of the pathology.

1.1.5 Diagnosis and Complementary Exams

Lung cancer was formerly diagnosed exclusively by radiography, but with the development of Computed Tomography (CT), which uses low doses of radiation to produce images of the tumour region, CT became the method of choice[16,21]. Figure 5 depicts a radiography and a CT scan used to diagnose lung cancer. Although lung cancer symptoms are seldom visible, the diagnosis of the pathology is mostly based on them, still, a CT scan with chest contrast, encompassing the neck and upper abdomen, can be suggested[8,10,22].

PET is a non-invasive technique that provides functional images, time-course detection, and quantification of the radiotracer all over the body[23]. PET or PET-CT scanning is advised not only for staging but also for detecting unnoticed metastatic disease and avoiding noncurative resections[10,24]. Despite the fact that PET scanning is a valuable technique, tissue biopsy is still necessary to validate PET scan results[10,24]. Endobronchial ultrasound-needle aspiration, endoscopic ultrasound-needle aspiration, and their combinations are the frequent needle methods employed for sampling[10,22,24]. When compared to surgical staging, needle methods have shown to be the most cost-effective diagnostic method for obtaining tissue[10,24].
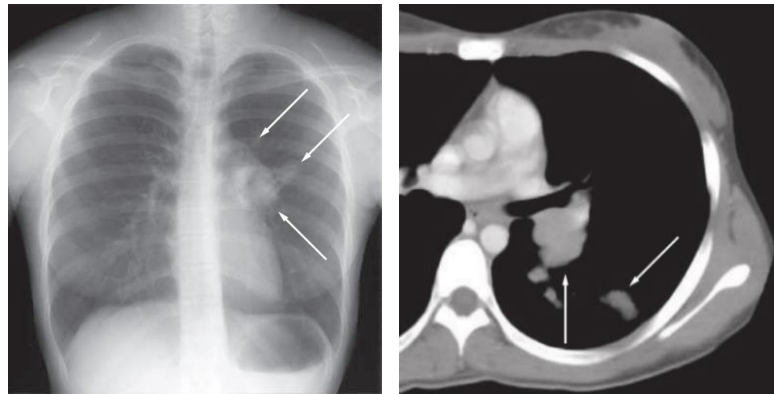
Figure 5 - On the picture on the left, a nodule with ill-defined boundaries (white arrows) may be seen in the left-middle lung region on the patient's chest X-ray; and on the picture on the right, a CT scan of a patient showing an enlarged left hilum and mediastinum, with the final diagnosis of SCLC, stage IIIA, adapted from[25].

Since lung cancer symptoms appear late, the vast majority of patients diagnosed with lung cancer suffer from advanced disease[22]. Unfortunately, current treatments are unlikely to cure patients, which is why certain new interesting indicators under investigation might be beneficial for early detection and prevention[22]. Autoantibodies, complement fragments, microRNAs, circulating tumour DNA, DNA methylation, blood protein profiling, and RNA airway or exhaled breath biomarkers, metabolomics, sputum cell imaging have all been investigated as tools for improving lung cancer diagnosis[10,26].

1.1.6 Staging

Sampling allows for more adequate staging and pathological diagnosis if the diagnostic CT shows distant metastases or supraclavicular or cervical lymph node involvement. Immunohistochemistry and molecular analysis often play an important role in staging[10].

The TNM system is often used to categorize lung cancer stages, with its divisions shown in figures 6, 7, and 8, and their classification in detail described in tables 2 and 3 for NSCLC and SCLC, respectively. The information in the figures and tables are complementary and together describe the TNM system.

Category T essentially specifies the size and extent of the primary tumour, while category N specifies the extent of regional lymph node involvement, and the last category M details the presence or absence of metastases in other parts of the body[8]. The numbers associated with these categories help in describing the extent of the cancer[8].
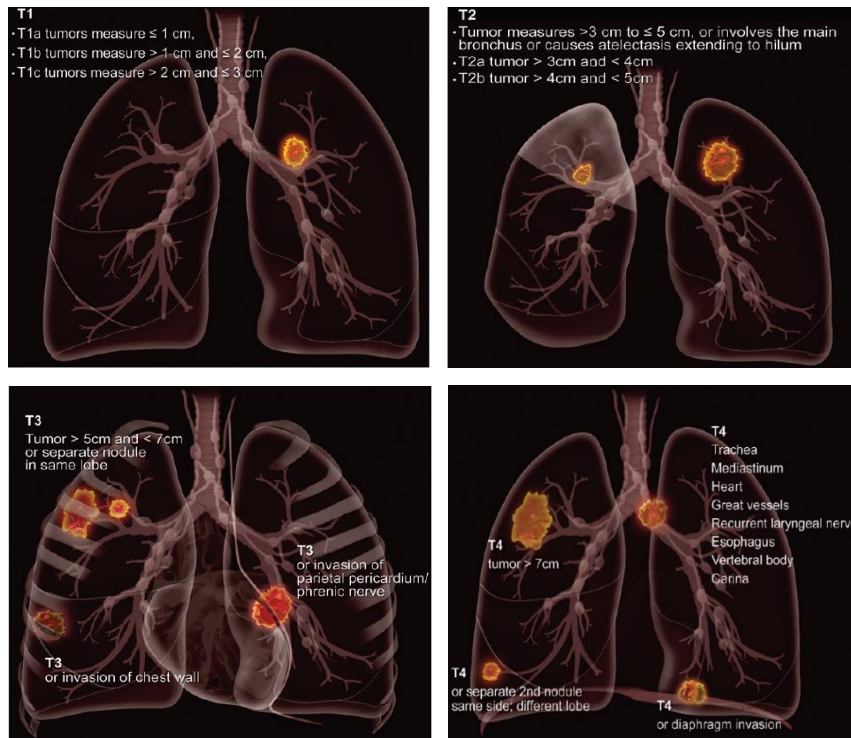
Figure 6 - Anatomical image depicting the T descriptors, adapted from[27].

Figure 7 - Anatomical image depicting N and M1 descriptors, adapted from[27].

NSCLC is classified into four stages, ranging from occult carcinoma to stage four (IV). The lower the stage, the less cancer has spread. When the primary tumour cannot be assessed, or the tumour is confirmed by the presence of malignant cells in sputum or bronchial washings but not visible by imaging or bronchoscopy, it is referred to as occult cancer[28]. When the tumour is only detected in the upper layers of the cells that border the air passageways is designed by stage 0 (carcinoma in situ)[28]. The division between stage I and stage II depends largely on the size of the tumour; Whilst stages III and IV classification depends on the size and location of the tumour and how far it has spread, for example, whether or not cancer has spread to the lymph nodes[28]. Stage IV mainly refers to the presence of distant metastases.
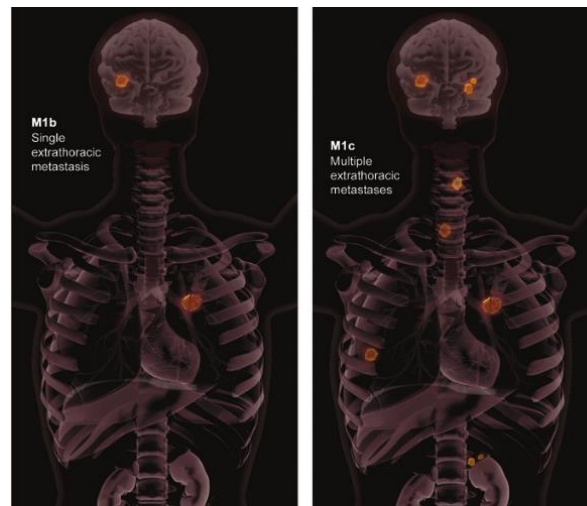
Figure 8 - Anatomical representation of the M1b and M1c descriptors, adapted from[27].

Table 2 - Stage grouping of the TNM classification of NSCLC, adapted from[28].

Stage	T	N	M
Occult Carcinoma	TX	N0	M0
0	Tis	N0	M0
IA1	T1mi	N0	M0
	T1a	N0	M0
IA2	T1b	N0	M0
IA3	T1c	N0	M0
IB	T2a	N0	M0
IIA	T2b	N0	M0
IIB	T1a,b,c	N1	M0
	T2a,b	N1	M0
	T3	N0	M0
IIIA	T1a,b,c	N2	M0
	T2a,b	N2	M0
	T3	N1	M0
	T4	N0	M0
	T4	N1	M0
IIIB	T1a,b,c	N3	M0
	T2a,b	N3	M0
	T3	N2	M0
	T4	N2	M0
IIIC	T3	N3	M0
	T4	N3	M0
IVA	Any T	Any N	M1a
	Any T	Any N	M1b
IVB	Any T	Any N	M1c

Patients with SCLC who have the malignancy restricted to the hemithorax, mediastinum, or supraclavicular lymph nodes are diagnosed with limited-stage disease (LS-SCLC); Or with extensive stage disease (ES-SCLC), in which the tumour has progressed beyond the supraclavicular areas[8]. However, this sort of staging is becoming less popular, and it is now more typical to use numbers to differentiate between SCLC types. The distinctions between stages on the current SCLC staging are comparable to those on the NSCLC staging.

Table 3 - SCLC tumour stage classification, adapted from[29].

Stage	T	N	M
Occult Carcinoma	TX	N0	M0
0	Tis	N0	M0
IA	T1a,b	N0	M0
IB	T2a	N0	M0
IIA	T2b	N0	M0
	T1a,b	N1	M0
	T2a	N1	M0
IIB	T2b	N1	M0
	T3	N0	M0
IIIA	T1a,b and T2a,b	N2	M0
	T3	N1, N2	M0
	T4	N0,N1	M0
IIIB	T4	N2	M0
	Any T	N3	M0
IV	Any T	Any N	M1

1.1.7 Treatment

As soon as a tumour has been diagnosed and staged, it is time to decide on the best therapy, and for that several aspects must be considered. The histology of the tumour, stage, patient health and comorbidities, genetics, and patient preferences influence the treatment options[8,16]. To the patient, an improvement in survival of at least several months or improved symptom management with fewer side effects is foreseen[8,16].

For patients without decreased lung function in stages I-II of NSCLC, a surgical lobectomy, whether video-assisted or not, is typically the preferred therapy[8,10,16,22]. Stage III is a diverse pathology with tumours that range from resectable to unresectable[8,22]. Surgery followed by chemotherapy is the usual treatment for patients with resectable IIIA[8,22]. Concurrent conformal radiation therapy (CRT) is the typical therapy for individuals with unresectable stage IIIA and IIIB cancers[22]. If CRT is not an option, sequential chemotherapy followed by radiation is a practicable and effective option[8,22]. In some circumstances, radiotherapy in stages such as IIIB could be applied to relieve symptoms and enhance the quality of life[8]. For a stage IV of NSCLC, palliative external radiation in combination with

chemotherapy, chemotherapy plus target therapy, or any form of laser therapy or internal endoscopic radiotherapy are all possible treatments[8,30].

NSCLC that has evolved or returned after initial treatment is known as recurrent or relapsed NSCLC[8]. Cancer might spread to other areas of the body, including the brain, and other organs. The treatment method for patients who have not ever had chemotherapy is identical to that for Stage IV NSCLC patients[8]. After surgical excision of the original major tumour, surgical resection of the second primary tumors can improve the patient's survival rate[8]. As there is a growing difficulty linked with poor prognosis, treatment for a patient with brain metastases may focus on symptom alleviation[8,16]. Whole brain radiotherapy (WBRT), surgical resection, stereotactic radiosurgery (SRS), systemic treatment, and radiosensitization, or any combination of the former modalities, can be employed to treat these patients[8].

The treatment options for SCLC are summarized in scheme 1. Palliative care is used to treat stage IV SCLC, with different chemotherapy regimens being the most frequent treatment choice[10,31].
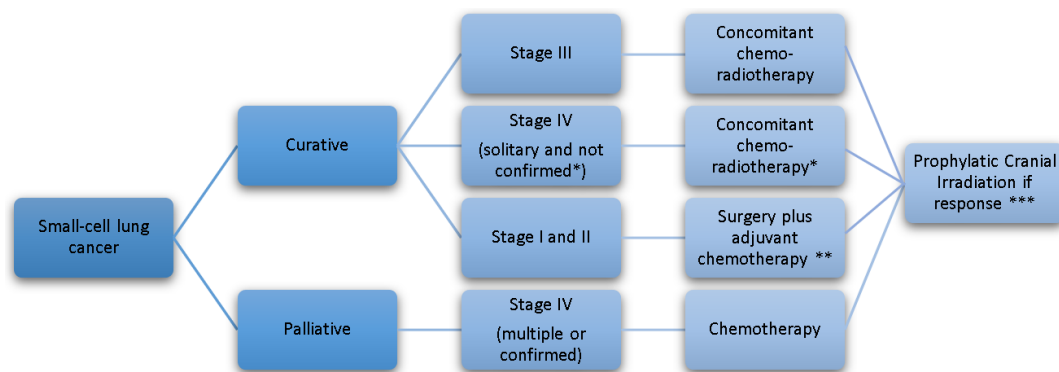
Scheme 1 - SCLC treatment; with * if no confirmation of solitary metastasis, radiotherapy may be added after first response evaluation and is omitted if there is metastatic involvement, ** for concomitant chemoradiotherapy instead, and *** or stable disease if disease is localised; adapted from[31].

Although chemotherapy and radiation generate strong initial responses, disease recurrence is common[8,31]. Chemotherapy and palliative therapy are used to treat recurrent SCLC. A small percentage of SCLC patients with symptoms related to tumour-induced airway blockage may possibly benefit from local therapy such as stenting, argon plasma coagulation, or photodynamic therapy (PDT)[10].

1.1.8 Prognosis

Lung cancer appearance and development are influenced not only by the genetic development and molecular characteristics of cancer cells but also by their interactions with the tumour environment, and with the immune system[16]. All of those factors influence treatment options, but also the prognosis.

NSCLC, which includes a diverse assortment of carcinomas with variable tumour biology and prognosis, accounts for nearly 85 % of lung malignancies. In general, advanced lung cancer has an exceedingly dismal prognosis, with only a 5 % 5-year survival rate.

SCLC is the most aggressive of all lung cancers when left untreated, with an average survival rate of 2 to 4 months after diagnosis[8]. SCLC accounts for about 15 % of all lung malignancies and is characterized by a great proliferative rate, a significant proclivity for early metastasis, and a poorer prognosis than NSCLC at every stage[32]. Brain metastases are common in SCLC patients, with 10 % of patients having brain metastases at the moment of diagnosis and another 40 - 50 % developing brain metastases later[32].

Accurate staging is of paramount importance in predicting prognosis and treatment. Since staging has been associated with a poor prognosis in the case of brain metastases, as these usually occur in more advanced stages of the disease, it is vital to find tools such as new compounds or biomarkers that can help with the detection and staging before the treatment options are more limited.

1.2 BODIPYs

BODIPY or 4,4-difluoro-4-bora-3a,4a-diaza-s-indacene is a dipyrromethene, with two pyrrolic units linked by a methylene bridge, complexed with boron. This particularly important dipyrromethene was discovered by Treibs and Kreuzer in 1968 and has been investigated for a wide range of applications.

The large structural and substitutive versatility of these fluorophores aids the definition of their spectroscopic, photophysical, and chemical characteristics[33–37]. Additionally, they have high photochemical stability, narrow absorption and emission bands with high peak intensities (absorbing high amounts of ultraviolet light), high molar absorption coefficient ε (λ) high quantum fluorescence yield (Φ), and fluorescence time (τ) in the nanosecond[33–35,37–40]. These compounds have also low toxicity and are thermally stable, and resistant to self-aggregation in solution, under physiological circumstances[33,37,38]. They are soluble in most organic solvents and are usually unaffected by the polarity or pH [23,33,35,37,38,40].

It is also essential to consider the factors that can contribute to the photodegradation processes during the use of BODIPYs in practice. The molecular structure of BODIPYs, as well as the nature of the medium, the properties of the absorbed light, the impact of the type of light, and the presence of atmospheric oxygen, are all variables that affect photodegradation[39].

1.2.1 Synthesis

Two major synthesis methods, depicted in scheme 2, are commonly used for the synthesis of the BODIPY core. Condensation of an acylium equivalent with a pyrrole is employed in the first method, in scheme 2[33,40]. The acylating agent in this reaction can be an

acid chloride, acid bromide, acid anhydride, or orthoester. BODIPY is formed when the extra base and boron trifluoride etherate (BF$_3$Et$_2$O) are added to the process[33,37,40].

The second method is based on a catalyzed condensation of pyrrole with an aldehyde; After oxidation with 2,3-dichloro-5,6-dicianobenzoquinone (DDQ), for instance, the oxidized dipyrromethane is placed in contact with excess base and BF$_3$Et$_2$O, obtaining BODIPY as the end product[33,37,40].
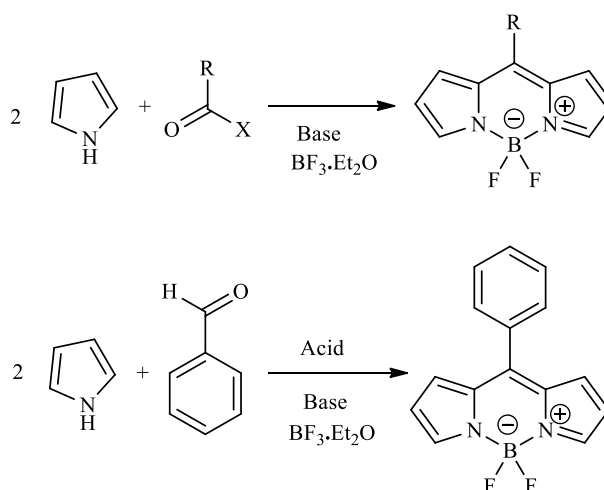
Scheme 2 - BODIPYs may be synthesized by the two different techniques, adapted from[33].

1.2.2 Structure

A monoanionic dipyrromethene ligand and a disubstituted electron-deficient boron, usually a cationic boron difluoride (BF$_2$) group, make the structure of a BODIPY dye[37]. BODIPYs have a distinct numbering system than the usually implemented for dipyrromethanes as demonstrated in scheme 3.
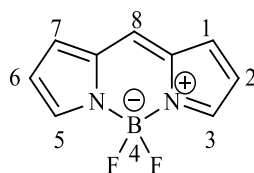
Scheme 3 - 4,4-difluoro-4-bora-3a,4a-diaza-s-indacene numbering system.

As illustrated in scheme 4, these compounds have three kinds of peripheral positions: *meso*, α, and β. BODIPY tracers have the greatest advantage that their structure contains eight locations that may be used to modify its characteristics[37].
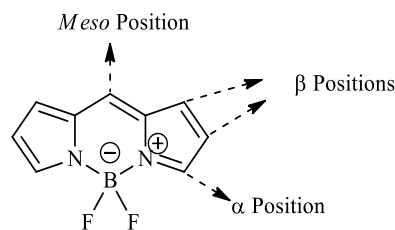
Scheme 4 - Nomenclature for the various BODIPY positions.

1.2.2.1 α, β and *Meso* Positions

BODIPYs are susceptible to oxidative nucleophilic replacements of α hydrogens, in which nucleophiles such as nitrogen and carbon are incorporated in a single step[34,41]. Furthermore, we can have a mono- or di-substitution of the 3, 5 positions of halogenated BODIPYs with oxygen, nitrogen, sulphur, or carbon nucleophiles[34,42,43].

The β position has two functionalization options: 2, 6 or 1, 7 with positions 2 and 6 being more susceptible to electrophilic substitution processes. Some groups usually associated with positions 2, 6 are formyl, carboxylic acids, or nitro groups. The influence of di-substitution 1, 7 on spectral characteristics is the less explored, however, these locations are low in electrons and have a reactivity comparable to positions 3, 5, and 8[35,44].

As the *meso* position can withstand a large variety of chemical reactions, there are many distinct functionalization techniques available in this position[45]. The broad range of groups that may be inserted at the 8-position results in a dye family with absorption and fluorescence emission spectra covering the major part of the visible spectrum[34].

1.2.2.2 Substitution Group Effects

The spectral properties of classic BODIPY chromophores are typically in the region of 470 - 530 nm[35]. BODIPYs in general are insensitive to the effects of solvents, but the incorporation of some substituents groups like donor groups or electron acceptors in the *meso* position can modify the response of the compounds to the environment in which they are found[45].

Significant deviations from the absorption and emission maximums in relation to the red region are obtained by substituting aryl, ethynylaryl, and styryl in positions 1-, 3-, 5- and/or 7, replacing the *meso*-carbon atom with nitrogen to form an aza-BODIPY or combinations thereof[35]. The introduction of electron-donating groups, such as alkoxy and amino groups in the *meso* position blue-shift the emission[45,46].

The presence of heteroatoms at positions 3 and 5, can also result in redshifts[34,35]. On moving from substituents with oxygen atoms, to those with nitrogen, sulphur, and selenium atoms and then to those with tellurium atoms, the absorption and emission spectra display a shift from the green to the Near-Infrared Region (NIR) region[35]. The extent of the redshift is mainly related to the electron-donating properties of the heteroatom[35].

The exchange of the two fluorine atoms in the boron centre for another anion offers another form of functionalization but does not significantly affect the maximum wavelength[34,35,37,46]. Replacement of the fluorines by carbon groups like aryl, alkyne, alkyl moieties, and oxygen nucleophiles (alkoxides or carboxylates) has led to a family of photostable, highly luminescent, redox-active BODIPYs[34,46].

1.2.3 Applications

The BODIPYs characteristics allow for almost unlimited structural changes, resulting in molecules with unique (electro) chemical, optical, and (photo) physical properties[37]. Its numerous applications did not begin to be discovered until around 1990.

They are used as fluorescent sensors, photoactive materials in organic photovoltaic devices, organic light-emitting devices, fluorescent nanocarriers, photoactivatable compounds, and triplet photosensitizers - PDT -, photocatalysts in organic reactions, among other applications[33,35–39,47]. Furthermore, boron dipyrromethene dyes are now accessible commercially as biological labels, bioimaging probes, and laser dyes[37].

The characteristics of BODIPYs are useful in bioimaging since fluorescence processes allow the use of spectroscopy in the NIR. The most commonly used fluorophores for bioimaging have a wavelength range of 650 to 900 nm, with a range of penetration between 1 and 3 mm[36,37,48]. Nevertheless, non-invasive fluorescence imaging in the second NIR window (NIR-II, 1000–1700 nm) has attracted much attention due to its deeper penetration (5–20 mm) in biological tissues and better contrast as a result of reduced photon absorption and/or scattering and reduced tissue autofluorescence[37]. In 1995, Boron dibenzopyrromethene dyes were patented with absorption and fluorescence emission beyond 700 nm[37]. In 2016, in the NIR-II region, two quinodimethane-bridged BODIPY dimers with great absorption around 1100 nm were investigated for selectively react with reactive oxygen species[49].

BODIPY and BODIPY-derived materials have been investigated as antibacterial agents, for labelling biological substances or targeting different biomolecules in the interior and outside of cells, and for the functionalization of drug micro- and nanocarriers for diagnostics[37,39]. BODIPYs in combination with Fluorine-18 as a tool for PET diagnostic scans have become increasingly investigated in recent years. Some work in the field, such as brain and myocardial perfusion imaging, has previously been published; in the case of myocardial perfusion, BODIPYs allowed the observation of ischemia[36,50–53].

1.3 Nuclear Medicine for Lung Cancer Diagnosis

PET systems which use radiopharmaceuticals, drugs labelled with a radioisotope, are exceptionally valuable in medical and scientific fields, particularly for cancer evaluation[23]. Some radiopharmaceuticals containing the radioisotope Fluorine-18 have been investigated to assess angiogenesis, cell proliferation, hypoxia, fatty acid metabolic activity, and metastasis in

lung cancer environments[54]. APPENDIX I, in particular table 7, covers several additional radiopharmaceuticals labelled with different radioisotopes such as ^{18}F, ^{68}Ga, ^{60}Cu used in lung cancer diagnostic research.

PET using ^{18}F-Fluorodeoxyglucose (^{18}F-FDG), a radiolabelled deoxyglucose analogue illustrated in scheme 5, is the radiopharmaceutical of choice for tumour metabolic activity assessment, as FDG has glucose-like first metabolic steps. The malfunction of glucose metabolic activity may be evaluated quantitatively *in vivo* by administering the radiopharmaceutical[55,56]. However, ^{18}F-FDG has some disadvantages, such as being less useful for brain metastases due to the intense physiological activity in that area, and the fact that there is ambiguity about whether it is tumour-specific, as it has a high rate of false positives in inflammatory and granulomatous diseases[54–56]. Also, the importance of the highest standardized uptake value (SUV_{max}) on PET scans with FDG is still discussed[56].
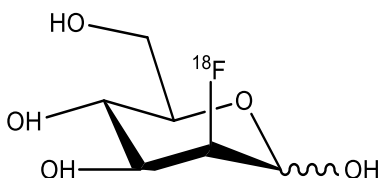
Scheme 5 – ^{18}F-FDG structure.

1.3.1 PET Imaging

PET as a non-invasive technique provides functional images, time-course detection, and quantification of a radiotracer all over the body[23]. This methodology allows the diagnose of diseases in early stages, evaluating the efficacy of certain treatments, and also the study of the biological sources of some diseases, providing accurate data on the radiotracer pharmacokinetics and physiological changes[23,57].

The physics of PET imaging is centred on a neutron-deficient radioisotope emitting a positron, which travels a small distance and interacts with an electron, annihilating both the electron and the positron and producing two high-energy photons[58]. The photons move in opposite directions along an approximately straight line, and PET scanner detectors, using scintillating crystals coupled to photomultipliers, detect photons outside the body[58].

Different factors establish the noise and resolution characteristics of the PET imaging process[58]. The noise is determined by the amount of 511 keV photons detected individually, in turn, the density of the scintillator, the scanner count-rate capabilities, and the amount of radiation delivered into the patient influence the number of photons detected[58]. In relation to the spatial resolution, this one is determined by the variability in calculating the 511 keV photon interaction spot in the scintillator[58]. As a result, this is influenced by the optics of the

scintillator, the number of optical photons emitted, and the fidelity of the photomultiplier tubes and related electronics[58].

The combination of two modalities can allow the acquisition of images that characterize the same living tissue in different ways. For example, when PET and CT are combined in one scan, as the one represented in figure 9, a synergistic combination of data regarding what (from PET) and where (from CT) is acquired. A PET/CT scan exposes a patient to between 23.7 and 26.4 mSv of radiation[59]. As a dose of up to 32 mSv added to the background radiation per experiment is already significant, the PET/CT scanning techniques must be optimized to reduce the radiation and cancer risk associated with them[59].
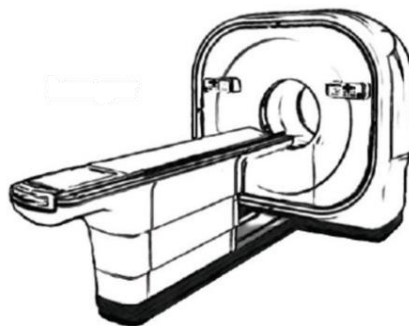
Figure 9 - Schematic PET/CT scan, adapted from[58].

1.3.2 Radioisotopes

Different conditions can be treated or diagnosed by administering radiopharmaceuticals to patients[1]. Cyclotrons and isotope generators can be used to produce radioisotopes, an atom with an unstable nucleus with many or few neutrons, which can later be linked to a drug for diagnostic or therapeutic applications[1]. Therefore, radioactivity consists of the emission of subatomic particles or high-energy electromagnetic radiation by the nuclei of radioisotopes, in order to achieve a more stable configuration[1].

However, in order to be used, radiopharmaceuticals must fulfil specific criteria. Firstly, they must be pyrogenic-free and sterile, dissolve in an aqueous medium or form a colloidal or a suspension of bigger particles, have a pH between 4 and 8, have a low radiation dosage, and constantly follow preparation and quality control guidelines[1]. Secondly, their half-life must be long enough for the scan and short enough to avoid unnecessary irradiation (an optimum effective half-life is around 1.5 times the duration of the diagnostic exam), with high target/non-target activity[1]. Certainly, the radionuclide must be available in sufficient amounts for the scan and must be able to promptly bind to the desired compounds. As the more expensive ones have limited utility, adequate cost-effectiveness must also be addressed.

Other factors to consider include radiochemical purity, radioisotopic purity, the presence of a carrier in the pharmaceutical, the presence of an isotope effect, the presence of

isotope exchange reactions, the radiation dose delivered to critical organs and the entire body, the presence of degradation products caused by chemical instability, and the presence of degradation products caused by self-irradiation of the pharmaceutical[1].

1.3.2.1 Fluorine-18

The radioisotope Fluorine-18 is the most important of the 18 distinct isotopes of fluorine[60]. The stable chemical element, Fluorine-19, has 9 protons and 10 neutrons, a high nuclear charge, and a $1s^2\,2s^2\,2p^5$ electronic distribution. Fluorine-19 is a chemical element with the atomic number 9 that is found in group 17 and period 2 of the periodic table. Because it can react with every periodic table element except krypton, neon, and helium, this element is particularly electronegative and exceedingly reactive.

Fluorine-18 has been a highly useful radioisotope for PET applications since its discovery in 1937[61]. Fluorine-18, or ^{18}F, is an unstable element with 9 protons and 9 neutrons. This radioisotope decay pattern is depicted in scheme 6. ^{18}F decays about 3% by electronic capture and approximately 97% by positron emission (β^+), with an energy of approximately 0.635 MeV, and with a half-life ($T_{1/2}$) of 109.7 minutes.
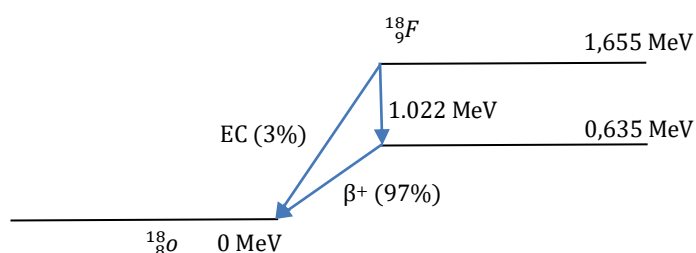
Scheme 6 - Scheme for the decay of Fluorine-18.

The physical and nuclear features of this radionuclide, as well as its high specific activity and ease of manufacture on a wide scale, make it unique[61,62]. It remains to add that the flexible chemistry of nucleophilic and electrophilic substitutions makes it easier to introduce Fluorine-18 directly or indirectly into the molecules of interest[62].

In tissues, ^{18}F has a low linear positron range, an average of 0.38 mm, and a maximum of 2.3 mm, resulting in a superior PET image resolution[61]. Another advantage of this radioisotope is that ^{18}F allows for reasonably extended imaging periods as well as production-distribution to clinical installations without an on-site cyclotron. In comparison with short-lived positron-emitting radionuclides such as Carbon-11, Nitrogen-13, and Oxygen-15 (half-lives of 20.3 minutes, 9.97 minutes, and 122 seconds, respectively), Fluorine-18 has a lower

positron emission energy. Thus, the total radiation dosage received by a patient exposed to ^{11}C, ^{13}N, or ^{15}O is substantially smaller[61–63].

Nuclear reactors and accelerators can generate Fluorine-18. The method of manufacturing has been to accelerate charged particles that cause a specific nuclear reaction on a specific target. Reactions 1 and 2 are the most often used to obtain Fluorine-18. The specific activity of the two chemical products of the following reactions is the most significant difference between them[62].

$$^{18}O + p \; \rightarrow \; ^{18}F + n \qquad \text{(reaction 1)}$$

$$^{20}Ne + d \; \rightarrow \; ^{18}F + \alpha \qquad \text{(reaction 2)}$$

The Oxygen-18 target in the first reaction is generally $[^{18}O]H_2O$, which is extremely enriched, though $[^{18}O]_2$-Oxygen has also been used[61,63]. An aqueous solution of ^{18}F-Fluoride ion is formed when the target is liquid $[^{18}O]H_2O$; when the target is $[^{18}O]_2$ gas, $^{18}F-F_2$ gas is obtained[62]. Though $^{18}F-F_2$ can also be obtained by irradiating ^{20}Ne with deuteron, in general the yield and specific activity are lower than those obtained with the first reaction[62,63].

The production method used is dependent on the desired subsequent chemical reactions; ^{18}F-Fluoride anion is produced for use as a nucleophile, while ^{18}F-Fluorine is produced for use in electrophilic methods[64]. Nucleophilic ^{18}F-Fluoride has in general a bigger specific activity, since to obtain electrophilic $^{18}F-F_2$, ^{19}F gas needs to be used as a carrier to extract the $^{18}F-F_2$ from the target[62]. The inclusion of a carrier ($^{19}F-F_2$) increases the bulk of the final radiotracer, which might contribute to receptor saturation and a decrease in PET signal, with possible pharmacological effects also associated[62].

Fluorine-18 is a radionuclide that is simple to produce, has a short half-life, is faultless for PET scans, and emits relatively low energy positrons, making metabolic process assessment inside the human body considerably safer[65]. Small biomolecules, as well as more complicated structures including peptides, proteins, and oligonucleotides, can be labelled with the radionuclide[61]. Some radiopharmaceuticals with this radioisotope have been investigated for lung cancer diagnosis.

1.3.3 Fluorine-18 Radiolabelling

Fluorine-18 may be associated with a variety of organic compounds without modifying their biological assets significantly[66,67]. Fluorine is a very electronegative element that has an atomic radius slightly larger than hydrogen; these particularities are used to replace hydrogen atoms in drug development, as it improves the lipophilicity of substances, allowing them to pass through the lipid membranes[60,67].

To produce a radiolabelled product, it is essential to choose precursor molecules with adequate leaving groups[67]. Furthermore, adding the ^{18}F to a precise position in the molecule requires a cautious choice of reagents as well as suitable conditions[60].

Direct radiofluorinations are performed on an immediate precursor to the target molecule, employing a one-step process; while indirect radiofluorinations are generally multi-step processes, however with the increasing complexity of the process, the greater the number of resulting products and the more intricate the purification process becomes[61]. The direct or indirect introduction of ^{18}F into molecules of interest can be performed through nucleophilic reactions, with ^{18}F-Fluoride anion, or electrophilic substitutions, with ^{18}F-Fluorine (^{18}F-F_2)[61,67].

1.3.3.1 Nucleophilic Radiofluoration

Labelling compounds with ^{18}F through nucleophilic methods is advantageous due to its greater selectivity and ability to provide compounds with high specific radioactivity for use in PET[61,67]. Nucleophilic substitution is known as a chemical process involving the addition of a nucleophilic molecule (negatively charged or having unpaired electron pairs) to a molecule containing a leaving group (electron drawing group attached to the parent molecule through a weak chemical bond)[68].

There are two types of nucleophilic reactions used to produce ^{18}F radiopharmaceuticals: a) aliphatic nucleophilic radiofluorination (S_N2) and b) aromatic nucleophilic radiofluorination (S_NAr)[61]. The indirect incorporation of ^{18}F into the aromatic ring occurs in S_NAr nucleophilic reactions, with the percentage of S_NAr nucleophilic reaction mostly depending on the nature of the leaving group, activating group, protecting group, temperature, and solvent[67].

Many Fluorine-18-labeled radiopharmaceuticals prepared by nucleophilic aliphatic fluorination comprise the introduction of ^{18}F, followed by a global deprotection step[61]. This is the case for the nucleophilic radiofluorination route to ^{18}F-FDG (3), depicted in scheme 7. ^{18}F-FDG is obtained by ^{18}F-Fluoride substitution of triflate (1), to give rise to structure (2), followed by hydrolysis of all acetyl protecting groups[61].
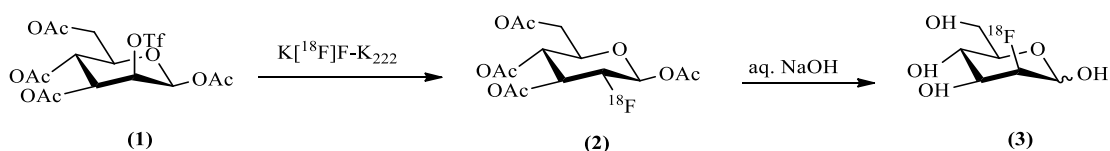
Scheme 7 - Nucleophilic aliphatic radiofluorination used to synthesized ^{18}F-FDG, adapted from[61].

To perform the synthesis of ^{18}F-FDG, different catalysts and phase transfer agents have been studied, and the one that proved to be the most effective for nucleophilic substitutions was the structure shown in scheme 8[68].
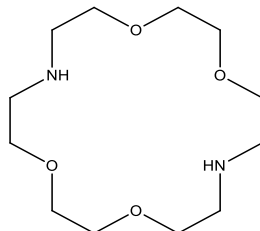
Scheme 8 - 1,4,10,13-tetraoxa-7,16-diazacyclooctadecane (Kryptofix 2.2.2).

1.3.3.2 Electrophilic Radiofluorination

When it comes to electrophilic radiofluorination, fluorine is delivered to an electron-rich reagent, like an alkene, aromatic ring, or carbonanion, producing a difluoro derivative of the parent molecule[61,68]. A widespread supplier of ^{18}F for electrophilic or radical fluorination is ^{18}F-F$_2$[61,63,67,68].

A relatively simple electrophilic reaction is to bubble ^{18}F-F$_2$ in a solution of the substrate to produce a Fluorine-18-labeled product[61,63]. This type of reaction is fast, which is why it is important in the production of some drugs. However, it has certain disadvantages, such as the fact that the gas is very reactive and is known to provide low yields of the final product and the fact that the oxidizing force of fluorine often leads to exothermic chain reactions with the formation of by-products[61,68].

The fluorination of an alkene can be used to obtain ^{18}F-FDG, as shown in scheme 9. It employs the reaction of molecular ^{18}F-Fluorine with 3,4,6-tri-O-acetylglucal (4) to give ^{18}F-FDG (3)[61]. One of the disadvantages of this method is that due to the highly reactive nature of ^{18}F-F$_2$, happens the concomitant production of undesired 2-[^{18}F]fluoro-2-deoxy-D-mannose (5), requiring a tedious separation procedure[61].
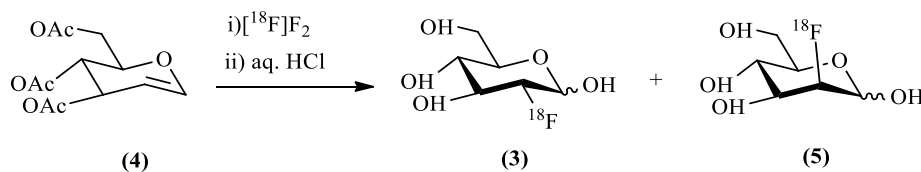
Scheme 9 - The pathway to ^{18}F-FDG through electrophilic radiofluorination, adapted from[61,68].

Electrophilic radiofluorinations have constrained applications since ^{18}F−F$_2$ has a lower specific activity as Fluorine-19 gas needs to be used as a carrier to extract the ^{18}F−F$_2$ from the

target. That way, only tracers of low-toxicity that do not necessarily require high specific radioactivity are obtained by electrophilic radiofluorination[61,62,67].

1.3.4 BODIPYs Radiofluorination

BODIPYs are chemicals that should be considered for diagnostic applications, such as PET scans, due to their stability and pH insensitivity characteristics. A nearly ideal molecule for diagnosis can be obtained by adding to their structure ^{18}F, a radioisotope that does not interact with cells or their components.

Typically, BODIPYs that are used as fluorophores are modified to produce redshift fluorescence. However, since ^{18}F can be introduced in their structure, BODIPYs can have a hybrid nature, PET/Fluorescence[51]. In recent years, the hybrid image has gained a lot of attention since PET provides quantitative data while the optical image provides real-time data with great sensitivity[51].

The technique that in the past was commonly employed to perform the BODIPYs radiolabelling with ^{18}F used boronic esters[23]. Over the years, several relevant pieces of research in the literature using different labelling techniques look into the incorporation of ^{18}F in the boron centre, as shown in scheme 10[23,51,66,69]. Radiolabelling techniques can be based on two or three steps through an intermediate, or based on hydroxide or direct isotopic exchange[23].

Although direct isotopic exchange may be impaired by the stability of the B-F bond in the BODIPYs structure, Lewis acid-promoted isotopic exchange is the most commonly used procedure, perhaps due to its ease of use and ability to offer a wider range of tracers with considerable high yields[23].
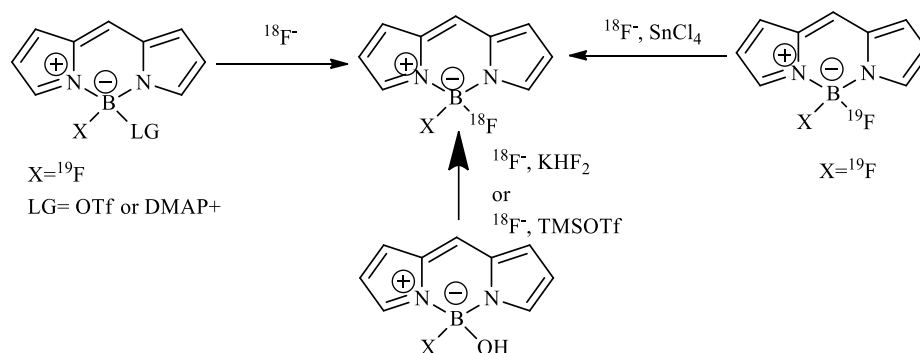
Scheme 10 - Triflate or DMAP substitution, hydroxyl substitution, and isotopic exchange are the main radiosynthesis techniques employed for BODIPY radiofluorination, adapted from[23].

Relatively weaker acids such as $ZnCl_2$ provided relatively good radiochemical yields (between 15 and 45 %) in BODIPYs, when the isotopic exchange was performed in acetonitrile with excess acid at elevated temperature[69]. However, the high temperature

employed in these reactions may trigger decomposition of the dye and by-product formation. So, among the most studied Lewis acids, the excess of SnCl$_4$ seemed to be the most effective with a higher quantitative yield (above 57 %), even when performed in acetonitrile at room temperature[51,69].

Lewis acid-promoted isotopic exchange has already been applied to the synthesis of some ^{18}F-BODIPY radiotracers containing several functional groups, such as peptides like RGD, represented in scheme 11, but also bombesin, MT-MMP1 substrates, and different inhibitors based on small molecules, like PARP1, PACMA31, and lipids[23,70].
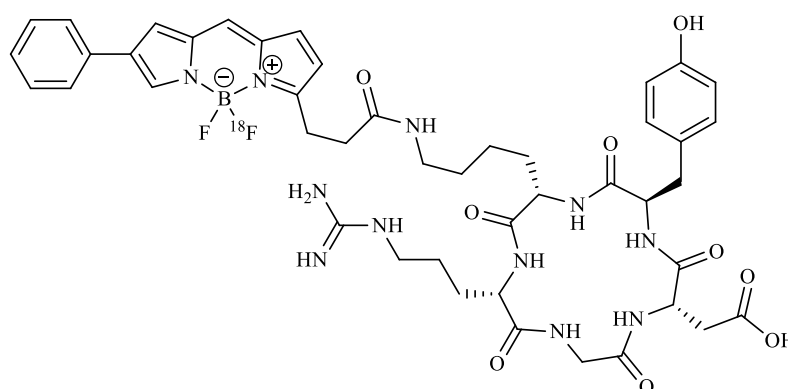
Scheme 11 - BODIPY labelled with Fluorine-18 and bioconjugated to an RDG peptide for use as a PET/Fluorescence glioblastoma imaging agent, adapted from[69].

All previously mentioned drugs, in addition to their synthesis and characterization, were subjected to *in vitro* studies in which their potential cytotoxicity was evaluated. It is important to start by doing these *in vitro* studies in order to understand the interactions of the compounds at the cellular level. After the compounds reveal the desired characteristics, the study of the radiolabelling process and the following *in vivo* studies are an option to assess the biodistribution of the radiopharmaceutical.

Objectives

2 - Objectives

The aim of this work was to synthesize new BODIPYs that could in the future have the radioisotope Fluorine-18 incorporated in their structure and therefore be used as tracers for PET imaging.

Thus, the goals of this dissertation were: first, synthesize BODIPYs as novel substrates for faster ^{18}F insertion, by aiming to substitute the ^{19}F with alkoxy groups in order to make easier the ^{18}F insertion into the boron centre; Second, perform a structural characterization of new alkoxy-BODIPYs versus the BODIPYs with ^{19}F in the boron centre; And at last, evaluate the cytotoxicity of the six structures depicted in scheme 12 through *in vitro* studies. It is important to find the most biocompatible since the compounds are aimed to be investigated in the future for intravenous injection to detect tumours.
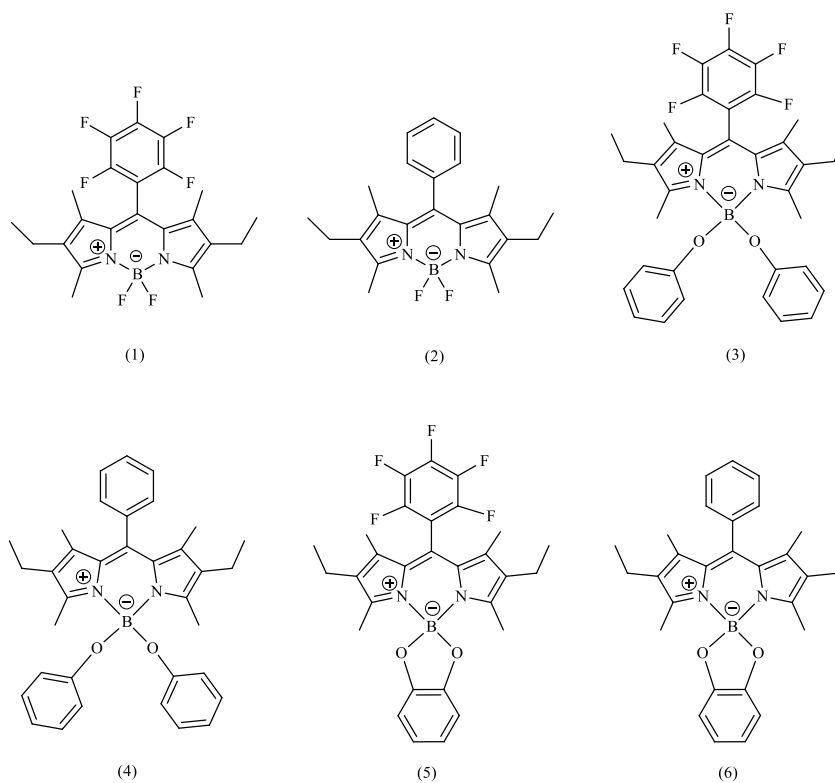
Scheme 12 - BODIPYs (1-6) synthesized and considered for *in vitro* assessment.

Experimental Procedures

3 – Experimental Procedures

3.1 Reagents, Instrumentation, and Synthesis

All reagents, silica gel and solvents used in the synthesis of all BODIPYs were supplied by one of the following companies Sigma-Aldrich, Acros Organics or Fluka. All were used without further purification. Analytical Thin Layer Chromatography (TLC) was performed on Merck silica gel plates with indicator F-254, and the results were observed with the aid of a double wavelength ultraviolet light (with 254 and 365 nm). Silica gel (230 - 400 mesh) was used to perform column chromatography and Fluka 60G silica gel to perform TLC on 20 x 20 cm glass plates.

3.1.1 Nuclear Magnetic Resonance Spectroscopy

^{1}H, ^{13}C, ^{11}B, and ^{19}F NMR spectra were obtained with a Bruker AVANCE III NMR, at 400 MHz for proton, 100 MHz for carbon, 128 MHz for boron, and 376 MHz for fluorine. As internal standards, protons from the solvent, CDCl$_3$, were used.

3.1.2 Mass Spectrometry

Mass spectrums were acquired with an ion trap MS: THERMO SCIENTIFIC, model LXQ, employing Electronic Spray Ionization (ESI). The samples were dissolved in dichloromethane and diluted in methanol acidified with 0.1 % of formic acid.

3.1.3 Absorption Spectroscopy

The absorption spectrums were obtained with a Shimadzu UV-2600 spectrophotometer, with a wavelength window ranging from 200 to 800 nm using 1 cm path length quartz cells.

3.1.4 Emission Spectroscopy

Steady-state fluorescence studies were performed using a Horiba-Jobin-Yvon Fluorog spectrometer. Fluorescence spectra were obtained by using optically diluted solutions in 1 cm path length quartz cells.

3.1.5 Procedures for the longer synthesis of BODIPYs 1 and 2

In a two-necked flask, 250 mL of dichloromethane (CH$_2$Cl$_2$) were added and placed under a nitrogen atmosphere for 10 to 15 minutes. Under stirring, 0.5 mL of 3-ethyl-2,5-dimethyl-pyrrole (3.70 mmol) were added. Next, 2.02 mmol of the corresponding aldehyde (2,3,4,5,6-pentafluorbenzoldehyde for BODIPY 1 or benzaldehyde for BODIPY 2) and 50 μL of trifluoroacetic acid (TFA) (0.65 mmol) were added. The mixture was left under stirring for 10 to

12 hours. Then, 0.40 g of 2,3-dichloro-5,6-dicyan-1,4-benzoquinone (DDQ) (1.76 mmol) was added and left stirring for 2 more hours. Latter, 3.8 mL of diisopropylethylamine (21.8 mmol) and 3.8 mL of boron trifluoride diethyl etherate (BF_3Et_2O) (30.3 mmol) were added and left to stir for 5 hours.

The mixture was washed with 30 mL of each solution: saturated sodium bicarbonate (Na_2HCO_3), saturated NaCl and distilled water. Sodium sulphate anhydrous (Na_2SO_4) was used to dry the solution. The mixture was filtered after the solvent was evaporated with a rotary evaporator.

Column chromatography on silica gel utilizing CH_2Cl_2:hexane (1:1) was employed to isolate the BODIPY. Analytical thin-layer chromatography was performed to confirm the compounds whenever necessary, and preparative TLC was performed with 60 mL of toluene, to separate the desired BODIPY.

3.1.6 Procedures for the shorter synthesis of BODIPYs 1 and 2

The longer synthesis of BODIPYs was the one we began with, but then a shorter one started to be used in our laboratory, as we could get BODIPYs without so many by-products and therefore fewer steps for compound purification were needed.

In a two-necked flask, nitrogen gas was bubbled into 20 mL of CH_2Cl_2 for 5 minutes. Then, 0.3 mL of 3-ethyl-2,5-dimethyl-pyrrole (2.22 mmol), 50 µL of TFA (0.65 mmol), and 0.97 mmol of the corresponding aldehyde (pentafluorbenzaldehyde for BODIPY 1 or benzaldehyde for BODIPY 2) were added. The mixture was left to stir under a nitrogen atmosphere. Ten minutes later, 0.27 g of DDQ (1.19 mmol) were added. Another ten minutes later, 4 mL of triethylamine (28.7 mmol) and 5mL of $BF_3.Et_2O$ (39.8 mmol) were added. Past half an hour, the agitation of the reaction was stopped.

Three distinct solutions were used to wash the solution: 30 mL of saturated $NaHCO_3$, 30 mL of distilled water, and 30 mL of saturated NaCl. The water content was then removed using anhydrous Na_2SO_4. The solvent was evaporated using a rotary evaporator after the mixture was filtered.

The BODIPY was isolated using column chromatography using CH_2Cl_2:hexane (1:1). To verify the compounds, analytical TLC was performed whenever necessary, and preparative TLC with 60 mL of toluene was done to isololate the desired BODIPY.

3.1.7 Procedures for the synthesis of BODIPYs 3 to 6

For the synthesis of BODIPYs 3 to 6, 10 mL of dichloromethane, 0.066 g of $AlCl_3$ (0.50 mmol), and 0.050 g of the respective BODIPY 1 (0.11 mmol) or BODIPY 2 (0.13 mmol) were placed in a 100 mL flask. The mixture was refluxed under a nitrogen atmosphere for 15 minutes at 60 °C, on a paraffin bath.

After 15 minutes, 2.5 equivalents of the respective alcohol reagent - phenol for BODIPYs 3 and 4, and catechol for BODIPYs 5 and 6 - were added to the purple solution; and 20 minutes later, the reflux was stopped. The products were washed with 30 mL of distilled water and 30 mL of concentrated NaCl, the water excess was removed with Na_2SO_4. Preparative thin-layer chromatography was performed with hexane:CH_2Cl_2 in the proportion 1:1 to isolate BODIPYs.

3.2 Structural Motifs Evaluation

Geometry optimization of all structures was performed by energy minimization with MM2 molecular mechanics calculations with a minimum RMS gradient of 0.01 using Chem3D software (CambridgeSoft v12).

3.3 *In vitro* Studies

Cytotoxicity studies such as 3-(4,5-dimethylthiazol-2-yl)-2,5-diphenyltetrazolium (MTT) bromide, Sulforhodamine B (SRB), and Haemolysis assays allow researchers to evaluate the cytotoxic effects of a drug in a controlled environment. The uptake of BODIPYs by cells was also studied to assess how much of the BODIPYs could be incorporated.

3.3.1 Cell Lines

A549 (ATCC CCL-185, *human alveolar basal epithelial adenocarcinoma cells*) and NCI-H1299 (ATCC CRL-5803, *human non-small cell lung carcinoma cells*) were the two cell lines that allowed the study of the effects of BODIPYs in a lung cancer environment.

The NCI-H1299 cell line was established from a metastatic lymph node in a lung of a patient who had previously received radiotherapy[71]. As for gene expression, these cells remain positive for keratin and vimentin but are negative for Neurofilament Triplet Protein[71]. This cells appear to have a homozygous partial deletion of the p53 protein and a lack of expression of the same protein[71]. Additionally, H1299 produces neuromedin B, which appears to be a regulatory peptide in lung cancer[71].

The A549 cell line comes from an adenocarcinoma of the epithelial tissue of the lung, which was first isolated in 1973. With a low density of the cell population, the cells contain only a few lamellar bodies; but in mature cells, in more populated cultures, lamellar bodies are abundant[72]. The cells of the A549 line produce, store in lamellar bodies and secrete phosphatidylcholine and, therefore, have several crucial biological properties of type II alveolar epithelial cell[72].

When dealing with cell cultures they were handled in strict sterile conditions, with all experiments made under a laminar flow hood, with aseptic techniques been used. In order to work with the cell lines, they were thawed and propagated in adherent culture flasks according to the recommendations of the respective supplier. For all studies, cell lines were grown at 37 °C in a

humidified atmosphere with 95 % air and 5 % CO_2 in a HeraCell 150 incubator. The culture medium used was Dulbecco's Modified Eagle Medium (DMEM (Gibco®, 11966-025)) with 1 % of antibiotic (100 U/mL de penicillin and 10 µg/mL streptomycin (Lonza Pen Strep, Amphotericin, B, 17-745E)), 0.25 mM of sodium pyruvate (Sigma, S8636), and 5 % of Fetal Bovine Serum (Sigma, F7524) for H1299 cell line, and 10 % for A549 cell line.

To conduct the *in vitro* studies, the cells had to be detached from the culture flasks using TrypLE Express™ (Gibco, 12605-028), for that end, cells were incubated with 2 mL of TrypLE for 5 minutes at 37 ºC. Following that, 4 mL of culture media was added, and the mixture was homogenized to inactivate the TrypLE. An equal amount of the cell suspension and the Trypan Blue solution (0.4 g of Trypan Blue in 100 mL of distilled water, a 0.4 % solution) were combined in an eppendorf to count the number of living cells using an inverted optical microscope (NIKON Eclipse, TS100). Thereon, the number of living and dead cells was counted with the aid of a hemocytometer. Following the counting, the volume of cell suspensions was adjusted with culture media to achieve the desired cellular concentration for each assay.

The BODIPYs solutions were prepared with dimethylsulfoxide (DMSO, Sigma, D4540) as a solvent, and they were tested in concentrations between 1 and 100 µM.

3.3.2 MTT Test

The MTT test is a colourimetric assay that measures cell metabolic activity. Viable cells have NAD(P)H-dependent oxidoreductase enzymes that convert MTT to formazan, as illustrated in scheme 13, and therefore cell metabolic activity may be determined after reading the absorbance of the samples.

The MTT solution was prepared with 5 mg of MTT (Sigma, M2128) for each millilitre of phosphate-buffered saline (PBS), i.e., 5 mg/mL, at a pH of 7.4. Approximately 200,000 cells/mL were incubated in 48-well plates (SPL Life Sciences, 30048) overnight to promote cell adhesion. After that, BODIPY concentrations ranging from 100 µM to 1 µM were applied, and the plates were incubated for 24, 48, and 72 hours. In all experiments, two types of controls were used: cells that had not been treated and cells that had been treated with DMSO.
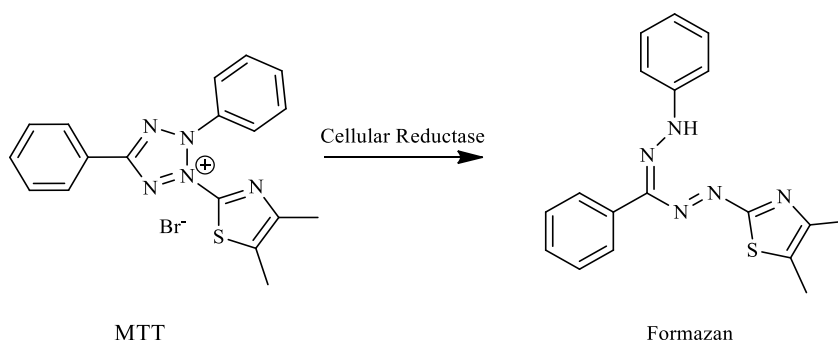
Scheme 13 - MTT is reduced to formazan crystals in metabolically active cells.

The culture media was then withdrawn, and the cells were washed with PBS. The cells were incubated for at least 2 hours with 100 μL of MTT at 37 °C and 5% CO_2 for the MTT to transform from a yellowish hue to the form of purple formazan crystals.

The insoluble formazan crystals were then dissolved in 100 μL of a solution of 0.04 M HCl in isopropanol. Finally, the absorbance was measured in an automated Enspire (Perkin Elmer) at a wavelength of 570 nm, using a wavelength reference of 620 nm. The following equation was used to compute the percentage of metabolic activity:

$$\% \, Metabolic \, Activity = \frac{(Treated \, Cells \, with \, BODIPY)_{(Abs \, 570nm - Abs \, 620nm)}}{(Treated \, Cells \, with \, Solvent)_{(Abs \, 570nm - Abs \, 620nm)}} \times 100 \quad (equation \, 1)$$

3.3.3 SRB Test

The SRB test is often used to assess drug-induced cytotoxicity and viability. This technique is based on the capacity of the protein-dye Sulforhodamine B to bind to proteins stoichiometrically under moderately acidic circumstances and be extracted using basic conditions, as shown in figure 10. The quantity of bounded dye may be used to infer about viability.

For the preparation of the SRB solution, 0.25 g of SRB (Sigma, 230162) were diluted in 500 mL of 1 % (v/v) acetic acid in ultra-purified water, obtaining a 0.05 % (w/v) solution. Approximately 200,000 cells/mL were incubated in 48-well plates (SPL Life Sciences, 30048) overnight to promote cell adhesion. BODIPYs were applied at 10 µM and 1 µM, and then the plates were incubated for 24, 48, and 72 hours. In all assays, two types of controls were used, cells without any treatment and cells treated with DMSO.

The growth media was removed, and then the plates were washed with PBS. To achieve the fixation, the cells were treated with 100 µM of acetic acid in methanol for at least 1 hour at 2° C. The solution was then withdrawn, and the plate was allowed to dry. After that, the cells were stained with 100 µM of SRB solution and left in the dark for at least another hour. Once the solution was removed and the plate washed, 100 µM of Tris-NaOH solution was added and the plate was kept in the dark for at least another hour while stirring.
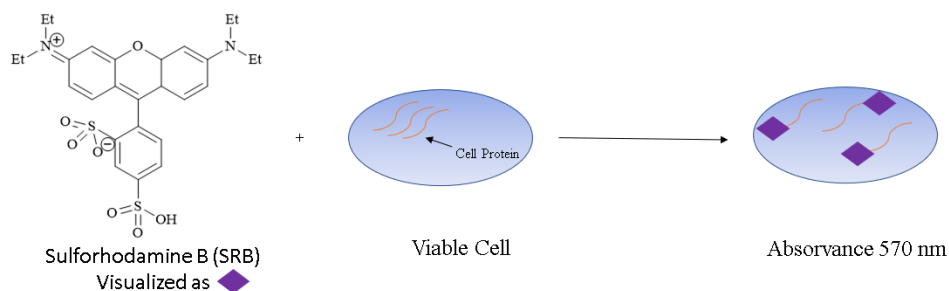
Figure 10 - Illustration of the SRB Cytotoxicity Assay, adapted from[73].

The absorbance was measured at a wavelength of 540 nm, using 690 nm as a wavelength reference, in an automatic *Enspire* (Perkin Elmer). The percentage of protein content was calculated with the following equation.

$$\% \: Protein \: Content = \frac{(Treated \: Cells \: with \: BODIPY)_{(Abs \: 570nm - Abs \: 620nm)}}{(Treated \: Cells \: with \: Solvent)_{(Abs \: 570nm - Abs \: 620nm)}} \times 100 \: \: (equation \: 2)$$

3.3.4 Haemolysis Test

Erythrocyte membrane can undergo substantial structural changes owing to drug treatment, therefore, the mechanical stability of red blood cells is a valuable measure for *in vitro* hemocompatibility screening[74].

Two solutions had to be prepared to perform the experiment. The first containing 0.85 % NaCl and 10 mM $CaCl_2$ prepared in ultrapure water. The second with Tryton-X 100 (1%) by diluting Triton-X 100 (100%) in ultrapure water.

After collecting 1 mL of blood, the samples were diluted in 30 volumes of a solution containing 0.85 % of NaCl and 10 mM $CaCl_2$. After centrifuging the mixture at 1300 g for 3 minutes and discarding the supernatant, another 30 mL of the initial solution was added. This procedure was carried out three times. Following the erythrocytes isolation, 2 % of the pellet was resuspended in 5 mL of 0.85 % of NaCl with 10 mM $CaCl_2$. The mixture was distributed on a 96-well plate. To have a comparison term, negative controls were the wells treated with DMSO, positive controls were the ones treated with Tryton-X 100 (1 %) to promote the lysis of cells, and then the effect of the BODIPYs on the red cells was evaluated by adding 10 µM and 1 µM of BODIPY 3 and 6 in the remaining wells. The plate was incubated for 1 hour and 2 hours under agitation at room temperature. Afterwards, the plate was centrifuged at 5200 g for 5 minutes. The supernatant was collected to another 96-well plate (SPL Life Sciences, 30096) and the quantification of the haemoglobin released was performed by the measure of the absorbance at 540 nm, in an automatic *Enspire* (Perkin Elmer).

The data obtained were normalized using the equation below.

$$\% \: Release \: of \: Hemoglobin = \frac{Abs \: (amostra)}{Abs \: (positive \: control) - Abs \: (negative \: control)} \times 100 \: \: \: (equation \: 3)$$

3.3.5 Cellular Uptake

This assay allows the perception of how much of the BODIPYs were incorporated by cells. To perform the uptake assay, about 500,000 cells were incubated in 24-well plates (SPL Life Sciences, 30024) with the following concentrations, 10 and 1 µM of BODIPYs 3 and 6, and the uptake was evaluated 4 hours, 2 hours, and 1 hour after the incubation to assess the variability of uptake as a function of time.

The medium of the plates was removed, and the plates were washed with PBS. Afterwards, 100 µL of DMSO were added to each well, and the well scrapping was performed.

The content of each well was collected to an eppendorf and subjected to centrifugation at 12 300 g for 10 minutes. The supernatants were collected to another eppendorf.

The fluorescence emission spectra and calibration curves were obtained based on the observation of a linear relationship between fluorescence emission and BODIPY concentration. Thus, 200 µL of a known concentration of BODIPY 3 and 6 in DMSO were added to a 96-well plate (SPL Life Sciences, 30096), and successive dilutions were performed until the detection limit of the fluorescence spectrometer was reached. Following, 100 µL of each solution of each eppendorf was placed on the plate to perform the measures. The absorption and emission wavelengths of the compounds were considered when measuring fluorescence intensity.

3.3.6 Statistical Analysis

The statistical analysis of the experimental values was performed using the software Graph Pad Prism version 8.4.3 for Windows, Graph Pad Software, USA.

Initially, the Shapiro-Wilk test was performed to know if the data was consistent with the assumption of sampling from a Gaussian distribution[75]. According to that, a parametric test was chosen. One-Sample t test was the test which was used to perform the statistical analysis, based on the aim of our work, to make inferences about one population by comparing the mean of some samples treated to a theoretical mean, the maximum normalization value, 100 %[75].

The multiple comparisons were corrected with the Bonferroni-Dunn test, so that statistically significant comparisons just by chance could be reduced[75]. Moreover, the significance level chosen was 0.05, and when $p < 0.05$ significances were represented by *, $p < 0.01$ were represented by **, and $p < 0.001$ by ***.

MTT, SRB, and Haemolysis data are represented in the form of mean and Confidence Interval (CI). The CI of the mean shows us how precisely the population mean was determined, and since only the most biocompatible BODIPYs will possibly be applied for diagnosis in the future, it is better to have a mean that best reflects the population in study.

Results and Discussion

4 – Results and Discussion

4.1 BODIPYs Characterization

To determine if the synthesized BODIPYs were the intended ones, NMR, Absorbance, Fluorescence, and Mass Spectra were used to characterize all of them. The obtained spectra, as well as a brief analysis and discussion, will be presented for each BODIPY.

BODIPY 1 with IUPAC name 2,8-diethyl-5,5-difluoro-1,3,7,9-tetramethyl-10-(perfluorophenyl)-5H-dipyrrolo[1,2-c:2',1'-f][1,3,2]diazaborinin-4-ium-5-uide was obtained with a yield of 20 %, and figures 11 to 16 show the results obtained from the characterisation.

(1)
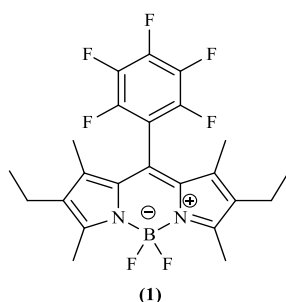
The methyl groups and aromatic protons associated with BODIPY 1 were properly identified in the ^{1}H NMR spectrum of figure 11. The acquired carbon spectrum is shown in figure 12, and it reveals the anticipated signs for this element. In figure 13 and 14, the ^{11}B and ^{19}F spectra also corroborate the structure by displaying all the required and predicted signals.

^{1}**H NMR (400 MHz, CDCl$_3$) δ (ppm):** 2.54 (s, 6H), 2.33 (q, J =7.6 Hz, 4H), 1.51 (s, 6H), 1.02 (t, J = 7.6 Hz, 6H).
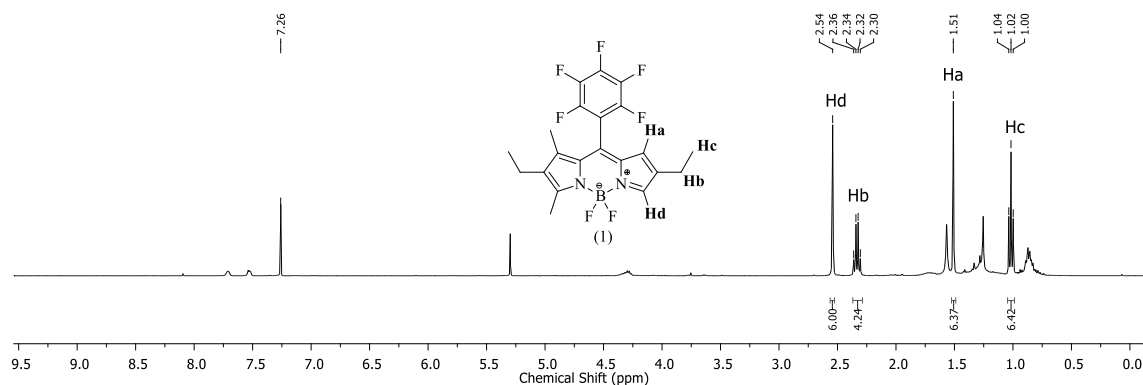
Figure 11 - ^{1}H NMR spectrum of BODIPY 1 (400 MHz, CDCl$_3$).

^{13}C NMR (100 MHz, CDCl3) δ (ppm): 156.14; 136.57; 133.93; 130.91; 130.35; 128.83; 121.16; 110.19; 17.08; 14.53; 12.73; 10.84.
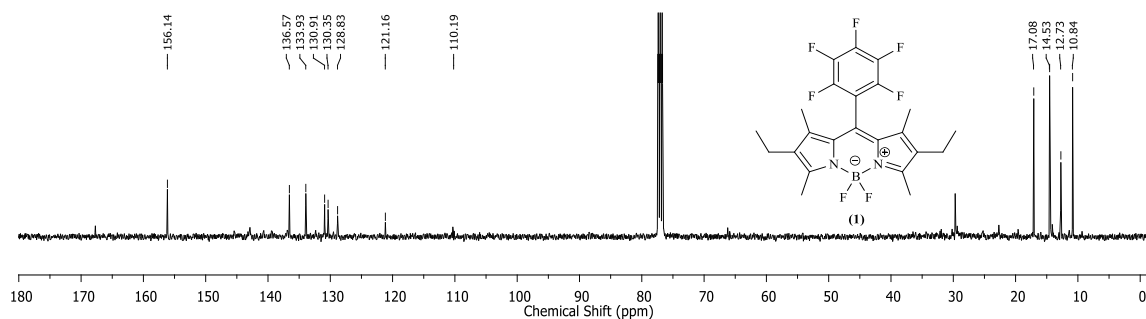
Figure 12 - ^{13}C NMR spectrum of BODIPY 1 (100 MHz, CDCl$_3$).

^{11}B NMR (128 MHz, CDCl$_3$) δ (ppm): 0.70(t, J =32.64 Hz).
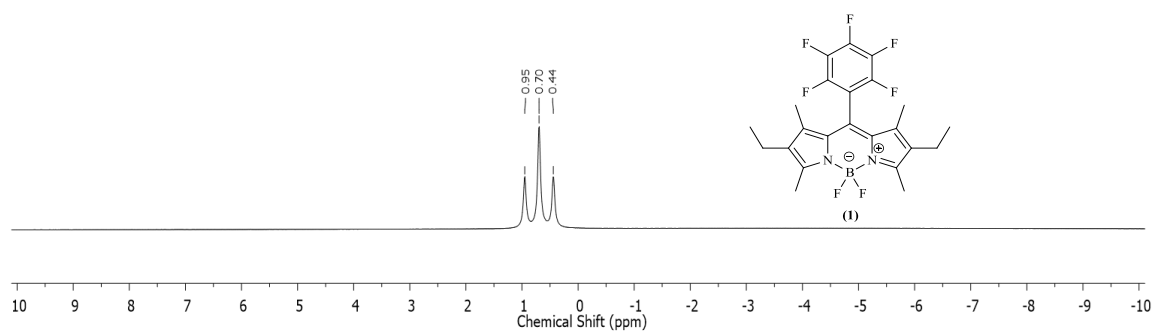
Figure 13 - ^{11}B NMR spectrum of BODIPY 1 (128 MHz, CDCl$_3$).

^{19}F NMR (376 MHz, CDCl$_3$) δ (ppm): -139.25(dd, J = 15.04 Hz, 7.14 Hz, 2F), -145.61 (dd, J = 32.71 Hz, 2F), -151.06 (t, J = 20.68 Hz, F), -159.82 (dt, J = 21.81, 6.40 Hz, 2F).
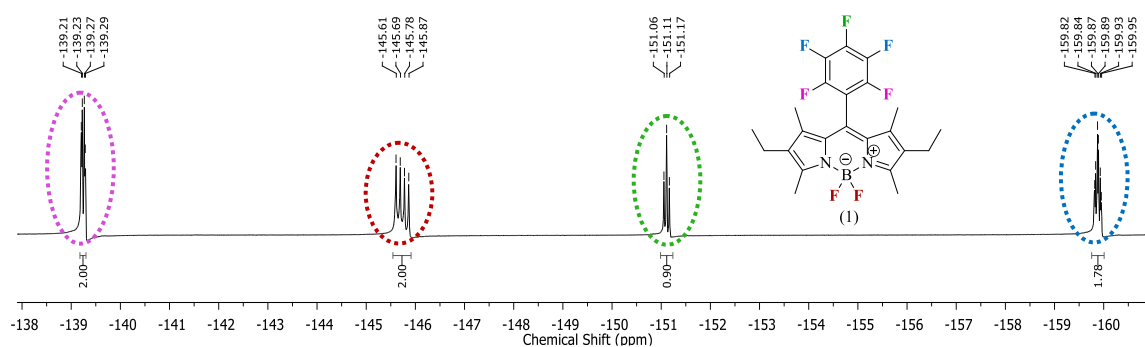
Figure 14 - ^{19}F NMR spectrum of BODIPY 1 (376, MHz, CDCl$_3$).

The mass spectrum, in figure 15, shows that the molecular ion was found at 471.30 m/z, as expected, and that the loss of a fluorine originated a peak at 451.30 m/z. Figure 16 depicts the absorption, excitation, and emission spectra of BODIPY 1, revealing a maximum of absorption at 526 nm and a maximum fluorescence at 549 nm.

MS m/z [M+H]$^+$ calculated for C$_{23}$H$_{22}$BF$_7$N$_2^+$: 471.23; Found: 471.30.
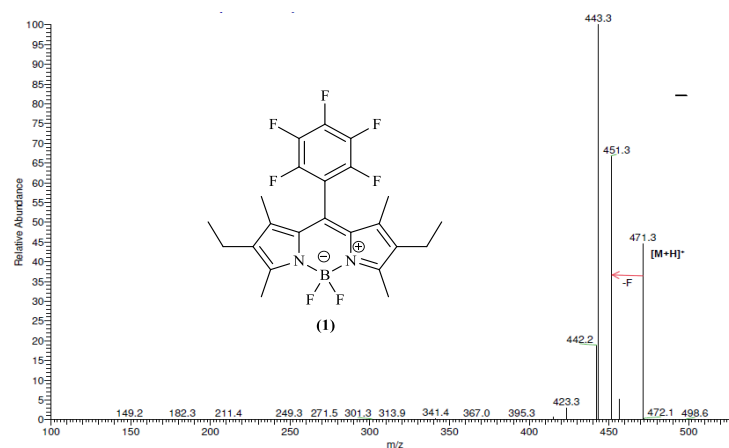
Figure 15 - Mass spectrum (positive mode) of BODIPY 1.
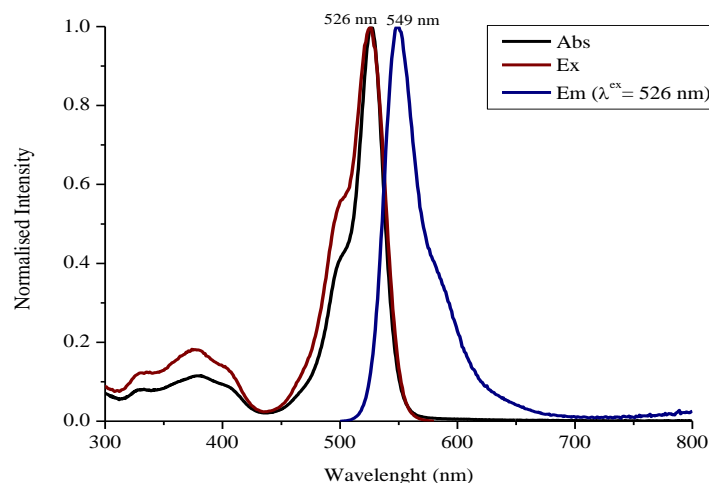
Figure 16 - Absorption, Excitation, and Emission Spectra from BODIPY 1, in hexane.

As a result of the characterisation data and its respective analysis, the structure of the BODIPY synthesized has been confirmed. The compound also exhibited interesting fluorescence properties, which might be useful for future PET/Fluorescence applications. This dual modality has already been explored in a BODIPY conjugated with an RGD peptide for assessment of integrin expression[76].

The characterization data for BODIPY 2 or 2,8-diethyl-5,5-difluoro-1,3,7,9-tetramethyl-10-phenyl-5H-dipyrrolo[1,2-c:2',1'-f][1,3,2]diazaborinin-4-ium-5-uide can be found from figure 17 to figure 22. This compound was synthesized with a yield of 43 %.

(2)
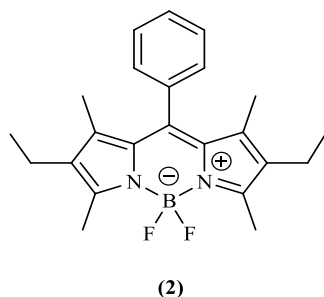
Figure 17 shows the proton NMR spectrum of BODIPY 2, in which the methyl groups and aromatic protons identified in the structure were also highlighted in the spectrum. Furthermore, as a result of the integration of the proton spectrum peaks, approximate values of the number of protons in the structure were obtained, which turned out to be very close to the anticipated values.

The carbon-13 spectrum, in figure 18, demonstrated the signals anticipated for the structure in analysis. Likewise, ^{11}B and ^{19}F NMR spectra, in figures 19 and 20, respectively, also supported the structure of the compound, showing all the necessary and required signals for each element.

^{1}H NMR (400 MHz, CDCl$_3$) δ (ppm): 7.71-7.70 (m, 2H), 7.54 -7.52 (m, 2H), 2.54 (s, 6H), 2.33 (q, J = 7.6 Hz, 4H), 1.51 (s, 6H), 1.02 (t, J = 7.6 Hz, 6H);
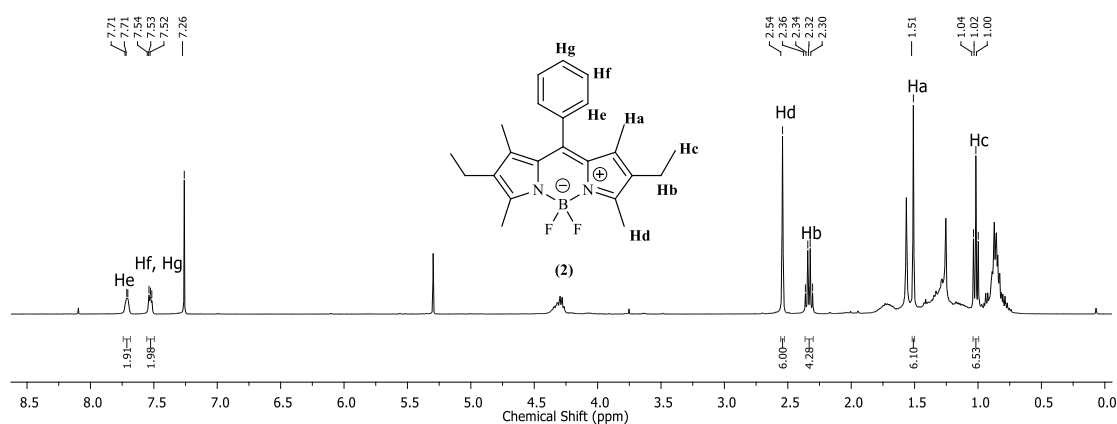
Figure 17 - ^{1}H NMR spectrum of BODIPY 2 (400 MHz, CDCl$_3$).

^{13}C NMR (100 MHz, CDCl$_3$) δ (ppm): 156.14, 136.57, 133.92, 130.91, 128.83, 26.61, 17.09, 14.54, 12.74, 10.85.

Figure 18 - ^{13}C NMR spectrum of BODIPY 2 (100 MHz, CDCl$_3$).

^{11}B NMR (128 MHz, CDCl3) δ (ppm):0.70 (t, *J* =32.64 Hz).
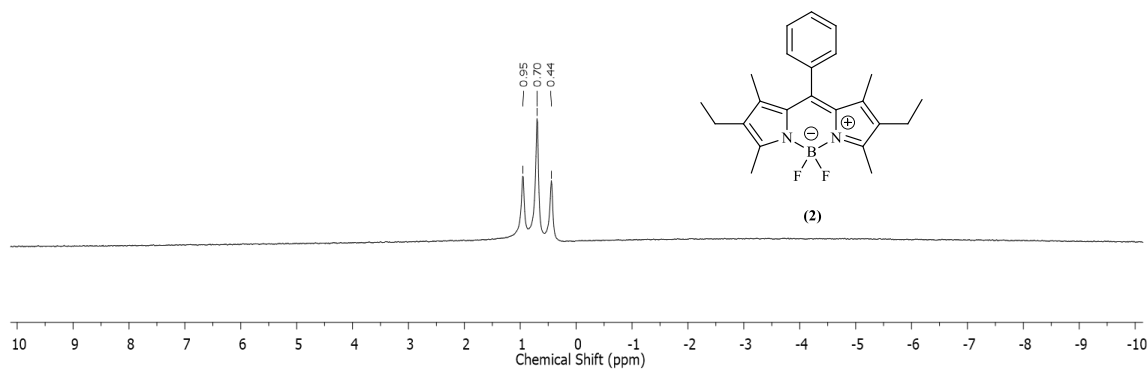
Figure 19 - ^{11}B NMR spectrum of BODIPY 2 (128 MHz, CDCl$_3$).

^{19}F NMR (376 MHz, CDCl$_3$) δ (ppm): -145.79 (dd, *J* =33.84 Hz, 2F).
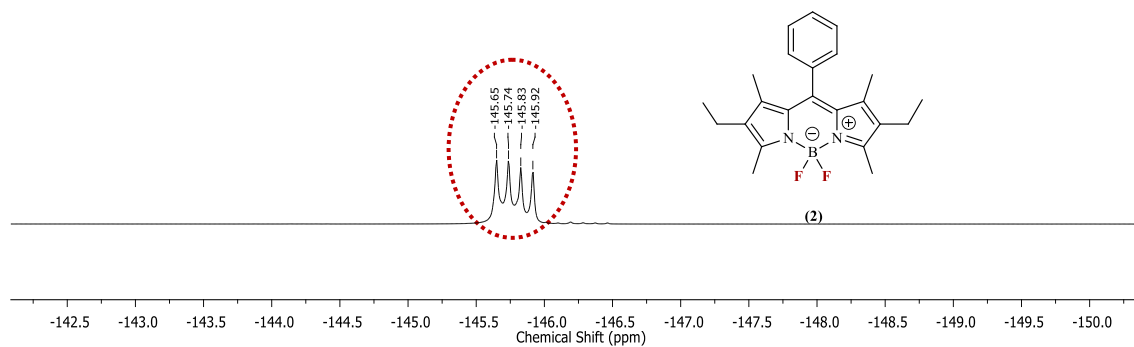
Figure 20 - ^{19}F NMR spectrum of BODIPY 2 (376, MHz, CDCl$_3$).

77

The mass spectrum in figure 21 revealed the molecular ion at 381.30 m/z as well as the loss of a methyl group, which resulted in the peak at 366.3 m/z. The absorption, excitation, and emission spectra of the compound depicted in figure 22 unveiled a maximum absorption at 533 nm and a maximum fluorescence at 542 nm.

MS m/z [M+H]$^+$ calculated for $C_{23}H_{28}BF_2N_2^+$: 381.28; **Found:** 381.30.

Figure 21 - Mass spectrum (positive mode) of BODIPY 2.
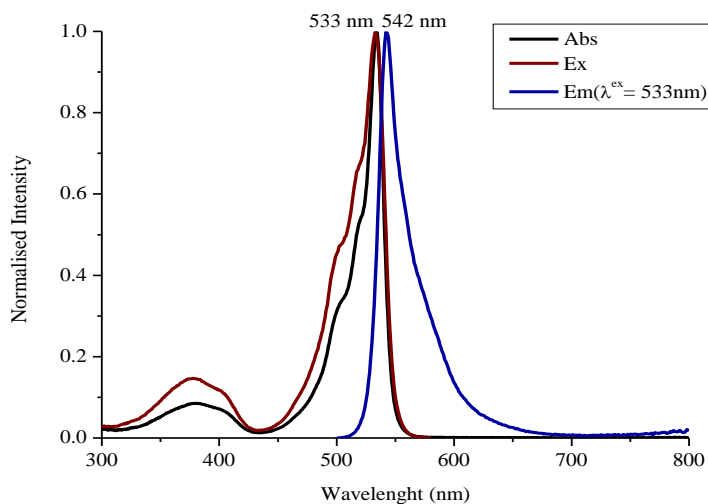
Figure 22 - Absorption, Excitation, and Emission Spectra from BODIPY 2, in hexane.

The first two BODIPYs can be considered as a first set of compounds synthetized, with the primary difference being the group attached to the *meso* position, i.e., pentafluorbenzaldehyde or benzaldehyde. Certain variations in the NMR spectra, as well as the values of the excitation wavelength and the emission peak maximum, were observed due to structural differences between BODIPY 2 and BODIPY 1. This second compound has also useful properties for PET/fluorescence dual imaging[76].

Regarding BODIPY 3 or 2,8-diethyl-1,3,7,9-tetramethyl-10-(perfluorophenyl)-5,5-diphenoxy-5H-dipyrrolo[1, 2-c:2',1'-f][1,3,2]diazaborinin-4-ium-5-uide, its characterization data is displayed in figures 23 to 28, and the yield of the synthesis was 69 %.

(3)
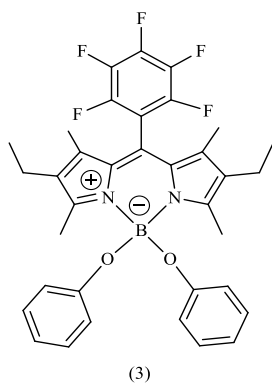
The ^{1}H NMR spectrum presented in figure 23 allowed the identification of methyl groups and aromatic protons of the third compound structure. The results of the integration of the spectrum peaks obtained revealed that the number of protons in each position of the structure synthetized was similar to the expected.

The ^{13}C, ^{11}B, and ^{19}F NMR spectra exhibited all the expected signals, as demonstrated by figures 24, 25, and 26.

^{1}H NMR (400 MHz, CDCl$_3$) δ (ppm): 7.06 (t, J = 7.2 Hz, 4H), 6.76 (t, J =7.2 Hz, 2H), 6.65 (d, J = 7.6 Hz, 4H), 2.51 (s, 6H), 2.20 (q, J = 7.6 Hz, 4H), 1.52 (s, 6H), 0.86 (t, J = 7.6 Hz, 6H).
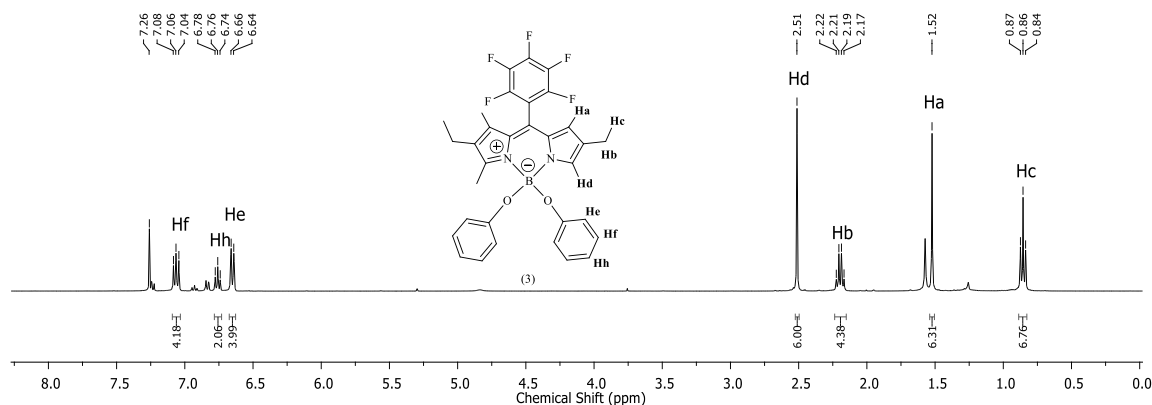
Figure 23 - ^{1}H NMR spectrum of BODIPY 3 (400 MHz, CDCl$_3$).

^{13}C NMR (100 MHz, CDCl$_3$) δ (ppm): 157.01, 156.48, 136.34, 134.50, 130.97, 129.10, 119.50, 118.40, 115.22, 17.08, 14.47, 13.05, 11.02.

Figure 24 - ^{13}C NMR spectrum of BODIPY 3 (100 MHz, CDCl$_3$).

^{11}B NMR (128 MHz, CDCl3) δ (ppm): 0.83 (s).
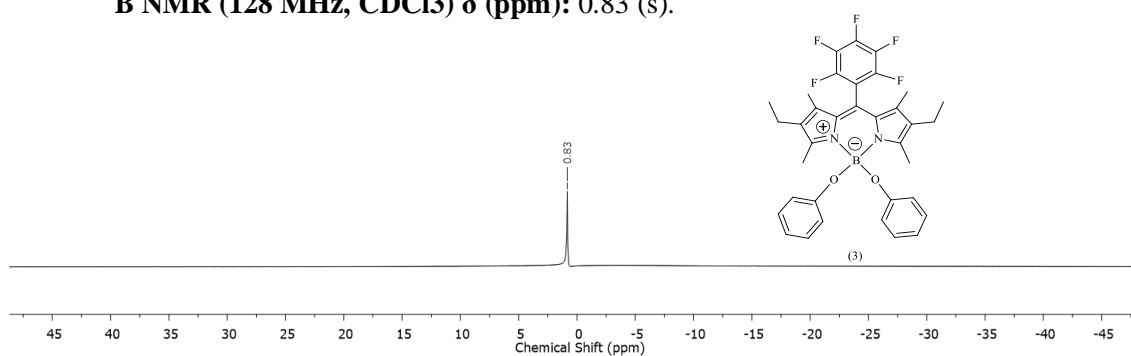
Figure 25 - ^{11}B NMR spectrum of BODIPY 3 (128 MHz, CDCl$_3$).

^{19}F NMR (376 MHz, CDCl$_3$) δ (ppm): -140.08 (dd, J= 22.56Hz,7.52Hz, 2F), -151.02 (t, J= 20.68Hz, 1F), -159.79 (dt, J= 21. 06Hz, 7.52Hz, 2F).
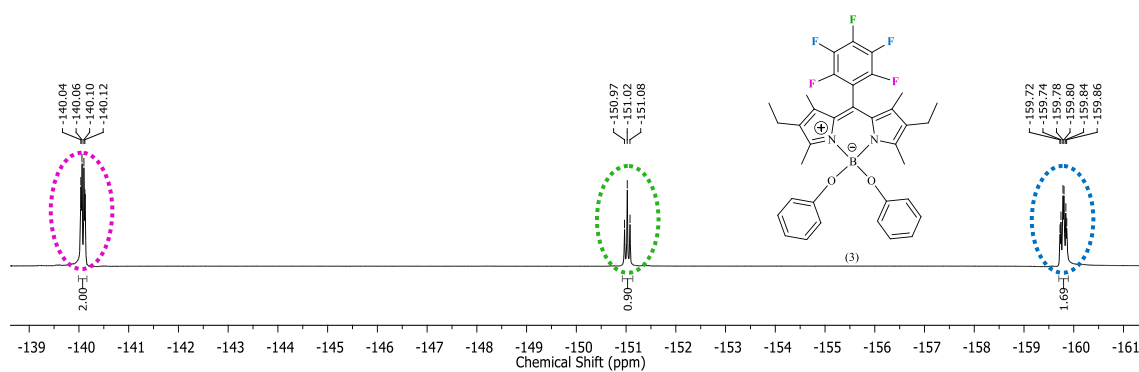
Figure 26 - ^{19}F NMR spectrum of BODIPY 3 (376, MHz, CDCl$_3$).

Figure 27 revealed the molecular ion at 641.20 m/z, which corresponds to the molecular ion plus the sodium ion[77]. The mass spectrum also revealed the loss of a phenoxy fragment, which resulted in the peak at 525.30 m/z.

The absorption, excitation, and emission spectra, in figure 28, unveiled that the compound has a maximum absorption at 545 nm and a maximum fluorescence emission at 563 nm.

MS m/z [M+H]$^+$ calculated for C$_{35}$H$_{33}$BF$_5$N$_2$O$_2$$^+$: 619.44; Found: 641.20.

Figure 27 - Mass spectrum (positive mode) of BODIPY 3.

Figure 28 - Absorption, Excitation, and Emission Spectra from BODIPY 3, in hexane.

Although this BODIPY exhibited fluorescence, the peak absorbance and fluorescence peak values were slightly different when compared to the other characterized compounds. However, these differences were not significant and can be explained by the fact that functionalization with phenolic groups can cause changes in the wavelength maxima[34,35].

BODIPY 4 or 2,8-diethyl-1,3,7,9-tetramethyl-5,5-diphenoxy-10-phenyl-5H-dipyrrolo[1,2-c:2',1'-f][1,3,2]diazaborinin-4-ium-5-uide was obtained with a yield of 59 %, and its characterization spectra is displayed from figure 29 to 33.

(4)

The ^{1}H NMR spectrum in figure 29 corroborated BODIPY 4 structure since it was possible to distinguish the methyl groups and aromatic protons, and the spectrum integration confirmed the number of protons in each position.

The majority of the predicted signals could be identified in the carbon spectrum in figure 30, as well as in the boron spectrum in figure 31. The elemental structure of BODIPY 4 was supported by all spectra obtained.

^{1}H NMR (400 MHz, CDCl$_3$) δ (ppm): 7.50 – 7.48 (m, 3H), 7.24 - 7.22 (m, 2H), 7.08 (t, J = 7.6 Hz, 4H), 6.77 (t, J = 7.2 Hz, 2H), 6.63 (d, J = 7.6 Hz, 4H), 2.52 (s, 6H), 2.19 (q, J = 7.6 Hz, 4H), 1.26 (s, 6H), 0.85 (t, J = 7.6 Hz, 6H).

Figure 29 - ^{1}H NMR spectrum of BODIPY 4 (400 MHz, CDCl$_3$).

^{13}C NMR (100 MHz, CDCl3) δ (ppm):156.90, 154.48, 138.10, 136.00, 133.29, 131.38, 128.92, 128.66, 128.39, 119.34, 118.80, 17.05, 14.52, 12.84, 11.73.
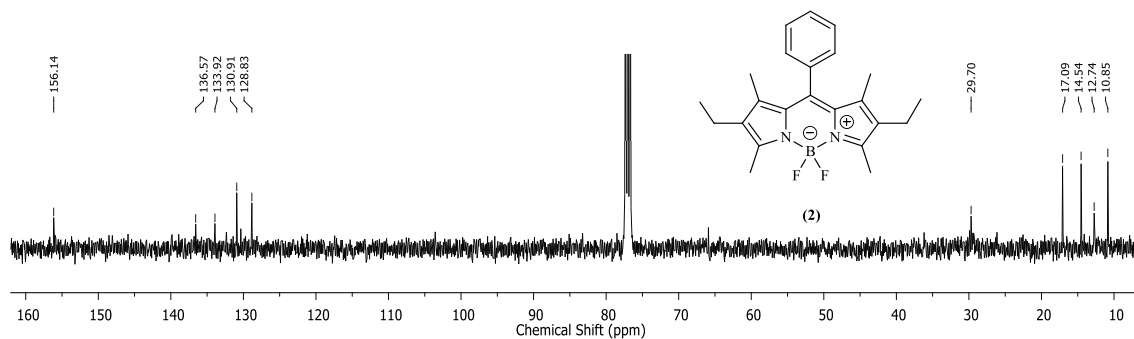

Figure 30 - ^{13}C NMR spectrum of BODIPY 4 (100 MHz, CDCl$_3$).

^{11}B NMR (128 MHz, CDCl3) δ (ppm): 0.91 (s).

Figure 31 - ^{11}B NMR spectrum of BODIPY 4 (128 MHz, CDCl$_3$).

The boron spectra of BODIPYs 3 and 4 exhibited a singlet signal, but the ^{11}B NMR spectra of BODIPYs 1 and 2 revealed triplets. Such variations are due to the impact of the spin of the atoms connected to the boron atom. While phenolic BODIPYs have oxygen atoms connected to the boron, BODIPYs 1 and 2 have two fluorine atoms coupled with the boron core, and the impact of the fluorine spin of ½ gives rise to the triplets seen in figures 13 and 19.

In relation to the mass spectrum, the molecular ion was found at 551.30 m/z as shown in figure 32. Since the result should be about 529.49 m/z, the difference is justified by the sodium ion presence, which is expected in these compounds taking into account the synthesis procedures and isolation[77].

The absorption, excitation, and emission spectra depicted in figure 33 revealed that the structure has an absorption maximum at 528 nm and a maximum fluorescence emission at 544 nm. These wavelengths are slightly different from the similar structure, BODIPY 3, being closer to the values obtained for BODIPY 2. Probably the group associated with the *meso* position has a greater influence on the absorbance and fluorescence maxima shifts than the groups associated with the boron atom.

MS m/z [M+H]$^+$ calculated for C$_{35}$H$_{38}$BN$_2$O$_2$$^+$: 529.49; **Found**: 551.30.
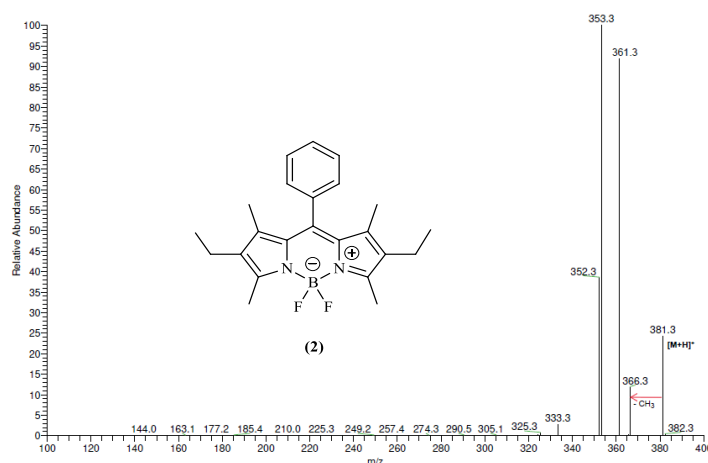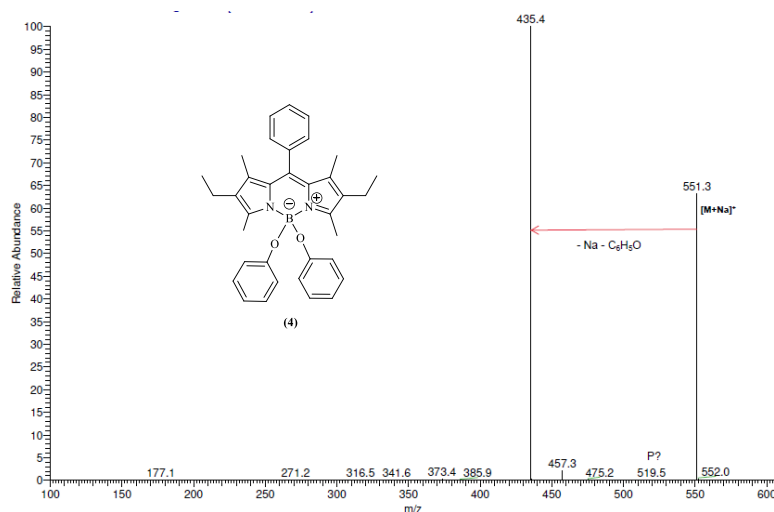

Figure 32 - Mass spectrum (positive mode) of BODIPY 4.
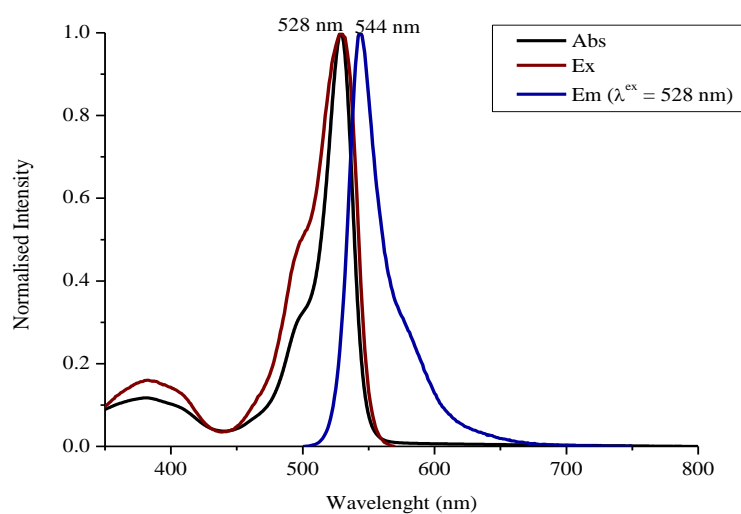
Figure 33 - Absorption, Excitation, and Emission Spectra from BODIPY 4, in hexane.

BODIPY 4 also exhibited considerable fluorescence, making it also a candidate for PET/Fluorescence imaging. Nevertheless, the fact that BODIPYs 3 to 4 contain phenol groups linked with the boron atom is the most important feature, since the exchange of phenol groups by ^{18}F can occur faster than the radiolabelling of BODIPYs 1 and 2. The first set of synthesized BODIPYs may have the isotopic exchange impaired due to the highly stable B-F bond, something that has been previously reported in the literature[23,69].

BODIPY 5 or 2',8'-diethyl-1',3',7',9'-tetramethyl-10'-(perfluorophenyl) spiro[benzo[d][1,3,2]dioxaborole-2,5'-dipyrrolo[1,2-c:2',1'-f][1,3,2]diazaborinin]-4'-ium-12-uide was synthesized with a 64% yield. Figures 34 to 39 provide the characterisation data for the fifth compound.

(5)
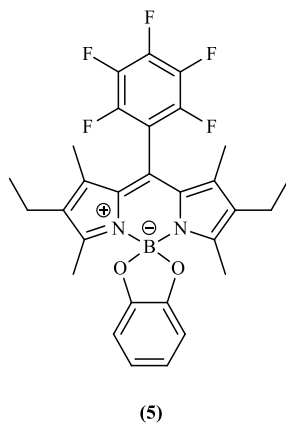
The ¹H NMR spectrum in figure 34 shows that the methyl groups and the aromatic protons were properly identified, and the values obtained from the integration confirmed the number of protons contained in the compound structure.

The NMR spectra of carbon, boron, and fluorine, figures 35, 36, and 37, all revealed the expected and anticipated signals for each element. Moreover, as predicted, due to the atoms associated with the boron atom in BODIPY 5, the spectrum of ¹¹B in figure 36 revealed a singlet.

¹H NMR (400 MHz, CDCl₃) δ (ppm): 6.76 (s, 4H), 2.27 (q, *J* = 7.6 Hz, 4H), 2.05 (s, 6H), 1.51 (s, 6H), 0.96 (t, *J* = 7.6 Hz, 6H).
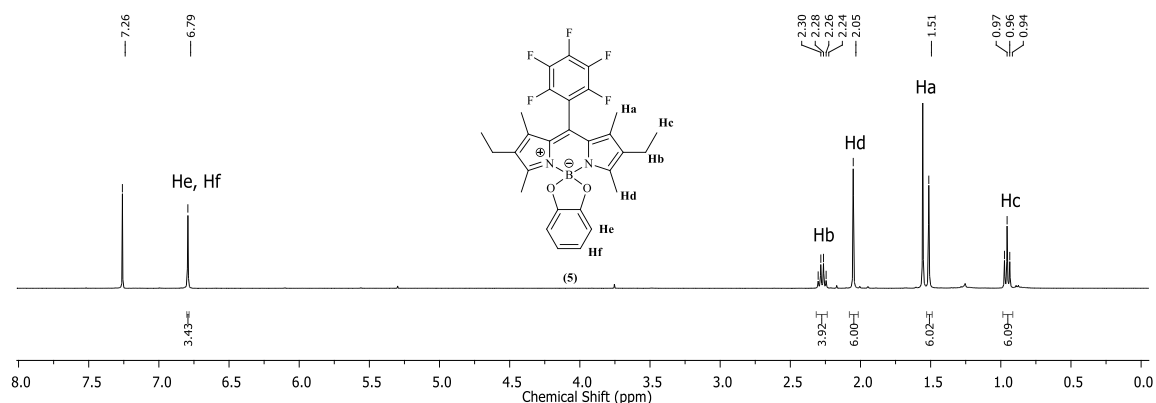
Figure 34 - ¹H NMR spectrum of BODIPY 5 (400 MHz, CDCl₃).

^{13}C NMR (100 MHz, CDCl$_3$) δ (ppm): 157.99, 151.96, 137.30, 134.57, 131.05, 119.71, 108.84, 17.09, 14.58, 12.92, 11.03.
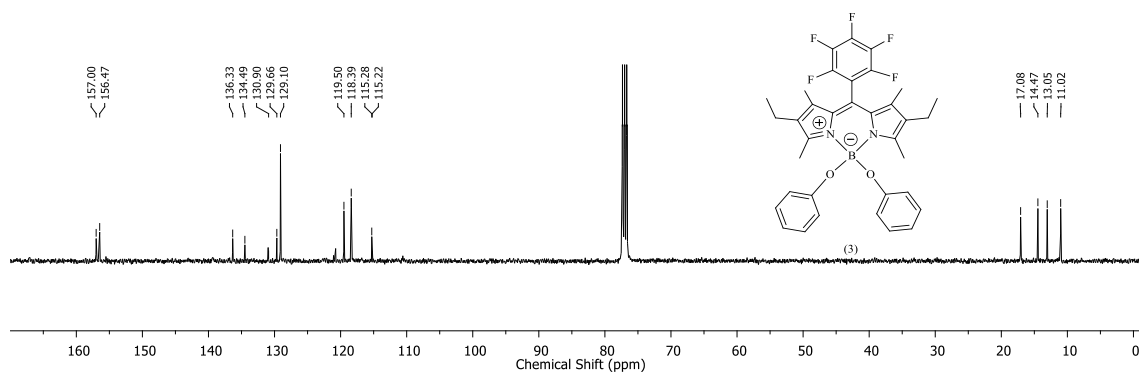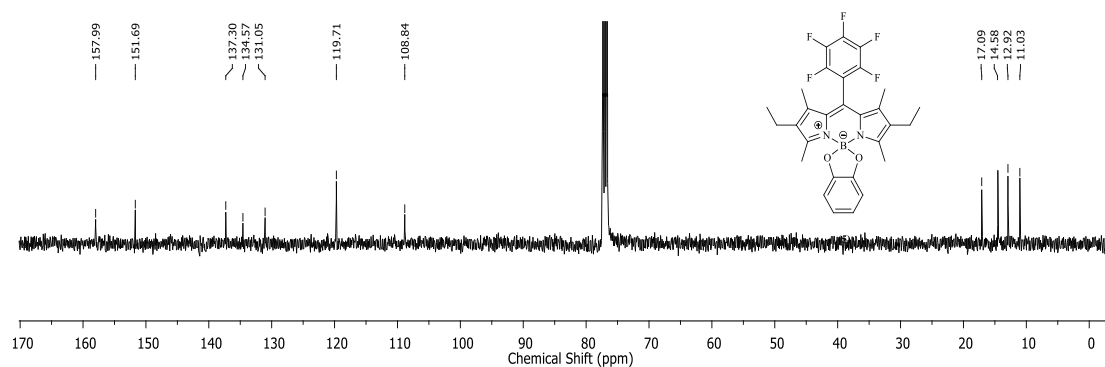

Figure 35 - ^{13}C NMR spectrum of BODIPY 5 (100 MHz, CDCl$_3$).

^{11}B NMR (128 MHz, CDCl3) δ (ppm): 7.15 (s).
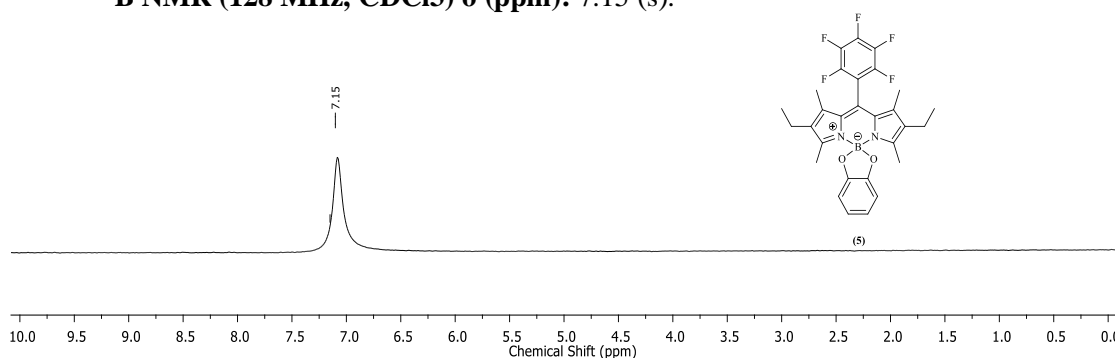
Figure 36 - ^{11}B NMR spectrum of BODIPY 5 (128 MHz, CDCl$_3$).

^{19}F NMR (376 MHz, CDCl$_3$) δ (ppm): -139.16 (dd, J = 22.56 Hz, 7.52 Hz, 2F), -151.09 (t, J = 22.56 Hz, 1F), -159.83 (dt, J = 22.56 Hz, 7.52Hz, 2F).
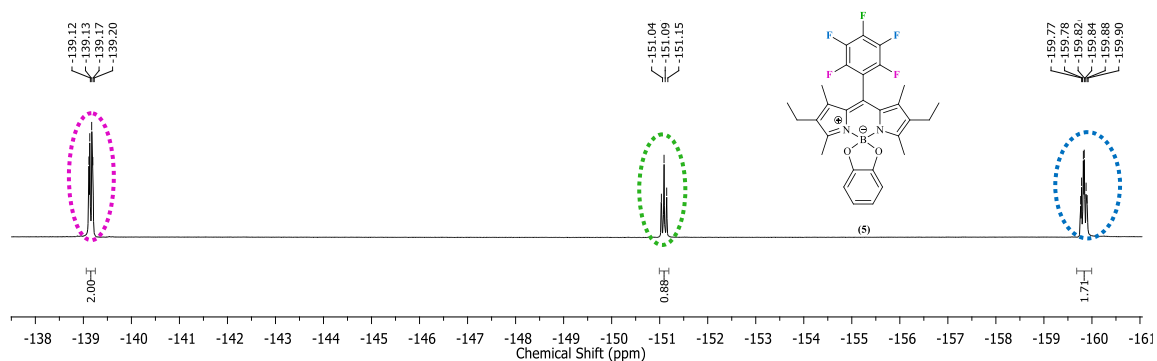
Figure 37 - ^{19}F NMR spectrum of BODIPY 5 (376, MHz, CDCl$_3$).

86

The molecular ion was identified at 541.30 m/z in figure 38; and the absorption, excitation, and emission spectra in figure 39 revealed that the compound has an absorption maximum at 546 nm and very weak fluorescence emission. This weak fluorescence was most likely quenched by the catechol group, as has already happened with other BODIPYs with the catechol group covalently linked to the boron atom[78,79]. Thus, the hybrid PET/fluorescence image is not a feasible application for this BODIPY.

MS m/z [M+H]$^+$ calculated for C$_{29}$H$_{27}$BF$_5$N$_2$O$_2$$^+$: 541.33; **Found:** 541.30.
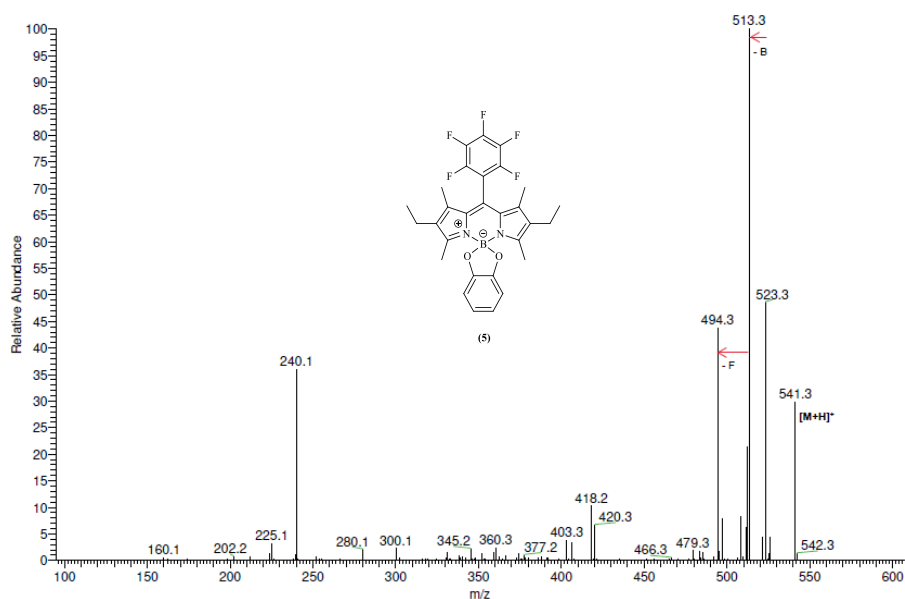
Figure 38 - Mass spectrum (positive mode) of BODIPY 5.
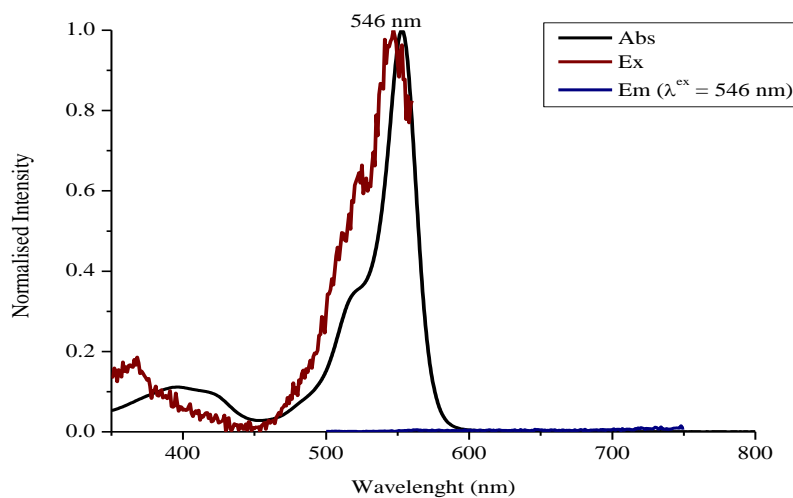
Figure 39 - Absorption, Excitation, and Emission Spectra from BODIPY 5, in hexane.

The characterization results for BODIPY 6 or 2',8'-diethyl-1',3',7',9'-tetramethyl-10'-phenylspiro[benzo[d][1,3,2]dioxaborole-2,5'-dipyrrolo[1,2-c:2',1'-f][1,3,2]diazaborinin]-4'-i   um-12-uide are summarized from figure 40 to 44. The synthesis yield for this compound was approximately 57 %.
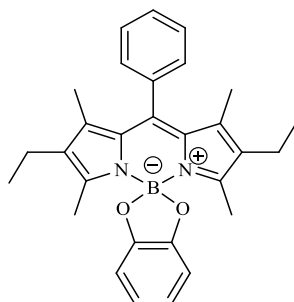
(6)

The methyl groups and the aromatic protons could be identified in the ^{1}H NMR spectrum of figure 40, and the values obtained from the integration of the peaks also confirmed the number of protons in the compound.

The other NMR spectra obtained, such as ^{13}C and [11]B, represented in figures 41 and 42, also corroborated the structure of BODIPY 6 by showing all the expected and predicted signals for each element.

^{1}H NMR (400 MHz, CDCl$_3$) δ (ppm): 7.49-7.47 (m, 3H), 7.31- 7.29 (m, 2H), 6.78 (s, 4H), 2.23 (q, $J = 7.6$ Hz, 4H), 2.24 (s, 6H), 1.27 (s, 6H), 0.91 (t, $J = 7.6$ Hz, 6H).
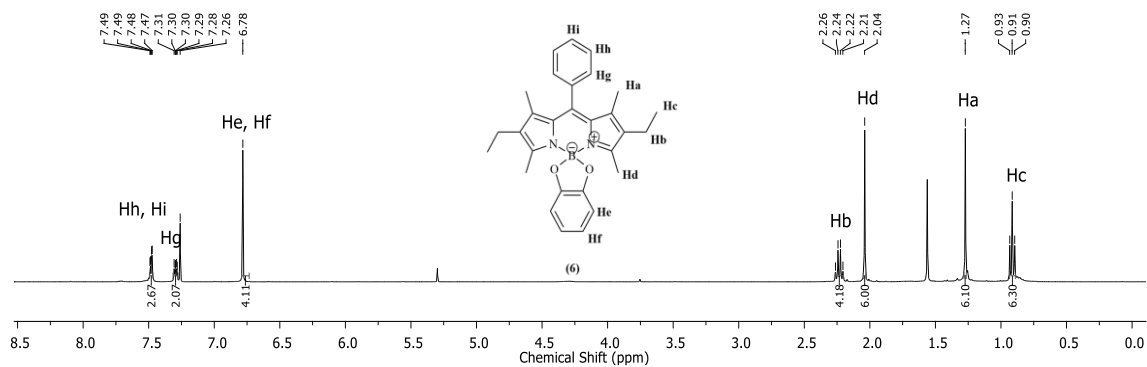
Figure 40 - ^{1}H NMR spectrum of BODIPY 6 (400 MHz, CDCl$_3$).

¹³C NMR (100 MHz, CDCl₃) δ (ppm): 155.60, 155.41, 151.99, 140.04, 139.18, 136.03, 133.40, 131.49, 129.06, 128.73, 128.33, 128.26, 119.39, 108.74, 17.07, 14.60, 12.69, 11.81.
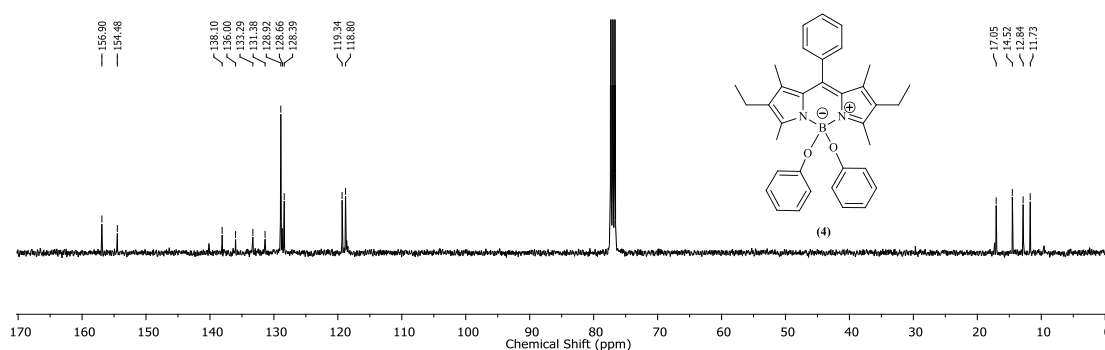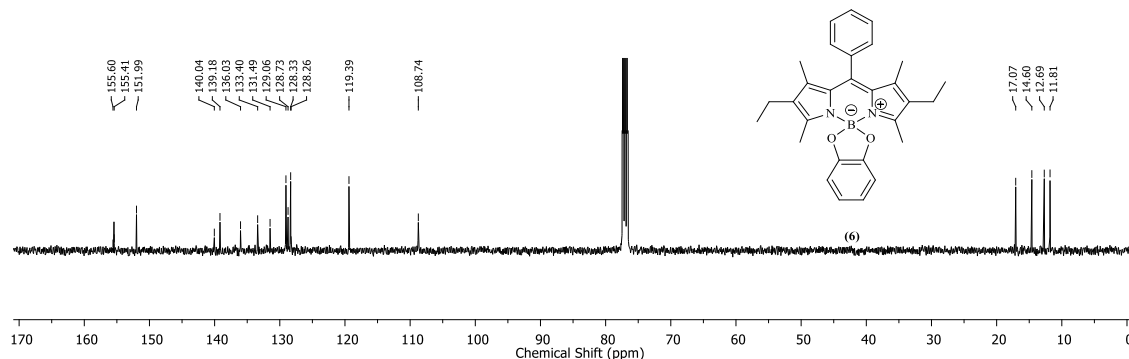

Figure 41 - ¹³C NMR spectrum of BODIPY 6 (100 MHz, CDCl₃).

¹¹B NMR (128 MHz, CDCl3) δ (ppm): 7.14 (s).
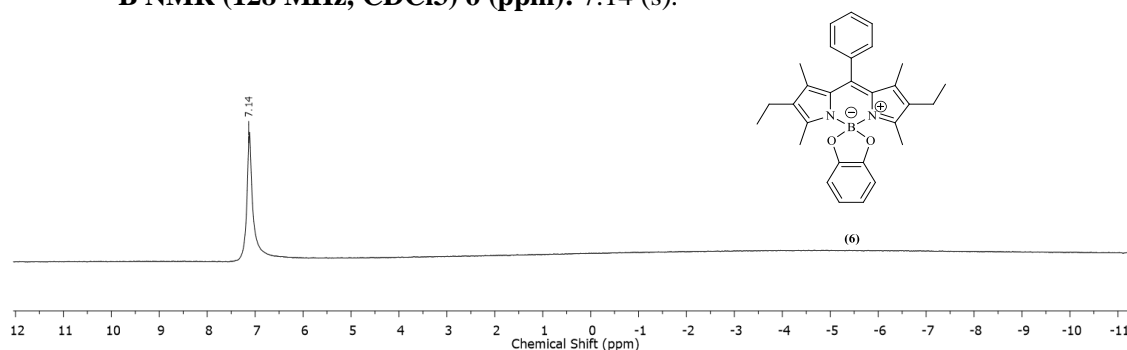
Figure 42 - ¹¹B NMR spectrum of BODIPY 6 (128 MHz, CDCl₃).

The molecular ion was identified at 551.40 m/z as expected. In addition, the considerable loss of two fragments, a boron fragment for the peak of 423.4 m/z and a fluorine fragment for the peak of 404.3 m/z, can be seen in figure 43.

The absorption, excitation, and emission spectra in figure 44 revealed that BODIPY 6 has an absorption maximum at 531 nm but has very weak fluorescence. Given the fact that the last two structures synthetized, BODIPY 5 and 6, showed weak fluorescence, and since the main similarity between the two structures is the catechol group linked to the boron atom, this group has the capacity to quench the fluorescence of both compounds[78,79].

This particularity of fluorescence quenching was explained in an article, in which BODIPYs with the catechol linked to the boron atom tended to undergo a rapid deactivation of the excitation state. A photoinduced electron transfer process must take place from the catechol to an orbital in the BODIPY to generate an intermediate state. This intermediate state has such a short lifetime that it quickly returns to the ground state, quenching the fluorescence of the compound[78].

**MS m/z [M+H]$^{+}$ calculated for C$_{29}$H$_{32}$BN$_2$O$_2^{+}$:** 451.38; **Found:**451.40.
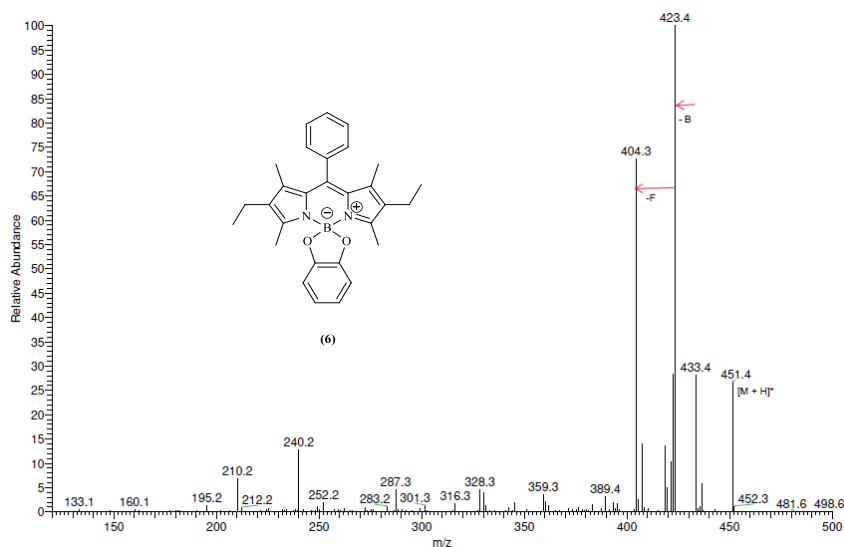
Figure 43 - Mass spectrum (positive mode) of BODIPY 6.
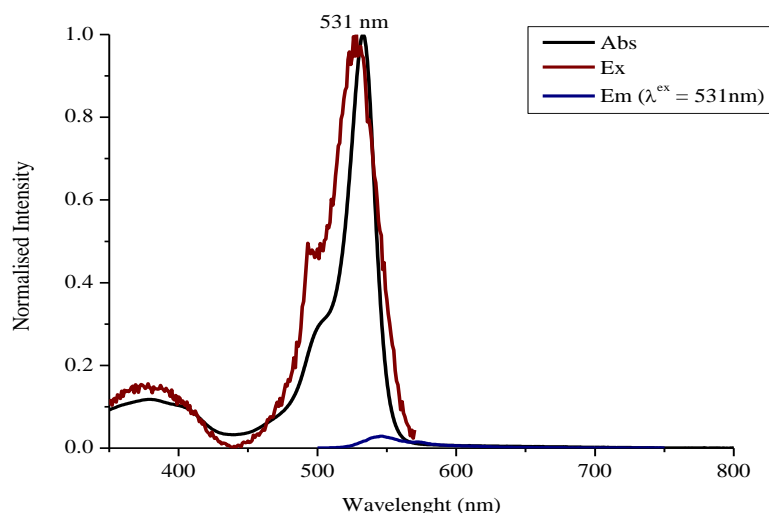
Figure 44 - Absorption, Excitation, and Emission Spectra from BODIPY 6, in hexane.

Six different BODIPYs were synthetised and characterized successfully. Two BODIPYs (1 and 2) with Fluorine-19 bound to the boron centre, two other BODIPYs (3 and 4) with Phenol groups, and the last ones (BODIPYs 5 and 6) with a catechol group bounded to the boron atom. NMR, Mass, Absorbance, and Fluorescence spectrums were used to corroborate the compounds and to perform the study of their characteristics. Overall, the ^{1}H, ^{13}C, ^{11}B, and ^{19}F spectrums all confirmed each element presence in each BODIPY, the mass spectrums showed the molecular ion, case of BODIPY (1, 2, 5, and 6), or at least the molecular ion with contamination with sodium, BODIPYs (3 and 4).

In general, all BODIPYs 1 to 4 revealed fluorescence in their spectra, contrasting with BODIPYs 5 and 6 spectra which revealed that these compounds have a very weak fluorescence emission, due to the group bounded to the boron atom.

All the developed BODIPYs have interesting characteristics for carrying out the radiolabelling procedure, and in our view the use of cyclic alkoxides, such as catechol derivatives, adds an additional beneficial feature linked to ring tension on the dialkoxide, which can speed up the procedure. Some of the radiolabelling approaches that have already been explored and used in BODIPYs, described in the literature were outlined in the third subchapter of the introduction and are also detailed in scheme 10[23,69].

4.2 Structural Motifs

Taking into consideration that the boron atom will be the centre where the exchange of alkoxy groups or fluorine atoms for ^{18}F will occur, it is important to evaluate some structural reasons that can help justify the use of cyclic alkoxides as a mean of speeding up the radiolabelling. An assessment of the N-B-N angles and the boron atom planarity regarding the plane of the pyrrole rings can be used to anticipate the ease with which the radiolabelling can occur with different speeds in different structures.
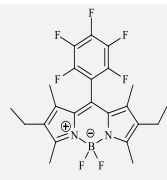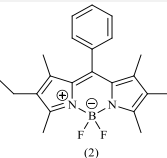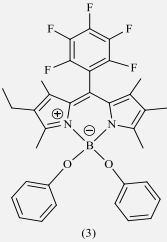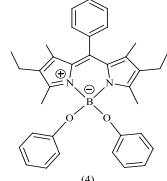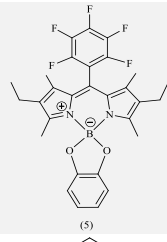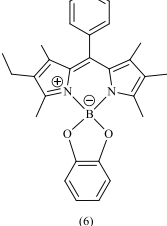
Table 4 displays the N-B-N angles found for each structure, revealing that similar structures have angles with relatively close values. The addition of alkoxy groups to the structure of BODIPYs induced a spatial rearrangement of the compounds, triggering changes in the amplitudes of the N-B-N angles. Phenoxy groups incremented the N-B-N angles (in the case of BODIPYs 3 and 4), while catechol groups reduced those angles (in the case of BODIPY 5 and 6). In both situations the alkoxy groups added an extra angle strain to the N-B-N angle of the BODIPYs with fluorine atoms bounded to the boron.

The variations in the planarities of the different compounds can help to determine how easily the atom can be the target of the exchange reaction of fluorines, phenols, or catechols for ^{18}F. In BODIPY 1 the boron was almost coplanar to the pyrrole rings, with a boron deviation from the pyrroles plane of just 0.059 Å, whilst in BODIPY 2 the deviation was 0.310 Å. This difference in the planarity of BODIPYs 1 and 2 may be related to the substituents in the *meso* position, i.e., the steric effects of the meso-phenyls. In BODIPY 3 and 4, the boron out-of-plane deviation was 0.036 Å and 0.063 Å, respectively; And in BODIPYs 5 and 6 was 0.719 Å and 0.612 Å. These deviations from the previous values for BODIPYs 1 and 2 might be attributed to the structural rearrangement required due to the volume of the substituent groups. It should be noted, however, that the deviations in BODIPYs with catechol groups bounded to the boron atom were higher, which may indicate a strained region after the catechol insertion.

The C-C-O angles were also considered, either in the phenol and catechol groups alone, or in the synthesized compounds, also described in table 4 and schematized in figure 45. The angle was 121.61 degrees in BODIPY 3 and 121.73 degrees in BODIPY 4, but 120.74 degrees in

phenol alone. Thus, it turns out that there is a small difference in angles after the phenol insertion, a small increase in its amplitude, which may be related to the volume of the groups inserted and the respective steric effect. The C-C-O angle in BODIPY 5 was 112.37 degrees and in BODIPY 6 was 112.35 degrees, however, this angle in catechol alone is 120.09 degrees. The angle amplitude decreased in BODIPYs 5 and 6; the additional strain in the oxygen area is another indication that the strained zone in these final compounds may contribute to a faster ^{18}F isotopic exchange reaction.

Table 4 - N-B-N angles obtained from MM2 molecular mechanics calculations.

Structure	Angle N-B-N (°)	Out of Plane Deviation (Å)	Angle C-C-O (°)
(1)	107.27	0.059	-
(2)	106.77	0.310	-
(3)	109.50	0.036	121.61
(4)	108.84	0.063	121.73
(5)	106.47	0.719	112.37
(6)	105.15	0.612	112.35
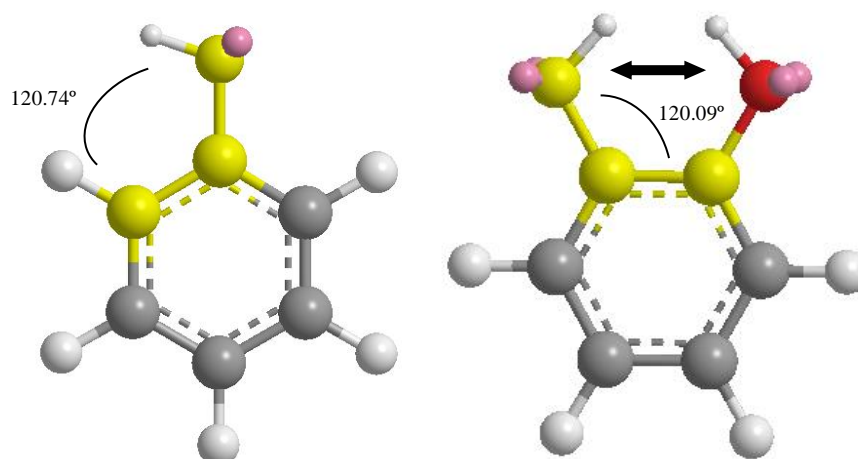
Figure 45 – Angle C-C-O analysed alone and in BODIPYs.

Probably, due to the strained region present in the BODIPYs 5 and 6 with the introduction of the catechol group, the radiolabelling procedure could be faster in those compounds than the ones with the phenol group, BODIPYs 3 and 4. The calculations performed in this subchapter do not prove with absolute certainty that the radiolabelling process will be faster in BODIPYs 5 and 6 than in those with fluorine or phenol associated with the boron atom, but they give an indication of the structural factors that are most likely to affect the kinetics of the reaction.

4.3 *In Vitro* Studies

Finding the most biocompatible BODIPYs is a critical step. As the compounds will be explored as radiotracers in the future, it is crucial to determine whether different concentrations of the different BODIPYs are cytotoxic.

MTT, SRB, Trypan Blue and Cellular Uptake assays were performed using two cancer cell lines from distinct types of NSCLC, (ATCC CCL-185) (*human alveolar basal epithelial adenocarcinoma cells*) and NCI-H1299 (ATCC CRL-5803) (*human non-small cell lung carcinoma cells*).

The Trypan Blue assay was employed for cell viability evaluation before starting all the other assays, and all the experiences had a viability superior to 90 %.

4.3.1 Metabolic Activity

The MTT test was used to evaluate cytotoxicity, and the effects of different concentrations of BODIPYs 1 to 6 on the metabolic activity of A549 and H1299 cell lines was assessed after 24, 48, and 72 hours of incubation.

(1)
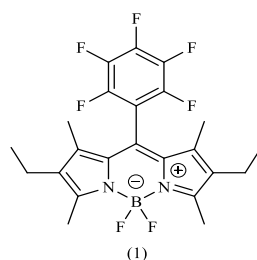
The experimental MTT results for BODIPY 1 for both cell lines are shown in figure 46. In graph A, only concentrations of 100 μM, 50 μM, and 25 μM seemed to lower the metabolic activity of the A549 cell line in a statistically meaningful way to 43.64 % (p<0.001), 52.27 % (p<0.001), and 73.11 % (p<0.001), respectively. The data indicate that 24 hours after the incubation with the compound, the cell response is concentration-dependent. BODIPY 1 caused statistically important impacts on A549 metabolic activity in the 48-hour test (graph B), with a mean of 64.42 % at 100 μM (p<0.01) and 89.22 % at 50 μM (p<0.01). In graph C, the lowest concentration had a statistically important impact, with an average metabolic activity of 112.2 % (p<0.01); also, cells treated with 100 μM had an average metabolic activity of 64.00 % (p<0.001), and 85.42 % (p<0.05) for 50 μM. The effect of concentration-dependent response is not lasting, in the large majority, cells recover from the effects of higher concentrations.

Two concentrations exhibited statistically relevant effects on the H1299 cell line, following a 24-hour incubation with BODIPY 1. Graph D shows a mean of 55.89 % (p<0.001) for 100 μM and 116.85 % (p<0.05) for 5 μM. In graph E, higher concentrations, such as 25 μM, 50 μM, and 100 μM, exhibited statistically relevant p-values, with average metabolic activity of 95.36 % (p<0.001), 78.96 % (p<0.001), and 47.06 % (p<0.001), respectively. After 72 hours, corresponding to graph F, 100 μM triggered a reduction of metabolic activity to 64.44 % (p<0.001), whereas 5 μM, 10 μM, and 25 μM tended to increase metabolic activity in a statistically noteworthy manner, to 123.38 % (p<0.05), 121.03 % (p<0.05), and 122.93 % (p<0.01), respectively. In general, the concentration-dependent response for the H1299 line only occurred in the 48-hour assay, with cells recovering and even increasing their metabolic activity in the 72-hour assay. It appears that the vast majority of concentrations tested caused greater activation of metabolic activity after a longer incubation period.

Considering the previous data, concentrations of up to 25 μM of BODIPY 1 were relatively safe for both cell lines. The concentration of 100 μM was the only one which had a metabolic activity below 70 %. The effects of lower dosages resulted in some cases in a small increase in metabolic activity, being more evident only for longer incubation periods. Overall, this drug may be an interesting candidate for diagnosis at lower concentrations.

A549

(A)

(B)

(C)

H1299

(D)

(E)

(F)

Figure 46 - MTT results represented in the form of average and CI, for BODIPY 1 for the A549 cell line (A) 24h, (B) 48h and (C) 72h, and for the H1299 cell line (D) 24h, (E) 48h and (F) 72h, respectively. Due to the normalization of the data previously done, the metabolic activity values obtained for the controls are comparable to 100 % of the metabolic activity; as a result, the controls are represented by the dashed line. Significances are represented by * for $p<0.05$, ** for values of $p<0.01$ and *** for $p<0.001$.

(2)

Considering the effects of BODIPY 2 in cells metabolic activity presented in figure 47, the negative impacts were particularly evident in the A549 cell line. Graph G shows that the cellular metabolic activities measured 24 hours after incubation with 1 μM, 25 μM, 50 μM and 100 μM had means of 93.58 % ($p<0.05$), 77.95 % ($p<0.05$), 68.41 % ($p<0.001$) and 61.35 % ($p<0.001$), respectively. In graph H, the 48-hour assay, 25 μM, 50 μM, and 100 μM continued to play a statistically important role in decreasing metabolic activity to 77.08 % ($p<0.01$), 75.61 % ($p<0.01$), and 68.33 % ($p<0.001$). In the longer experiment, all doses had a statistically meaningful effect on decreasing metabolic activity, graph I. Concentrations of 1 μM, 5 μM, and 10 μM reduced metabolic activity to 85.04 %, 87.85 %, and 83.30 %, respectively (all with

p<0.01); whilst 25 µM, 50 µM, and 100 µM reduced metabolic activity to 76.12 %, 78.54 %, and 76.24 %, respectively (all with p<0.001). The negative effects of BODIPY 2 on the metabolic activity of the A549 cell line appear to grow with time, indicating that the compound is more harmful after longer incubation periods.

After 24 hours of incubation, concentrations of 50 µM and 100 µM reduced H1299 metabolic activity in a statistically relevant way to 80.62 % (p<0.01) and 74.68 % (p<0.001), respectively (graph J). In the 48-hour assay, all concentrations above 10 µM had a statistically relevant influence on metabolic activity; cells treated with 10 µM had a mean of 86.05 % (p<0.05), whereas those treated with 25 µM had an average metabolic activity of 81.74 % (p<0.001), 50 µM led to an average of 76.55 % (p<0.001) and finally cells treated with 100 µM had a mean metabolic activity of 79.59 % (p<0.001). After 72 hours of incubation with the compound, concentrations of 25 µM and 50 µM caused a statistically relevant reduction in H1299 metabolic activity to 87.65 % (p<0.01) and 92.69 % (p<0.01), respectively. On the whole, higher concentrations had more pronounced effects in decreasing the metabolic activity of H1299 in the three incubation periods, additionally, the 10 µM concentration appeared to have had transient toxicity in the 48-hour assay.

Figure 47 - MTT results represented in the form of average and CI, for BODIPY 2 for the A549 cell line (G) 24h, (H) 48h and (I) 72h, and for H1299 cell line (J) 24h, (K) 48h and (L) 72h, respectively. Due to the normalization of the data previously done, the metabolic activity values obtained for the controls are comparable to 100 % of the metabolic activity; as a result, the controls are represented by the dashed line. Significances are represented by * for p<0.05, ** for values of p<0.01 and *** for p<0.001.

BODIPY 2 had more negative impacts on the A549 cell line than BODIPY 1. The more pronounced effects associated to this BODIPY were more noticeable at concentrations ranging from 25 µM to 100 µM. Considering the aforementioned findings, this BODIPY does not appear to be safe for diagnostic usage, since even low concentrations appeared to have had some cytotoxicity.

(3)
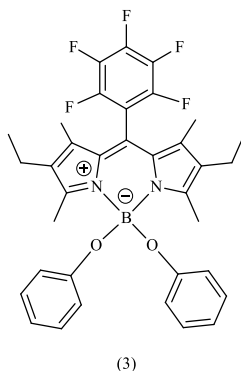
Figure 48 shows the MTT results obtained for the three incubation periods with BODIPY 3. For the 24-hour assay with the A549 cell line, graph M, the concentration of 100 µM was the only one that caused a statistically significant decrease in metabolic activity to 85.89 % (p<0.05). After 48 hours of incubation with the compound, which corresponds to graph N, the concentrations that appeared to be most relevant in triggering an increase in A549 metabolic activity were 25 µM and 5 µM, to 118.61 % (p<0.05) and 112.10 % (p<0.05), respectively. In the 72-hour experiment, no concentration had a statistically meaningful effect. Aside from the concentration of 100 µM in the 24-hour experiment, no other concentration statistically substantially influenced the reduction of the metabolic activity of the A549 cell line. In the 48-hour assay, two concentrations appeared to have had a statistically considerable effect on the rise in metabolic activity, although only temporarily.

Higher doses decreased H1299 metabolic activity in a statistically significant way for the 48- and 72-hour assays. In graph Q, concentrations of 25 µM, 50 µM and 100 µM resulted in reductions of metabolic activity to 80.77 % (p<0.001), 76.82 % (p<0.001), and 75.37 % (p<0.001), respectively. While, in the 72-hour experiment whose data is shown in graph R, 50 µM of BODIPY 3 caused a more statistically relevant reduction in metabolic activity than 100 µM and 25 µM. The mean cell metabolic activity with 100 µM was 80.84 % (p<0.05), 76.46 % (p<0.001) with 50 µM and 83.9 % (p<0.05) with 25 µM. In the H1299 cell line, the third compound had some relevant cytotoxic effects, but mostly at concentrations above 10 µM.

BODIPY 3 had less effect on cell metabolic activity when compared to BODIPYs 1 and 2. The third BODIPY had a more pronounced effect on the H1299 cell line and only at higher concentrations such as 25 µM, 50 µM, and 100 µM. Therefore, this compound displayed interesting attributes to be used as a diagnostic drug, at least in concentrations up to 10 µM.
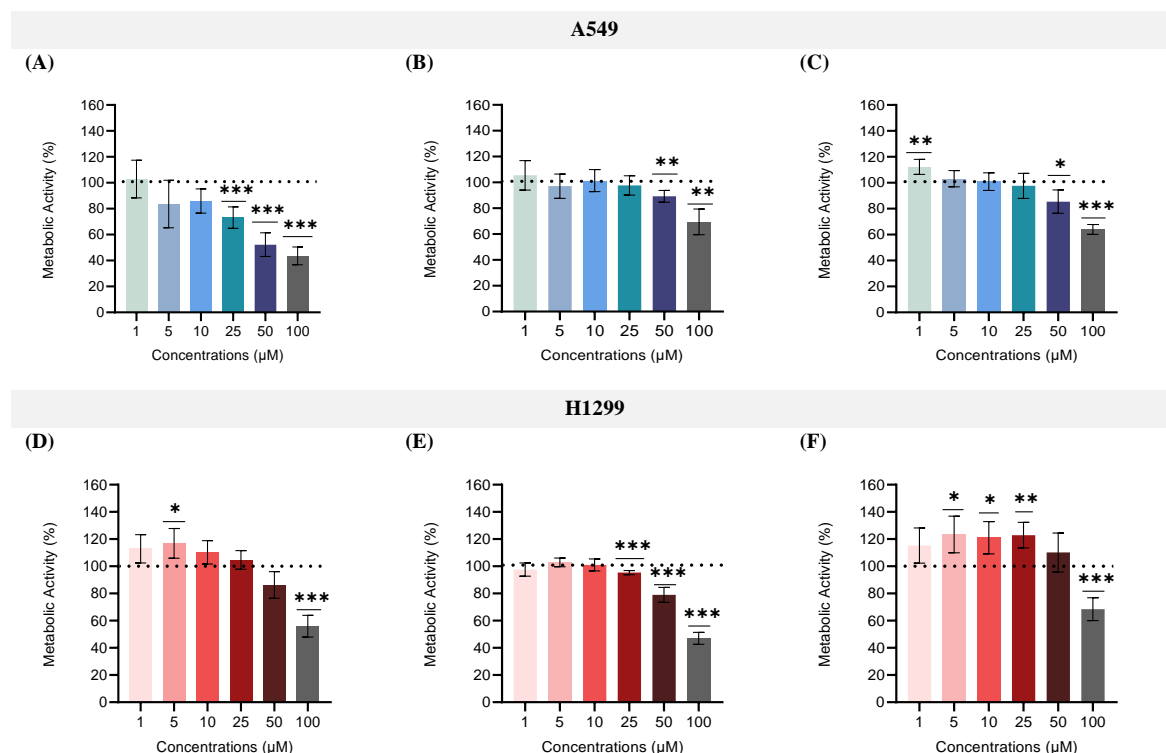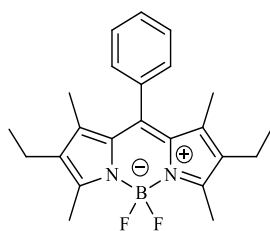
A549

H1299

Figure 48 - MTT results represented in the form of average and CI, for BODIPY 3 for the A549 cell line (M) 24h, (N) 48h and (O) 72h, and for H1299 cell line (P) 24h, (Q) 48h and (R) 72h, respectively. Due to the normalization of the data previously done, the metabolic activity values obtained for the controls are comparable to 100 % of the metabolic activity; as a result, the controls are represented by the dashed line. Significances are represented by * for $p<0.05$, ** for values of $p<0.01$ and *** for $p<0.001$.
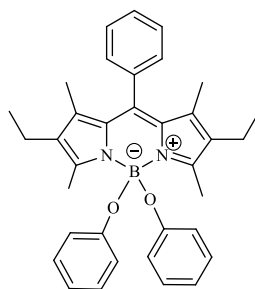
(4)

The results of the 24-hour assay revealed that all concentrations affected the A549 cell line in a statistically relevant way, but with different degrees of significance; when cells were treated with 1 μM the mean metabolic activity was 75.41 % ($p<0.01$), when the treatment was with 5 μM the mean was 81.35 % ($p<0.05$) and 10 μM caused a reduction to 78.19% ($p<0.01$). In the S graph, in figure 49, it is also possible to verify that concentrations such as 25 μM, 50 μM, and 100 μM triggered reductions to 71.98 %, 68.18 %, and 75.82 % (all with $p<0.001$). After 48 hours of incubation with BODIPY 4, for lower concentrations there was an increase in metabolic activity, revealing a temporary recovery. On the T graph, cells treated with 1 μM had a mean of 113.56 % ($p<0.001$), 5 μM led to a mean of 112.07 % ($p<0.05$), and when cells were treated with

98

10 µM, metabolic activity averaged 119.35 % (p<0.001). However, in the longer assay, graph U, the compound tended to have cytotoxic effects and, in some cases, triggering greater reductions in metabolic activity than those verified for the 24-hour assay. After 72 hours of incubation, A549 cells treated with 1 µM had a mean of 78.78 % (p<0.001), whereas 25 µM, 50 µM and 100 µM triggered a decrease to 48.07 % (p<0.001), 25.01 % (p<0.001) and 56.30 % (p<0.001), respectively.

Regarding the effects of incubation of the compound with the H1299 cell line, in the 24-hour assay (graph V) no concentration significantly affected metabolic activity. In the 48-hour trial, graph W, 1 µM of BODIPY 4 triggered a statistically substantial decrease in H1299 metabolic activity to 78.10 % (p<0.01). At last, in graph X, all concentrations had a statistically relevant influence on metabolic activity. It is possible to verify that there was a reduction in the mean metabolic activity to 72.58 %, 77.37 %, 74.15 %, 66.13 %, 60.14 %, 59.33 %, in relation to each concentration ranging from 100 µM to 1 µM (all with p<0.001). The effects of BODIPY 4 in the H1299 cell line as a function of time were more evident in the longer trial, in contrast to what happened with the A549 cell line which in all experiments at least part of the concentrations triggered statistically relevant changes in cell's metabolic activity. Even so, in the 72-hour assay, both cell lines had considerable reductions in metabolic activity, with means below 70 % and in some cases below 50 %.

Figure 49 - MTT results represented in the form of average and CI, for BODIPY 4 for the A549 cell line (S) 24h, (T) 48h and (U) 72h, and for H1299 cell line (V) 24h, (W) 48h and (X) 72h, respectively. Due to the normalization of the data previously done, the metabolic activity values obtained for the controls are comparable to 100 % of the metabolic activity; as a result, the controls are represented by the dashed line. Significances are represented by * for p<0.05, ** for values of p<0.01 and *** for p<0.001.

(5)
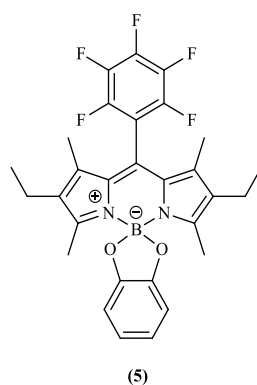
All data obtained and the respective statistical analysis of the 24-, 48- and 72-hour MTT assays with BODIPY 5 are summarized in figure 50, from graphs Y to DD.

When metabolic activity was assessed 24 hours after A549 cells were treated with BODIPY 5, all concentrations except 1 µM had a statistically significantly contribution to the metabolic activity reduction to 54.94 % ($p<0.001$) in the case of 5 µM, 60.38 % ($p<0.001$) for 10 µM, 64.45 % ($p<0.001$) for 25 µM, 60.61 % ($p<0.001$) for 50 µM and 63.02 % ($p<0.001$) for 100 µM, as demonstrated by Y graph. In the 48-hour assay, the same concentrations had a statistically significant impact in lowering metabolic activity. The Z graph shows that cells treated with 5 µM, 10 µM, 25 µM, 50 µM and 100 µM of BODIPY 5 had a metabolic reduction to 71.95 %, 73.12 %, 76.88 %, 74, 06 % and 75.18 % (all with $p<0.001$). A slight temporary recovery can be observed, as there was an increase in the mean values of metabolic activity. After 72 hours of incubation, there was a statistically relevant reduction in the metabolic activity of cells at all concentrations, with a reduction in means compared to the 48-hour assay. In the AA graph, from 1 µM to 100 µM, the means were 64.11 %, 55.77 %, 57.59 %, 59.63 %, 60.67 %, 59.48 % (all with $p<0.001$). Considering data obtained for the A549 cell line, BODIPY 5 tended to have considerable detrimental effects on metabolic activity, with greater reductions in metabolic activities as a function of time.

In the assay with a shorter incubation period with the H1299 cell line, all concentrations except 1 µM played a statistically relevant role in reducing metabolic activity, as it happened with the A549 cell line. In the BB graph, the mean reduction after cell treatment with 5 µM was 59.18 % ($p<0.01$), 10 µM triggered a reduction to 51.69 % ($p<0.001$), 25 µM to 53.48 % ($p<0.001$), 50 µM to 55.76 % ($p<0.01$) and 100 µM resulted in a mean metabolic activity of 56.03 % ($p<0.001$). In the 48-hour trial, H1299 had a temporary recovery as had A549, with only three concentrations substantially reducing the cell's metabolic activity. In the CC graph, 10 µM of the compound led to a mean of 72.97 % ($p<0.001$), whereas cells treated with 25 µM and 50 µM had a mean of 76.47 % ($p<0.05$) and 74.72 % ($p<0.05$), respectively. After 72 hours of incubation, all concentrations were statistically relevant to trigger the reduction in metabolic activity; in the DD graph the mean metabolic rate for cells treated with concentrations between 1 µM and 100 µM of the compound was 73.08 % ($p<0.001$), 57.84 % ($p<0.001$), 55.83 % ($p<0.001$), 55.94 %

(p<0.001), 57.17 % (p<0.001) and 58.75 % (p<0.001), respectively. Although a temporary recovery occurred in the 48-hour trial, the compound showed substantial negative effects in the 24- and 72-hour assays.
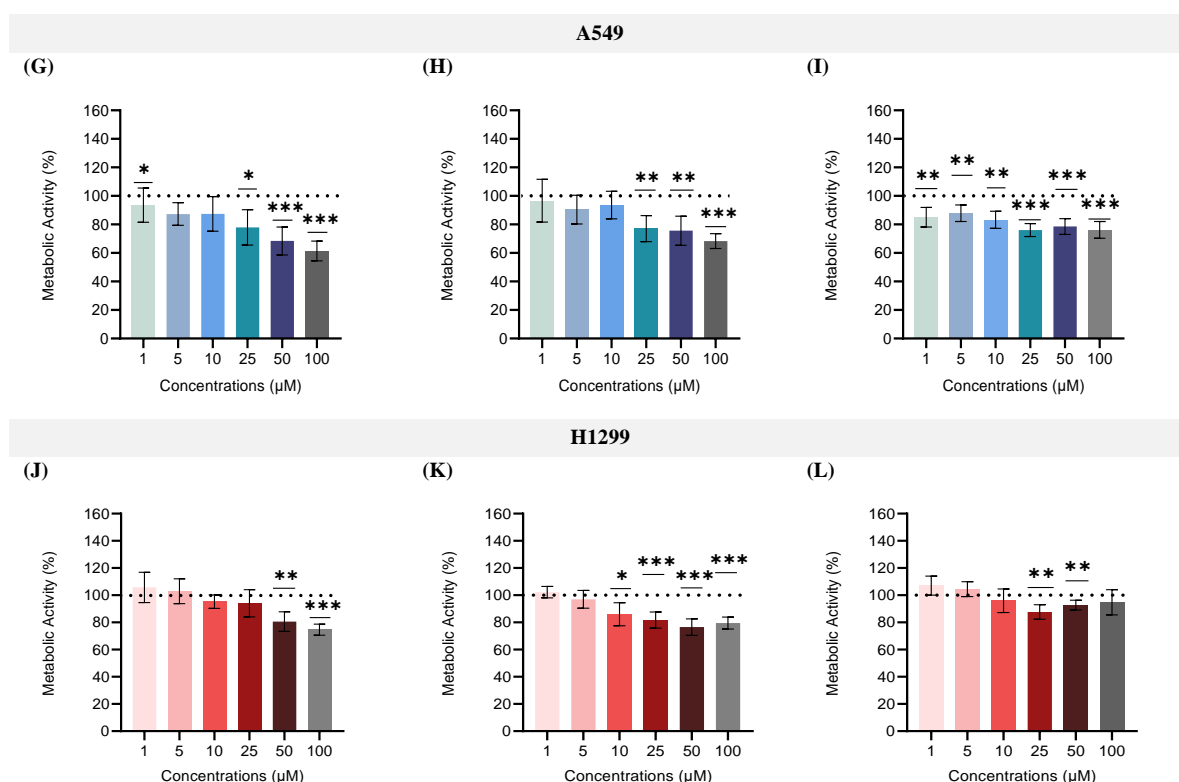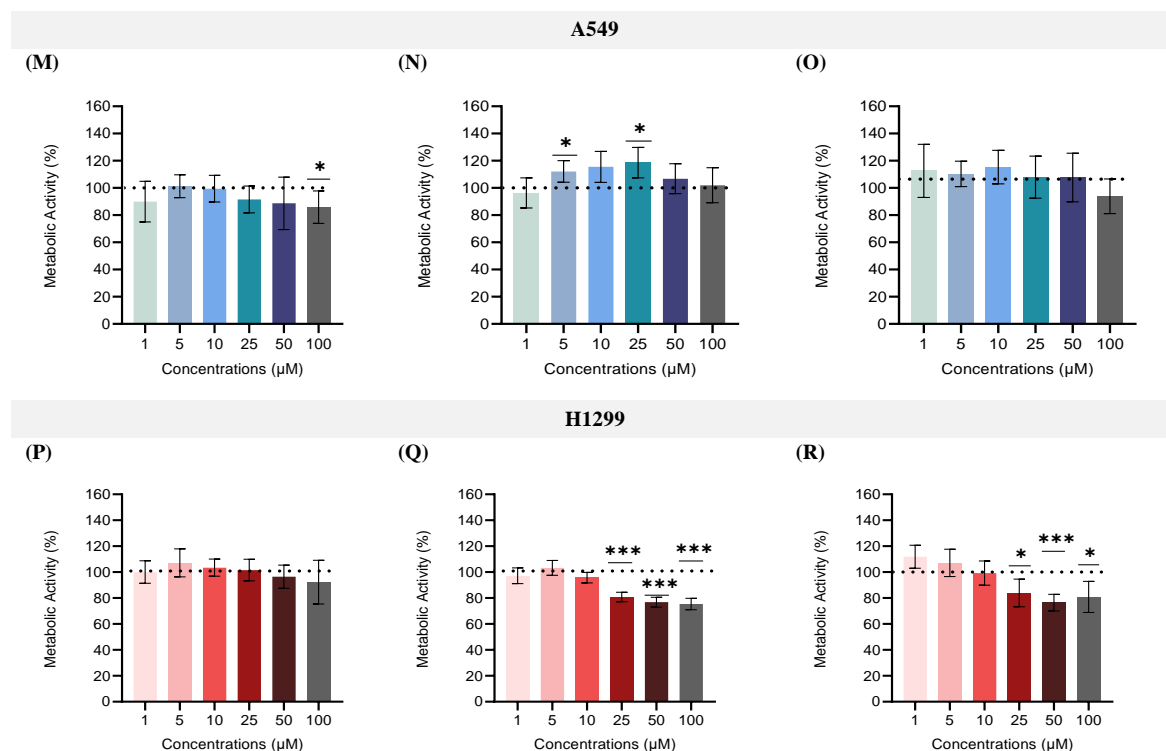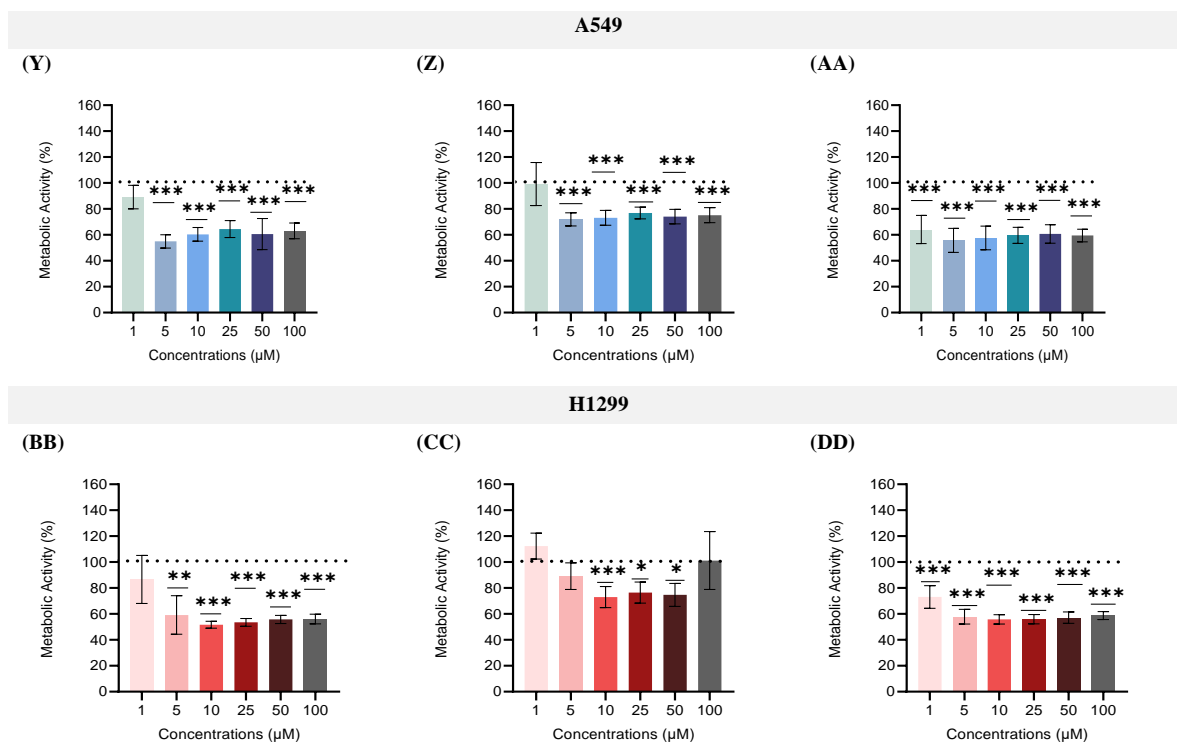

Figure 50 - MTT results, in the form of average and CI, for BODIPY 5 for the A549 cell line (Y) 24h, (Z) 48h and (AA) 72h, and for H1299 cell line (BB) 24h, (CC) 48h and (DD) 72h, respectively. Due to the normalization of the data previously done, the metabolic activity values obtained for the controls are comparable to 100 % of the metabolic activity; as a result, the controls are represented by the dashed line. Significances are represented by * for p<0.05, ** for values of p<0.01 and *** for p<0.001.

BODIPY 5 proved to have had a detrimental impact on the metabolic activity of cells in both cell lines, but more specifically in the 24-hour and 72-hour assays. Considering the above, some cytotoxicity may be associated with this compound, especially when compared to the other BODIPYs results. Since this compound seems to have more pronounced effects on cells, it could be investigated for some therapeutic application related to lung cancer, but not for the diagnosis of the pathology. Ever since, to make the diagnosis, the tumour environment should not be affected in any way or as little as possible by the drug used, so that the most accurate diagnosis possible can be achieved, and therefore be able to define a suitable treatment plan for each pathological condition.

(6)
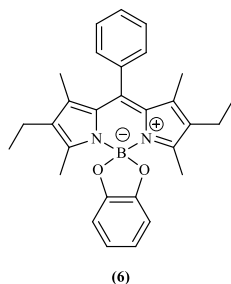
Data from the A549 cell line after treatment with BODIPY 6 did not reveal a statistically significant influence on cell metabolic activity until the 72-hour assay, as displayed in the graphs of figure 51. In the GG graph, the only concentration that caused a statistically significant decrease in metabolic activity was 100 µM to 88.80 % (p<0.05). Except for one concentration in the longer incubation period, this compound did not have a statistically substantial influence on metabolic activity of the A549 cell line.

In the H1299 cell line, the scenario was a little different, concentrations between 10 µM and 50 µM had a statistically relevant influence in increasing metabolic activity in the 24-hour and 48-hour trials, indicating that such concentrations were likely to somehow trigger metabolic activity. In the HH graph, the mean metabolic activity was 111.59 % (p<0.05) for 10 µM, 117.98 % (p<0.001) for 25 µM and 115.22 % (p<0.001) for 50 µM of BODIPY 6. The values of the statistically significant means in graph II were relatively close to those in the HH graph. In graph II, the metabolic activity was on average 110.70 % (p<0.05) for 10 µM, 116.42 % (p<0.01) for 25 µM and 114.67 % (p<0, 01) for 50 µM. In the final trial, only 1 µM of BODIPY 6 played a statistically relevant role in reducing the mean to 88.43 % (p<0.05). When treated cells were incubated for 24 and 48 hours, a certain range of doses was found to have a significant impact on boosting metabolic activity. The 72-hour experiment, however, did not reveal this rise in metabolic activity, and there was some recovery to the normal metabolic activity.

Overall, the results were relatively consistent with regard to the effects of the compounds on both cell lines. BODIPYs 1, 3 and 6 were the ones that showed results showing no or low cytotoxicity, at least in terms of metabolic activity. However, the two with the best results by far were BODIPYs 3 and 6 with the most consistent data on both cell lines and safe for cells at concentrations up to 10 µM. These last two compounds did not show significant cytotoxicity and therefore may have potential applications for the diagnostic field.

Other BODIPYs that are also being investigated for the diagnosis of lung cancer, but through Nuclear Magnetic Resonance, when their metabolic activity was assessed in a concentration range similar to those studied here, presented metabolic activity values above 90 %[80]. Still, when compared to this study, the data obtained for BODIPYs 3 and 6 for concentrations between 1 µM and 10 µM showed values above 80%, which represent good results.
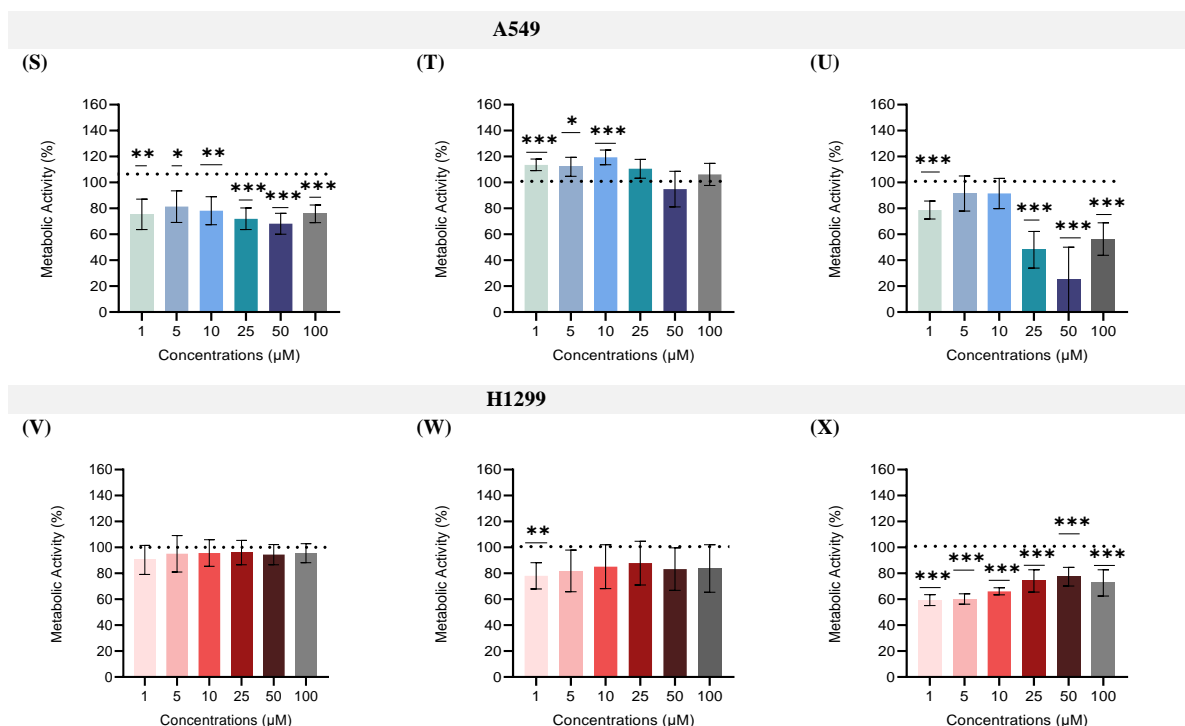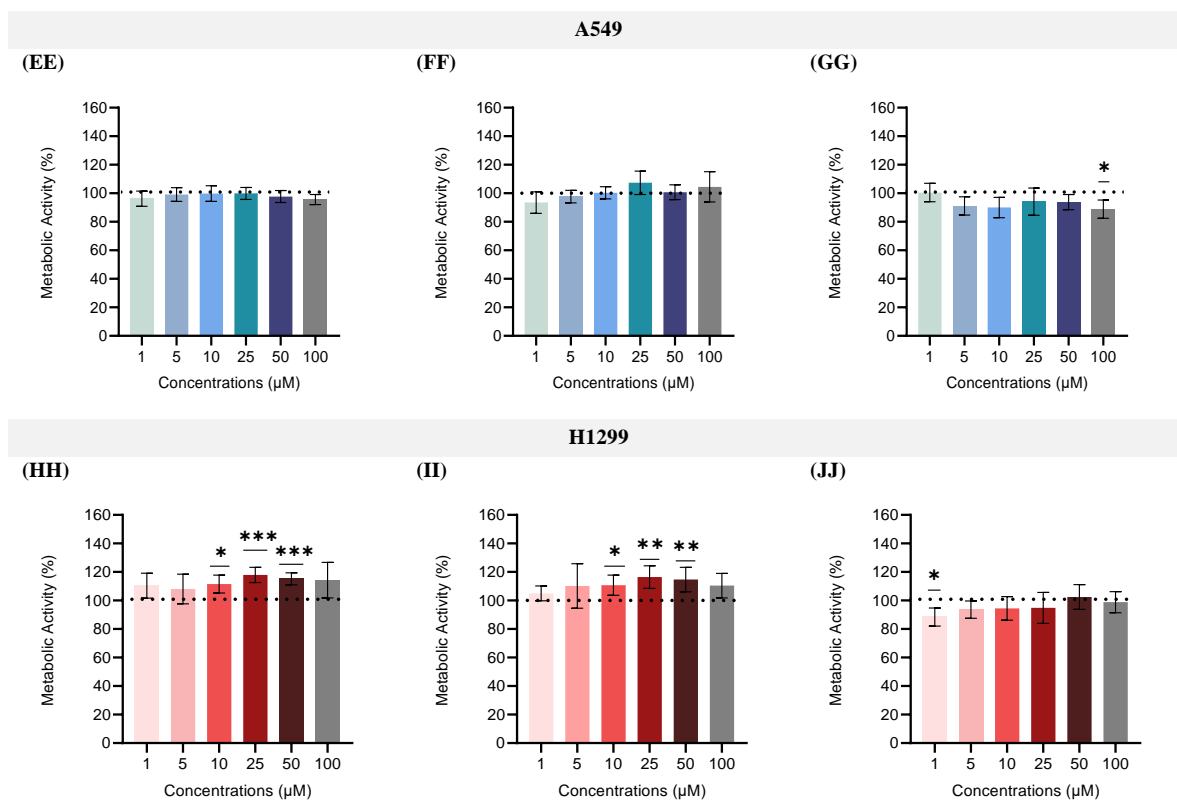
Figure 51 - MTT results, in the form of average and CI, for BODIPY 6 for the A549 cell line (EE) 24h, (FF) 48h and (GG) 72h, and for H1299 cell line (HH) 24h, (II) 48h and (JJ) 72h, respectively. Due to the normalization of the data previously done, the metabolic activity values obtained for the controls are comparable to 100 % of the metabolic activity; as a result, the controls are represented by the dashed line. Significances are represented by * for $p < 0.05$, ** for values of $p < 0.01$ and *** for $p < 0.001$.

4.3.2 Cell Viability

After assessing the effects of the different concentrations of the six BODIPYs on metabolic activity of two lung cancer cell lines, evaluating cell viability using at least two of the concentrations investigated above would be a method of verifying the effects of the compounds. Given that the SRB assay findings allow for the assessment of cell viability and cytotoxicity, the effects of 10 µM and 1 µM for each of the six compounds were evaluated, and the resulting data was reported in figure 52.

In the A549 cell line, the results of the SRB assay after 24 hours showed that BODIPY 1 at a concentration of 10 µM caused a statistically relevant reduction in viability to 78.74 % ($p < 0.01$), also BODIPY 5 in this assay at 10 µM had an influence on the viability reduction to 95.82 % ($p < 0.010$). In the same assay, graph KK, BODIPY 6 at 1 µM and 10 µM triggered a reduction in viability to 70.38 % ($p < 0.001$) and to 78.71 % ($p < 0.01$), respectively. In the 48-hour experiment, MM graph, BODIPY 1 was the only one to trigger a reduction statistically noteworthy to 79.24 % ($p < 0.001$) for 10 µM and to 87.84 % ($p < 0.05$) for 1 µM. The OO graph

reveal that after 72 hours of incubation, all BODIPYs except BODIPY 5 had a statistically considerable influence in decreasing viability, particularly at 10 μM. In this last assay with A549, the mean viability was 87.01 % (p<0.01) when cells were treated with 10 μM of BODIPY 1, and it was 90.70 % (p<0.05) for cells treated with 10 μM of BODIPY 2, and 83.46 % (p<0.01) for treatment with 1 μM of BODIPY 3. Also, in OO graph, both concentrations of BODIPYs 4 and 6 led to a relevant decrease of viability to 69.84 % (p<0.001) with 10 μM and to 86.57 % (p<0.01) with 1 μM of BODIPY 4; and with viability at 90.83 % (p<0.01) for 10 μM and 83.08 % (p<0.001) for 1 μM of BODIPY 6. All BODIPYs led to changes in cell viability in the cell line A549, with most effects being more evident in the longer incubation period, with the maximum difference from the normalized value being about 30.16 % for BODIPY 4.

In the shorter assay with the H1299 cell line, whose data are represented in the LL graph, BODIPY 5 had a statistically important role in reducing viability to 89.43 % (p<0.01) at 1 μM, additionally, BODIPY 6 also triggered a statistically notable reduction to 73.42 % (p<0.001) at 10 μM and to 70.14 % (p<0.001) at 1 μM. In the NN graph which corresponds to the data obtained from the 48-hour assay, BODIPYs 3 and 5 both at 1 μM had a relevant influence on cell viability, resulting in means of 87.43 % (p < 0.05) and 77.03 % (p<0.01), respectively. All BODIPYs except BODIPY 2 showed a statistically meaningful impact in decreasing viability in the longer experiment, notably at the 1 μM. In the PP graph, BODIPYs 1, 3 and 5 all at 1 μM caused a statistically relevant reduction in viability to 82.30 % (p<0.05), 76.96 % (p<0.01) and 78.58 % (p<0.01), respectively. Also in this last assay, both concentrations of BODIPYs 4 and 6 caused a statistically relevant reduction in cell viability; BODIPY 4 at 10 μM triggered a reduction to 82.57 % (p <0.001) and 1 μM to 72.30 % (p < 0.001); cells treated with 10 μM and 1 μM of BODIPY 6 had a mean viability of 74.11 % (p<0.01) and 62.61 % (p<0.001), respectively. All BODIPYs except BODIPY 2 led to changes in cell viability in the H1299 cell line, with the maximum difference being 37.39 % for BODIPY 6 in the 72-hour assay.

Overall, all BODIPYs resulted in changes in cell viability, with the greatest effects being more evident in the longer trials. A drug may have some cytotoxicity associated when it has viability values below 70 %[81]. That said and taking into account that the viability changes obtained were at most 30.16 % for the A549 line and 37.39 % for the H1299 line, it is possible to state that all BODIPYs do not seem to have major cytotoxic effects on cell's viability[81]. In view of the MTT and SRB results, BODIPY 3 and 6 were the ones with the best results in both assays, with metabolic activity above 80 % and viability above 70 % for concentrations of 10 μM and 1 μM.

The BODIPYs whose cytotoxicity was continued to be assessed by measuring haemoglobin release by erythrocytes, and incorporation by cell membranes using cell uptake assays were investigated at the same concentrations as those used in the metabolic activity and cell viability assays. If the compounds exhibit little or no cytotoxicity at 1 μM and 10 μM, it is quite likely that at lower concentrations the compounds would be non-cytotoxic as well.
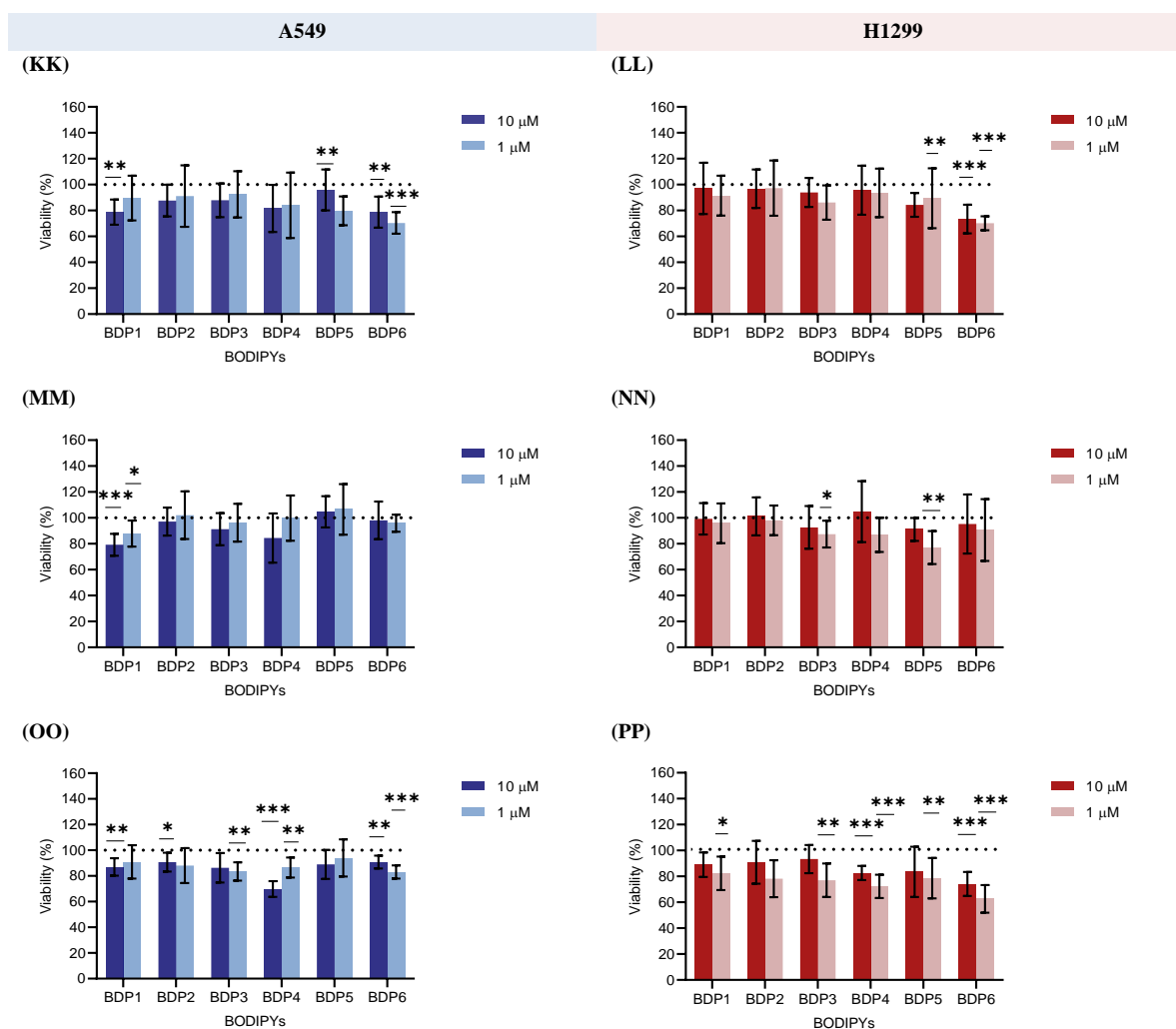
Figure 52 - SRB assay results for all BODIPYs (1-6) represented as mean and CI: for cell line A549 graph (KK) 24h assay, (MM) 48h assay, and (OO) 72h assay; and for cell line H1299 graph (LL) 24h assay, (NN) 48h assay and (PP) 72h assay. Due to the normalization of the data previously done, the cell viability values obtained for the controls are comparable to 100 % of the viability; as a result, the controls are represented by the dashed line. Significances are represented by * for $p < 0.05$, ** for values of $p < 0.01$ and *** for $p < 0.001$.

4.3.3 Haemolysis

After evaluating the effects of the compounds on metabolic activity and cell viability, it is necessary to assess the cytotoxicity of BODIPYs to blood cells. This is important not only because BODIPYs are being investigated for intravenous injection, but also because red blood cells interact with a wide range of cells and tissues in the body. Haemolysis is a flexible and useful technique to access cell cytotoxicity, because of the ease with which erythrocytes may be isolated. Figure 53 illustrates the results of the haemolysis assay.

Graph UU depicts the percentage of haemoglobin released after one hour of incubation with BODIPYs 3 and 6 at two different concentrations. BODIPY 3 increased haemoglobin

release to 13.74 % at 10 μM and to 12.46 % at 1 μM. BODIPY 6 had a more detrimental effect on red blood cell membranes at both concentrations, with haemoglobin release of 20.68 % at 10 μM and 14.70 % at 1 μM.

After 2 hours of incubation with the two compounds, graph VV, BODIPY 3 triggered a release of 26.74 % at 10 μM and 28.70 % at 1 μM; Whilst BODIPY 6 caused a release of 31.39 % at 10 μM and 26.48 % at 1 μM. Both BODIPYs provoked greater lysis in the second incubation period.
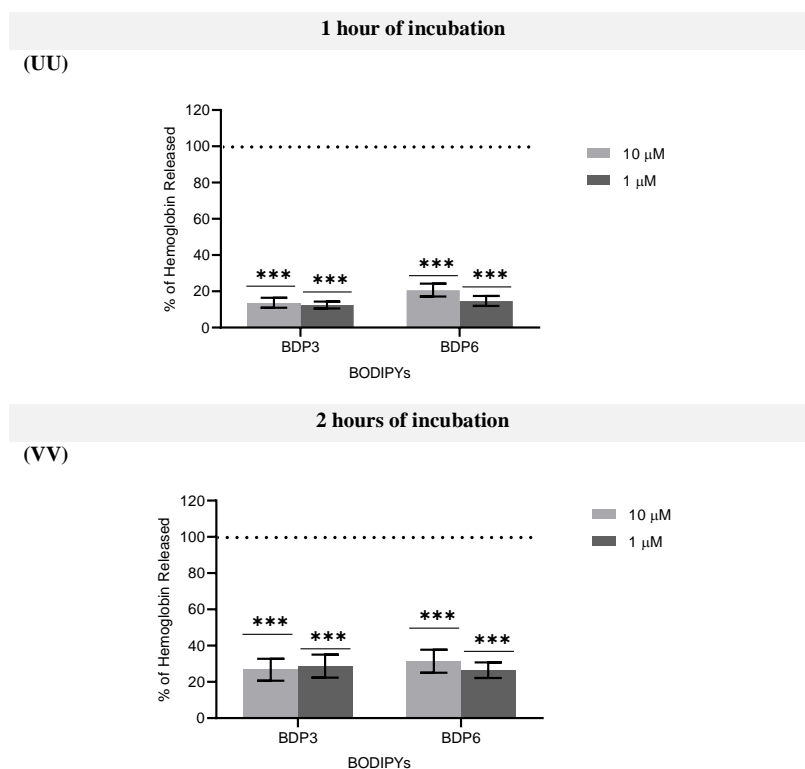
Figure 53 - Haemolysis results from (UU) 1 hour of incubation and (VV) 2 hours of incubation of BODIPYs 3 and 6 with red blood cells. Due to the normalization of the data previously done, the haemolysis values obtained for the controls are comparable to 100 % of haemoglobin release; as a result, the controls are represented by the dashed line. Significances are represented by * for $p < 0.05$, ** for values of $p < 0.01$ and *** for $p < 0.001$.

All comparisons were made considering the maximum release induced by Tryton X-100, the positive control. This surfactant causes damage to red cell membranes and can therefore be used to assess increased haemoglobin release. The increased release of haemoglobin in the body can have toxic consequences or initiate processes that stress the kidneys or other organs, that is why haemolysis is such an essential *in vitro* cytotoxicity assay[82].

The values obtained were good when compared to the normalization value and can help to demonstrate that the compounds appear to have low cytotoxicity, specially BODIPY 3 which

was the one with better results. Even though, haemolysis assays usually are carried out with an incubation period of 1 hour, since if the compound tends to cause damage, this should be evident in a shorter incubation period; in this study, we used the 2-hour incubation period to try to assess some extent of the effects, and indeed the values were slightly higher for the second incubation period. Following an article in which a formulation is considered haemolytic if it has haemolytic activity above 25 %, the values previously obtained for the first period of incubation were below this limit[83]. Even the values obtained for the second incubation period were not much superior to the limit imposed, revealing erythrocyte membrane stability in the presence of BODIPYs[82,83].

4.3.4 Cellular Uptake

Data so far from BODIPYs 3 and 6 have revealed that these compounds have some biocompatibility, with the cancer cell lines and with red blood cells. So, trying to figure out if the compound is internalized and in what range of values this might occur would be great to understand if there are interactions between the compound and the plasma membrane that allow the cellular uptake of BODIPYs.

To find out how much of BODIPYs 3 and 6 were incorporated by the cell lines, A549 and H1299, a calibration curve was obtained with a serial dilution of a previously prepared solution of each compound. Figures 54 and 55 have associated a graph with data obtained from the measured intensities for each of the different concentrations as a function of the range of wavelengths read; and also, the calibration curves obtained by linear fitting the maximum fluorescence as a function of each concentration value. Each calibration curve is associated with the equation from the fitting and the corresponding adjusted R-squared.

As the linear fit model was not suitable for the entire data set, the data were divided into two groups, and the linear fit was performed for both sets, obtaining two R squares better than the R square obtained for the whole dataset.

The following linear fit equations were used to calculate the concentrations of BODIPY 3 internalized by the cells, represented in the QQ and RR graphs of figure 56. In the following equations, F represents the fluorescence intensity and C represents the concentration in nanomolar.

$$F = 962.47C + 4949.78 \text{ for F between } [0, 160\,000] \qquad \text{(equation 4)}$$

$$F = 196.75C + 150305 \text{ for F between }]160\,000, 360\,000] \qquad \text{(equation 5)}$$

The plot of intensities as a function of wavelength for BODIPY 6 depicted in figure 55 suggests that this compound has a very weak fluorescence when compared to the graph in figure 54. This feature had already been mentioned previously by the characterization data, more specifically by the analysis performed on the data in figure 44.
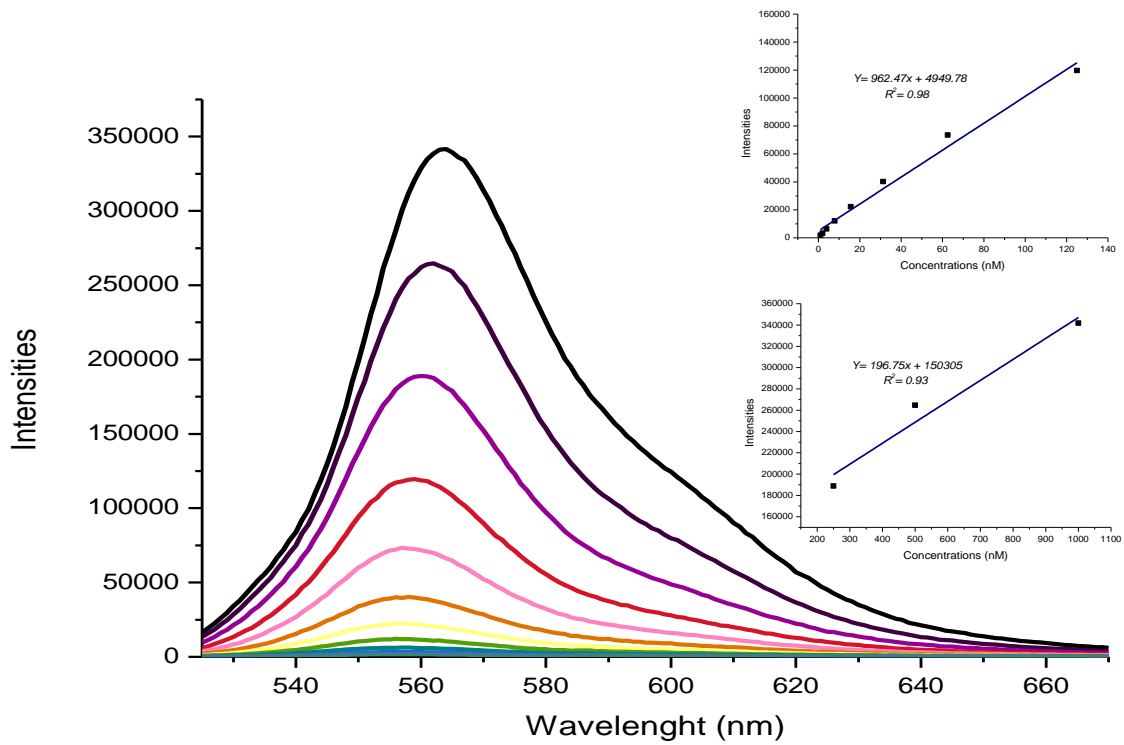
Figure 54 - Fluorescence intensity spectrum of a dilution series of known concentrations of BODIPY 3 used to obtain the calibration curves, on the left side; And the two calibration curves obtained with a linear fitting, on the right side. The measurement of fluorescence intensity was performed taking into account the maximum absorption at 545 nm and the fluorescence emission peak at 563 nm.

Even so, it was possible to determine the amounts of BODIPY 6 incorporated by the cells using equations 12 and 13. However, only concentrations with fluorescence greater than 500 were considered since the linear fitting could only be made for higher fluorescence values.

In the following equations, F represents the fluorescence intensity and C represents the concentration in nanomolar.

$$F = 24.74C + 356.57 \text{ for F between } [500, 3000] \qquad \text{(equation 6)}$$

$$F = 8.27C + 3481.48 \text{ for F between }]3000, 12000] \qquad \text{(equation 7)}$$

The maximum fluorescence obtained for the samples was replaced in the respective equation and the resulting concentrations were represented in figure 56 in the form of mean and standard deviation. All the uptake values in the form of mean and CI can be checked in APPENDIX II.
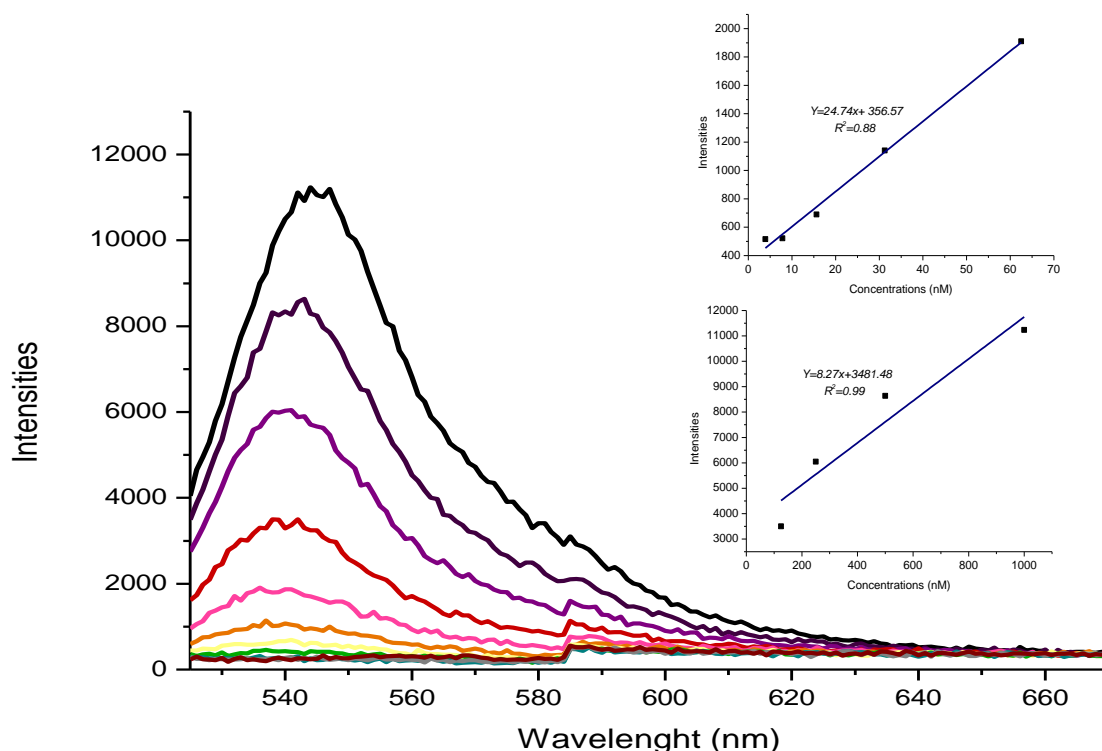
Figure 55 - Fluorescence intensity spectrum of a dilution series of known concentrations of BODIPY 6 used to obtain the calibration curves, on the left side, and the two calibration curves obtained with a linear fitting, on the right side. The measurement of fluorescence intensity was performed taking into account the maximum absorption at 531 nm.

The cellular uptake assay was carried out across three distinct time periods, 4 hours, 2 hours, and 1 hour, these intervals were chosen considering the duration of the PET scan, approximately 2 hours. So, knowing how much of the BODIPYs would be taken up by the cells during the scan and a little later would be important to get an idea of the response of cells to the compounds.

In the shortest incubation time, data displayed on the QQ plot revealed that 1 hour after A549 were incubated with 1 μM of BODIPY 3 the cell uptake was 12.24 nM and was 14.01 nM for H1299. After 2 hours of incubation with 1 μM of the third compound, A549 incorporated 26.12 nM and H1299 had uptaken 24.09 nM. After 4 hours of incubation, the A549 had integrated 37.04 nM of the compound, whereas the H129 had incorporated 30.68 nM.

The RR graph shows data for cells incubated with 10 μM of BODIPY 3. After 1 hour, 46.78 nM and 77.87 nM were incorporated by A549 and H1299, respectively. Following 2 hours of incubation, the mean compound incorporation was 93.72 nM for A549 and 97.56 nM for H1299. After 4 hours of incubation, 130.01 nM and 126.86 nM were the concentrations incorporated by A549 and H1299, respectively.

Now taking into account the BODIPY 6 uptake data, the SS and TT graphs show that these values were lower than those found for BODIPY 3. After 1 hour of incubation with 1 μM of the sixth compound, A549 had an uptake of 11,47 nM and H1299 had an incorporation of 11,88

nM. For a longer incubation period, 2 hours, with the same concentration, the mean cell uptake was 22.02 nM for A549 and 14.22 nM for H1299. After 4 hours, the mean uptake values for A549 were 29.50 nM and 24.82 nM for H1299.

With a higher concentration, graph TT, there was also greater incorporation of the compound. After 1 hour of incubation with 10 μM of BODIPY 6, the cell line A549 incorporated 33.63 nM, whereas the cell line H1299 integrated 56.84 nM. After 2 hours of incubation, A549 had an uptake of 68.88 nM and H1299 an uptake of 65.23 nM. In the longest incubation period tested, 4 hours, there was a slight decrease in the mean uptake values, with 53.94 nM for A549 and 54.21 nM for H1299.
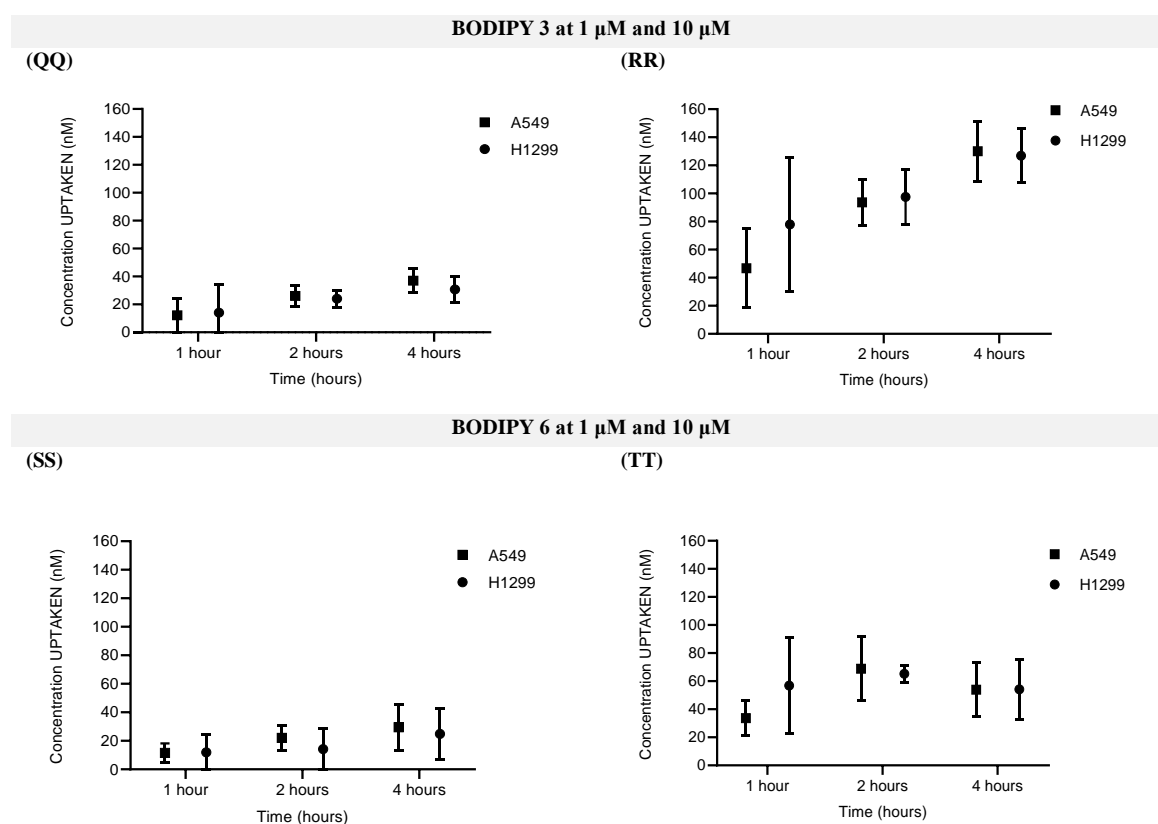
Figure 56 - Uptake results presented in the form of mean and SD, graph (QQ) for 1 μM and (RR) for 10 μM of BODIPY 3, respectively; and (SS) for 1 μM and (TT) for 10 μM of BODIPY 6 for A549 and H1299 cell lines.

In most of the conditions tested, the uptake values for both compounds in H1299 were lower than the values in the A549 cell line. As the H1299 are cells from a patient who had already received radiotherapy, the cellular mechanisms of compounds incorporation may have changed, or the BODIPYs simply have more difficulty getting through the membranes[71].

In general, for both cell lines and concentrations tested, compound incorporation tended to increase with increasing incubation duration. A possible explanation is that in order to establish the equilibrium of compound concentrations within and outside the cells may be needed a longer incubation period. This fact may also be related to the drug incorporation mechanism itself or to the interactions of the compound with the cellular environment.

Another condition studied in this trial was the different concentrations of each BODIPY. When cells were incubated with 10 µM, the percentage of incorporation shown in tables 5 and 6 was not higher than those obtained when cells were incubated with 1 µM. Among the two BODIPYs studied in this trial, BODIPY 3 had higher uptake values, at both concentrations, when compared to BODIPY 6. Despite, the values in the tables below were relatively low for both BODIPYs, this is not a reason to exclude the compounds for diagnostic applications. In the literature, a BODIPY for myocardial perfusion imaging had its *in vitro* uptake evaluated after 1.5 hours of incubation with 25 µM revealed incorporation values between 1 % and 3 %[50]. Despite the modest values achieved in that last investigation, revealing some similarities with the ones obtained by us, *in vivo* evaluation of BODIPY labelled with Fluorine-18 indicated preferential accumulation in the their targeted tissue, the heart[50].

Radiolabelling compounds with Fluorine-18 can increase uptake values, since fluorine is commonly used to improve the lipophilicity of substances, allowing them to pass more easily through lipid membranes[60,67]. BODIPYs 3 and 6 have phenol and catechol groups linked to boron, groups that will likely contribute to faster radioactive labelling due to the ring stress on the dialkoxide. Therefore, the uptake studies must be performed following the radiolabelling in order to determine whether ^{18}F insertion can actually increase compound uptake or not.

Table 5 - Mean concentrations of BODIPY 3 uptaken by cells in the form of percentage.

	1 µM		10 µM	
	A549	**H1299**	**A549**	**H1299**
1 hour	1.22 %	1.40 %	0.47 %	0.78 %
2 hours	2.61 %	2.41 %	0.94 %	0.98 %
4 hours	3.71 %	3.07 %	1.30 %	1.27 %

Table 6 - Mean concentrations of BODIPY 6 uptaken by cells in the form of percentage.

	1 µM		10 µM	
	A549	**H1299**	**A549**	**H1299**
1 hour	1.49 %	1.26 %	0.33 %	0.57 %
2 hours	2.20 %	1.42 %	0.69 %	0.65 %
4 hours	2.95 %	2.48 %	0.54 %	0.54 %

A comparison with a normal cell line like for example MRC-5 cell line, fibroblasts, should also be performed to know which effects could the BODIPYs have in normal cells, with such comparisons have already been performed to study other drugs[84,85].

Conclusions

5 - Conclusions

A major goal of this research was to synthesize and assess the cytotoxicity of six BODIPYs with distinct properties that might be beneficial for ^{19}F-^{18}F isotopic exchange in the boron core. Additionally, it was intended to provide the means to reduce radiolabelling time, allowing for a longer scan time, as a new alternative or complementary method to glucose fluorides for the diagnosis of lung cancer.

Six different BODIPYs were synthetised and characterized successfully. BODIPY 1 to 4 showed considerable fluorescence and therefore can be investigated for dual PET/Fluorescence imaging. In contrast, BODIPYs 5 and 6 showed very weak fluorescence, which is related to the extinction triggered by the catechol group when covalently linked to the boron atom of BODIPYs.

The use of cyclic alkoxides such as catechol derivatives brings an additional favourable parameter related to ring stress on the dialkoxide that can further accelerate the radiolabelling. Based on the structural motif analysis, BODIPYs 5 and 6 are likely to have a greater influence on the reaction kinetics due to their extra strain in the oxygen area and greater deviation of boron from the pyrrole plane.

MTT and SRB data revealed that BODIPYs 3 and 6 did not show relevant cytotoxicity at concentrations up to 10 µM. Although the haemolysis assay showed that BODIPY 6 had a greater effect on red cell lysis at both times of incubation, both BODIPYs did not contribute to trigger a major lysis of the red cell membrane. Last of all, uptake values revealed that the compounds had low uptake, with BODIPY 3 showing slightly higher uptake than BODIPY 6 in both cell lines.

Although the uptake values were not as good as expected, the inclusion of Fluorine-18 in the BODIPYs structure can facilitate their passage across the lipid membranes, thereby increasing cellular uptake. For this purpose, BODIPYs 3 and 6 have alkoxy groups attached to the boron atom, a feature we were interested in, and which may optimize radiolabelling kinetics.

As future work, biocompatibility studies of the compounds on the MRC-5 cell line or other normal cell line of lung tissue should be performed as a way to compare the data obtained to the eventual effects on normal cells. If biocompatibility can be proven for BODIPYs 3 and 6 for a normal cell line, then the kinetic evaluation of new alkoxy-BODIPYs versus the identical BODIPYs with ^{19}F in the boron centre should be investigated. After the radiolabelling of BODIPYs 3 and 6, their uptake should be reassessed in cell lines and the *in* with the EasyPET system. This last task should be regarded as future collaboration with ICNAS. Furthermore, in order to better understand how BODIPYs uptake occurs, it may be useful to try to uncover the mechanism by which BODIPYs enter the cancer cells. Finally, considering that at least BODIPY 3 showed interesting characteristics for dual-mode imaging this possibility should also be considered for a PET/fluorescence modality for *in vivo* studies.

References

6 - References

1. Hendee, W. R. & Ritenour, E. R. Chapters 1 to 9. in *Medical Imaging Physics* (John Wiley & Sons, Inc., 2002). ISBN:0471382264.
2. Gao, D., Zhang, B., Liu, Y., Hu, D., Sheng, Z., Zhang, X. & Yuan, Z. Molecular Engineering of Near-Infrared Light-Responsive BODIPY-Based Nanoparticles with Enhanced Photothermal and Photoacoustic Efficiencies for Cancer Theranostics. *Theranostics* **9**, 5315–5331 (2019) DOI:10.7150/thno.34418.
3. Tang, Q., Xiao, W., Huang, C., Si, W., Shao, J., Huang, W., Chen, P., Zhang, Q. & Dong, X. pH-Triggered and Enhanced Simultaneous Photodynamic and Photothermal Therapy Guided by Photoacoustic and Photothermal Imaging. *Chem. Mater.* **29**, 5216–5224 (2017) DOI:10.1021/acs.chemmater.7b01075.
4. Hu, W., Ma, H., Hou, B., Zhao, H., Ji, Y., Jiang, R., Hu, X., Lu, X., Zhang, L., Tang, Y., Fan, Q. & Huang, W. Engineering Lysosome-Targeting BODIPY Nanoparticles for Photoacoustic Imaging and Photodynamic Therapy under Near-Infrared Light. *ACS Appl. Mater. Interfaces* **8**, 12039–12047 (2016) DOI:10.1021/acsami.6b02721.
5. Betts, J. G., Desaix, P., Johnson, E., Johnson, J. E., Korol, O., Kruse, D., Poe, B., Wise, J. A., Womble, M. & Young, K. A. The Respiratory System. in *Anatomy & Physiology* 1033–1084 (OpenStax, 2013). ISBN:978-1-938168-30-7.
6. Fois, S. S., Paliogiannis, P., Zinellu, A., Fois, A. G., Cossu, A. & Palmieri, G. Molecular Epidemiology of the Main Druggable Genetic Alterations in Non-Small Cell Lung Cancer. *Int. J. Mol. Sci.* **22**, 612 (2021) DOI:10.3390/ijms22020612.
7. Miller, Y. E. Pathogenesis of Lung Cancer. *Am. J. Respir. Cell Mol. Biol.* **33**, 216–223 (2005) DOI:10.1165/rcmb.2005-0158OE.
8. Lemjabbar-Alaoui, H., Hassan, O. U., Yang, Y.-W. & Buchanan, P. Lung Cancer: Biology and Treatment Options. *Biochim. Biophys. Acta - Rev. Cancer* **1856**, 189–210 (2015) DOI:10.1016/j.bbcan.2015.08.002.
9. Global Cancer Observatory. International Agency for Reserch on cancer. World Health Organization. Respiratory System and Intrathoracic Organs. Trachea, Bronchus and Lung. *GLOBOCAN, International Agency for Research on Cancer* vol. 419 1–2 https://gco.iarc.fr/today/data/factsheets/cancers/15-Lung-fact-sheet.pdf (2020) (accessed:18 August 2021).
10. Neal, R. D., Sun, F., Emery, J. D. & Callister, M. E. Lung cancer. *BMJ* **365**, l1725 (2019) DOI:10.1136/bmj.l1725.
11. World Health Organization. *WHO Global Report On Trends in Prevalence of Tobacco Smoking 2000-2025*. (2018) ISBN:978-92-4-000003-2.
12. Multi bars - Estimated number of deaths in Portugal, both sexes, all ages. *GLOBOCAN, International Agency for Research on Cancer* https://gco.iarc.fr/today/home (2021) (accessed:11 September 2021).
13. World Health Organization. *WHO report on cancer: setting priorities, investing wisely and providing care for all*. (2020). ISBN:9789240001299.
14. de Groot, P. M., Wu, C. C., Carter, B. W. & Munden, R. F. The Epidemiology of Lung Cancer. *Transl. Lung Cancer Res.* **7**, 220–233 (2018) DOI: 10.21037/tlcr.2018.05.06.
15. Malhotra, J., Malvezzi, M., Negri, E., La Vecchia, C. & Boffetta, P. Risk factors for Lung Cancer Worldwide. *Eur. Respir. J.* **48**, 889–902 (2016) DOI:10.1183/13993003.00359-2016.
16. Hirsch, F. R., Scagliotti, G. V., Mulshine, J. L., Kwon, R., Curran, W. J., Wu, Y. L. & Paz-Ares, L. Lung Cancer: Current Therapies and New Targeted Treatments. *Lancet* **389**, 299–311 (2017) DOI: 10.1016/S0140-6736(16)30958-8.
17. Wen, Y., Zhu, C., Li, N., Li, Z., Cheng, Y., Dong, J., Zhu, M., Wang, Y., Dai, J., Ma, H., Jin, G., Dai, M., Hu, Z. & Shen, H. Fine Mapping in Chromosome 3q28 Identified Two Variants Associated with Lung Cancer Risk in Asian Population. *J. Cancer* **10**, 1862–1869 (2019) DOI:10.7150/jca.28379.
18. Altorki, N. K., Markowitz, G. J., Gao, D., Port, J. L., Saxena, A., Stiles, B., McGraw, T. &

Mittal, V. The Lung Microenvironment: an Important Regulator of Tumour Growth and Metastasis. *Nat. Rev. Cancer* **19**, 9–31 (2019) DOI:10.1038/s41568-018-0081-9.

19. Tan, A. C. Targeting the PI3K/Akt/mTOR Pathway in Non-Small Cell Lung Cancer (NSCLC). *Thorac. Cancer* **11**, 511–518 (2020) DOI:10.1111/1759-7714.13328.

20. Travis, W. D., Brambilla, E., Nicholson, A. G., Yatabe, Y., Austin, J. H. M., Beasley, M. B., Chirieac, L. R., Dacic, S., Duhig, E., Flieder, D. B., Geisinger, K., Hirsch, F. R., Ishikawa, Y., Kerr, K. M., Noguchi, M., Pelosi, G., Powell, C. A., Tsao, M. S. & Wistuba, I. The 2015 World Health Organization Classification of Lung Tumors. *J. Thorac. Oncol.* **10**, 1243–1260 (2015) DOI:10.1097/JTO.0000000000000630.

21. Oudkerk, M., Devaraj, A., Vliegenthart, R., Henzler, T., Prosch, H., Heussel, C. P., Bastarrika, G., Sverzellati, N., Mascalchi, M., Delorme, S., Baldwin, D. R., Callister, M. E., Becker, N., Heuvelmans, M. A., Rzyman, W., Infante, M. V., Pastorino, U., Pedersen, J. H., Paci, E., Duffy, S. W., de Koning, H. & Field, J. K. European Position Statement on Lung Cancer Screening. *Lancet Oncol.* **18**, e754–e766 (2017) DOI:10.1016/S1470-2045(17)30861-6.

22. Postmus, P. E., Kerr, K. M., Oudkerk, M., Senan, S., Waller, D. A., Vansteenkiste, J., Escriu, C. & Peters, S. Early and Locally Advanced Non-Small-Cell Lung Cancer (NSCLC): ESMO Clinical Practice Guidelines for Diagnosis, Treatment and Follow-up. *Ann. Oncol.* **28**, iv1–iv21 (2017) DOI:10.1093/annonc/mdx222.

23. Munch, M., Rotstein, B. H. & Ulrich, G. Fluorine-18-Labeled Fluorescent Dyes for Dual-Mode Molecular Imaging. *Molecules* **25**, 6042 (2020) DOI:10.3390/molecules25246042.

24. Silvestri, G. A., Gonzalez, A. V., Jantz, M. A., Margolis, M. L., Gould, M. K., Tanoue, L. T., Harris, L. J. & Detterbeck, F. C. Methods for Staging Non-small Cell Lung Cancer. *Chest* **143**, e211S-e250S (2013) DOI:10.1378/chest.12-2355.

25. Yonemori, K., Kunitoh, H. & Sekine, I. Small-Cell Lung Cancer with Lymphadenopathy in an 18-year-old Female Nonsmoker. *Nat. Clin. Pract. Oncol.* **3**, 399–403 (2006) DOI:10.1038/ncponc0534.

26. Seijo, L. M., Peled, N., Ajona, D., Boeri, M., Field, J. K., Sozzi, G., Pio, R., Zulueta, J. J., Spira, A., Massion, P. P., Mazzone, P. J. & Montuenga, L. M. Biomarkers in Lung Cancer Screening: Achievements, Promises, and Challenges. *J. Thorac. Oncol.* **14**, 343–357 (2019) DOI:10.1016/j.jtho.2018.11.023.

27. Kandathil, A., Kay, F. U., Butt, Y. M., Wachsmann, J. W. & Subramaniam, R. M. Role of FDG PET/CT in the Eighth Edition of TNM Staging of Non–Small Cell Lung Cancer. *RadioGraphics* **38**, 2134–2149 (2018) DOI:10.1148/rg.2018180060.

28. Goldstraw, P., Chansky, K., Crowley, J., Rami-Porta, R., Asamura, H., Eberhardt, W. E. E., Nicholson, A. G., Yokoi, K., *et al.* The IASLC Lung Cancer Staging Project: Proposals for Revision of the TNM Stage Groupings in the Forthcoming (Eighth) Edition of the TNM Classification for Lung Cancer. *J. Thorac. Oncol.* **11**, 39–51 (2016) DOI:10.1016/j.jtho.2015.09.009.

29. Lababede, O., Meziane, M. & Rice, T. Seventh Edition of the Cancer Staging Manual and Stage Grouping of Lung Cancer. *Chest* **139**, 183–189 (2011) DOI:10.1378/chest.10-1099.

30. Besse, B., Adjei, A., Baas, P., Meldgaard, P., Nicolson, M., Paz-Ares, L., Reck, M., Smit, E. F., Syrigos, K., Stahel, R., Felip, E., Peters, S., Stahel, R., Felip, E., Peters, S., Kerr, K., Besse, B., Vansteenkiste, J., Eberhardt, W., Edelman, M., Mok, T., O'Byrne, K., Novello, S., Bubendorf, L., Marchetti, A., Baas, P., Reck, M., Syrigos, K., Paz-Ares, L., Smit, E. F., Meldgaard, P., Adjei, A., Nicolson, M., Crinò, L., Van Schil, P., Senan, S., Faivre-Finn, C., Rocco, G., Veronesi, G., Douillard, J.-Y., Lim, E., Dooms, C., Weder, W., De Ruysscher, D., Le Pechoux, C., De Leyn, P. & Westeel, V. 2nd ESMO Consensus Conference on Lung Cancer: Non-Small-Cell Lung Cancer First-Line/Second and Further Lines of Treatment in Advanced Disease. *Ann. Oncol.* **25**, 1475–1484 (2014) DOI:10.1093/annonc/mdu123.

31. Früh, M., De Ruysscher, D., Popat, S., Crinò, L., Peters, S. & Felip, E. Small-Cell Lung Cancer (SCLC): ESMO Clinical Practice Guidelines for Diagnosis, Treatment and Follow-up. *Ann. Oncol.* **24**, vi99–vi105 (2013) DOI:10.1093/annonc/mdt178.

32. Rudin, C. M., Brambilla, E., Faivre-Finn, C. & Sage, J. Small-Cell Lung Cancer. *Nat. Rev.*

Dis. Prim. **7**, 3 (2021) DOI:10.1038/s41572-020-00235-0.

33. Boens, N., Leen, V. & Dehaen, W. Fluorescent Indicators Based on BODIPY. *Chem. Soc. Rev.* **41**, 1130–1172 (2012) DOI:10.1039/C1CS15132K.

34. Boens, N., Verbelen, B. & Dehaen, W. Postfunctionalization of the BODIPY Core: Synthesis and Spectroscopy. *European J. Org. Chem.* **2015**, 6577–6595 (2015) DOI:10.1002/ejoc.201500682.

35. Lu, H., Mack, J., Yang, Y. & Shen, Z. Structural Modification Strategies for the Rational Design of Red/NIR Region BODIPYs. *Chem. Soc. Rev.* **43**, 4778–4823 (2014) DOI:10.1039/C4CS00030G.

36. Tao, J., Sun, D., Sun, L., Li, Z., Fu, B., Liu, J., Zhang, L., Wang, S., Fang, Y. & Xu, H. Tuning the Photo-Physical Properties of BODIPY Dyes: Effects of 1, 3, 5, 7- Substitution on Their Optical and Electrochemical Behaviours. *Dye. Pigment.* **168**, 166–174 (2019) DOI: 10.1016/j.dyepig.2019.04.054.

37. Boens, N., Verbelen, B., Ortiz, M. J., Jiao, L. & Dehaen, W. Synthesis of BODIPY Dyes Through Postfunctionalization of the Boron Dipyrromethene Core. *Coord. Chem. Rev.* **399**, 213024 (2019) DOI:10.1016/j.ccr.2019.213024.

38. Gai, L., Lu, H., Zou, B., Lai, G., Shen, Z. & Li, Z. Synthesis and Spectroscopic Properties of BODIPY Dimers with Effective Solid-State Emission. *R. Soc. Chem.* **2**, 8840–8846 (2012) DOI:10.1039/c2ra21040a.

39. Kritskaya, A. Y., Berezin, M. B., Antina, E. V. & Vyugin, A. I. Effect of Aryl-, Halogen-, and Ms-Aza-Substitution on the Luminescent Properties and Photostability of Difluoroborates of 2,2′-Dipyrrometenes. *J. Fluoresc.* **29**, 911–920 (2019) DOI: 10.1007/s10895-019-02403-2.

40. Loudet, A. & Burgess, K. BODIPY Dyes and Their Derivatives: Syntheses and Spectroscopic Properties. *Chem. Rev.* **107**, 4891–4932 (2007) DOI:10.1021/cr078381n.

41. Leen, V., Gonzalvo, V. Z., Deborggraeve, W. M., Boens, N. & Dehaen, W. Direct Functionalization of BODIPY Dyes by Oxidative Nucleophilic Hydrogen Substitution at the 3- or 3,5-Positions. *Chem. Commun.* **46**, 4908–4910 (2010) DOI: scite.ai/reports/10.1039/c0cc00568a.

42. Rohand, T., Baruah, M., Qin, W., Boens, N. & Dehaen, W. Functionalisation of Fluorescent BODIPY dyes by Nucleophilic Substitution. *Chem. Commun.* 266–268 (2006) DOI:10.1039/b512756d.

43. Li, L., Nguyen, B. & Burgess, K. Functionalization of the 4,4-difluoro-4-bora-3a,4a-diaza-s-indacene (BODIPY) Core. *Bioorg. Med. Chem. Lett.* **18**, 3112–3116 (2008) DOI:10.1016/j.bmcl.2007.10.103.

44. Leen, V., Miscoria, D., Yin, S., Filarowski, A., Molisho Ngongo, J., Van Der Auweraer, M., Boens, N. & Dehaen, W. 1,7-disubstituted Boron Dipyrromethene (BODIPY) Dyes: Synthesis and Spectroscopic Properties. *J. Org. Chem.* **76**, 8168–8176 (2011) DOI:10.1021/jo201082z.

45. Xochitiotzi-Flores, E., Islas-Mejía, A. A., García-Ortega, H., Romero-Ávila, M., Mendez-Stivalet, J. M., Carreón-Castro, M. D. P., Santillan, R., Maldonado-Domínguez, M., Arcos-Ramos, R. & Farfán, N. On the Structure of meso-Substituted F-BODIPYs and Their Assembly in Molecular Crystals: An Experimental-Theoretical Approach. *J. Organomet. Chem.* **805**, 148–157 (2016) DOI: 10.1016/j.jorganchem.2016.01.021.

46. Squeo, B. M. & Pasini, M. BODIPY platform: a tunable tool for green to NIR OLEDs. *Supramol. Chem.* **32**, 56–70 (2020) DOI:10.1080/10610278.2019.1691727.

47. Gupta, I. & Kesavan, P. E. Carbazole Substituted BODIPYs. *Front. Chem.* **7**, 1–31 (2019) DOI: 10.3389/fchem.2019.00841.

48. Liu, X., Chen, B., Li, X., Zhang, L., Xu, Y., Liu, Z., Cheng, Z. & Zhu, X. Self-Assembly of BODIPY based pH-Sensitive Near-infrared Polymeric Micelles for Drug Controlled Delivery and Fluorescence Imaging Applications. *Nanoscale* **7**, 1–20 (2015) DOI: 10.1039/C5NR04655F.

49. Ni, Y., Lee, S., Son, M., Aratani, N., Ishida, M., Samanta, A., Yamada, H., Chang, Y.-T., Furuta, H., Kim, D. & Wu, J. A Diradical Approach towards BODIPY-Based Dyes with Intense Near-Infrared Absorption around λ =1100 nm. *Angew. Chemie Int. Ed.* **55**, 2815–

2819 (2016) DOI:10.1002/anie.201511151.

50. Liu, S., Li, D., Shan, H., Gabbaï, F. P., Li, Z. & Conti, P. S. Evaluation of 18F-labeled BODIPY Dye as Potential PET Agents for Myocardial Perfusion Imaging. *Nucl. Med. Biol.* **41**, 120–126 (2014) DOI: 10.1016/j.nucmedbio.2013.09.006.

51. Kim, H., Kim, K., Son, S., Choi, J. Y., Lee, K., Kim, B., Byun, Y. & Choe, Y. S. 18 F-Labeled BODIPY Dye: A Potential Prosthetic Group for Brain Hybrid PET/Optical Imaging Agents. *ACS Chem. Neurosci.* **10**, 1445–1451 (2019) DOI: 10.1021/acschemneuro.8b00480.

52. Liu, M., Ma, S., She, M., Chen, J., Wang, Z., Liu, P., Zhang, S. & Li, J. Structural Modification of BODIPY: Improve its Applicability. *Chinese Chem. Lett.* **30**, 1815–1824 (2019) DOI:10.1016/j.cclet.2019.08.028.

53. Chansaenpak, K., Wang, H., Wang, M., Giglio, B., Ma, X., Yuan, H., Hu, S., Wu, Z. & Li, Z. Synthesis and Evaluation of [18 F]-Ammonium BODIPY Dyes as Potential Positron Emission Tomography Agents for Myocardial Perfusion Imaging. *Chem. - A Eur. J.* **22**, 12122–12129 (2016) DOI:10.1002/chem.201601972.

54. Theodoropoulos, A. S., Gkiozos, I., Kontopyrgias, G., Charpidou, A., Kotteas, E., Kyrgias, G. & Tolia, M. Modern Radiopharmaceuticals for Lung Cancer Imaging with Positron Emission Tomography/Computed Tomography Scan: A Systematic Review. *SAGE Open Med.* **8**, 205031212096159 (2020) DOI:10.1177/2050312120961594.

55. Akhoundova, D., Hiltbrunner, S., Mader, C., Förster, R., Kraft, J., Schwanhäusser, B., Bankel, L., Kollias, S., Treyer, V., Rushing, E. J., Lee, S.-Y., Andratschke, N., Hüllner, M. & Curioni-Fontecedro, A. 18F-FET PET for Diagnosis of Pseudoprogression of Brain Metastases in Patients With Non–Small Cell Lung Cancer. *Clin. Nucl. Med.* **45**, 113–117 (2020) DOI:10.1097/RLU.0000000000002890.

56. Wang, S., Lin, D., Yang, X., Zhan, C., Zhao, S., Luo, R., Wang, Q. & Tan, L. Clinical Significance of PET/CT Uptake for Peripheral Clinical N0 Non-Small Cell Lung Cancer. *Cancer Med.* **9**, 2445–2453 (2020) DOI:10.1002/cam4.2900.

57. Arosio, V., Caccia, M., Castro, I. F., Correia, P. M. M., Mattone, C., Moutinho, L. M., Santoro, R., Silva, A. L. M. & Veloso, J. F. C. A. The EasyPET: A Novel Concept for an Educational Cost-Effective Positron Emission 2D Scanner. *2016 IEEE Nucl. Sci. Symp. Med. Imaging Conf. Room-Temperature Semicond. Detect. Work.* 1–8 (2016) DOI: 10.1109/nssmic.2016.8069360.

58. Vaquero, J. J. & Kinahan, P. Positron Emission Tomography: Current Challenges and Opportunities for Technological Advances in Clinical and Preclinical Imaging Systems. *Annu. Rev. Biomed. Eng.* **17**, 385–414 (2015) DOI:10.1146/annurev-bioeng-071114-040723.

59. Huang, B., Law, M. W.-M. & Khong, P.-L. Whole-Body PET/CT Scanning: Estimation of Radiation Dose and Cancer Risk. *Radiology* **251**, 166–174 (2009) DOI:10.1148/radiol.2511081300.

60. Boechata, N., Pinto, A. da C. & Bastosa, M. M. Métodos Seletivos de Fluoração de Moléculas Orgânicas. *Quim. Nov.* **38**, 1323–1338 (2015) DOI: 10.5935/0100-4042.20150140.

61. Banister, S., Roeda, D., Dollé, F. & Kassiou, M. Fluorine-18 Chemistry for PET: A Concise Introduction. *Curr. Radiopharm.* **3**, 68–80 (2010) DOI: 10.2174/1874471011003020068.

62. Jacobson, O., Kiesewetter, D. O. & Chen, X. Fluorine-18 Radiochemistry, Labeling Strategies and Synthetic Routes. *Bioconjug. Chem.* **26**, 1–18 (2015) DOI:10.1021/bc500475e.

63. Preshlock, S., Tredwell, M. & Gouverneur, V. 18F-Labeling of Arenes and Heteroarenes for Applications in Positron Emission Tomography. *Chem. Rev.* **116**, 719–766 (2016) DOI:10.1021/acs.chemrev.5b00493.

64. Luis, C., Castaño-Guerrero, Y., Soares, R., Sales, G. & Fernandes, R. Avoiding the Interference of Doxorubicin with MTT Measurements on the MCF-7 Breast Cancer Cell Line. *Methods Protoc.* **2**, 29 (2019) DOI: 10.3390/mps2020029.

65. Fowler, J. S. A. P. W. *Synthesis of Carbon-11, Fluorine-18, and Nitrogen-13 Labeled*

Radiotracers for Biomedical Applications. Synthesis of Carbon-11, Fluorine-18, and Nitrogen-13 Labeled Radiotracers for Biomedical Applications (National Academies Press, 1982). ISBN:978-0-309-32944-6.

66. Li, Z., Lin, T., Liu, S., Huang, C., Hudnall, T. W., Gabbaï, F. P. & Conti, P. S. Rapid Aqueous [18F]-Labeling of a BODIPY Dye for Positron Emission Tomography/Fluorescence Dual Modality Imaging. *Chem. Commun.* **47**, 9324 (2011) DOI:10.1039/c1cc13089g.

67. Goud, N. S., Joshi, R. K., Bharath, R. D. & Kumar, P. Fluorine-18: A Radionuclide with Diverse Range of Radiochemistry and Synthesis Strategies for Target based PET Diagnosis. *Eur. J. Med. Chem.* **187**, 111979 (2020) DOI:10.1016/j.ejmech.2019.111979.

68. Yu, S. Review of 18F-FDG synthesis and quality control. *Biomed. Imaging Interv. J.* **2**, (2006) DOI:10.2349/biij.2.4.e57.

69. Liu, S., Lin, T., Li, D., Leamer, L., Shan, H., Li, Z., Gabbaï, F. P. & Conti, P. S. Lewis Acid-Assisted Isotopic 18 F- 19 F Exchange in BODIPY Dyes : Facile Generation of Positron Emission Tomography/Fluorescence Dual Modality Agents for Tumor Imaging. *Theranostics* **3**, 181–189 (2013) DOI: 10.7150/thno.5984.

70. Carlucci, G., Carney, B., Brand, C., Kossatz, S., Irwin, C. P., Carlin, S. D., Keliher, E. J., Weber, W. & Reiner, T. Dual-Modality Optical/PET Imaging of PARP1 in Glioblastoma. *Mol. Imaging Biol.* **17**, 848–855 (2015) DOI:10.1007/s11307-015-0858-0.

71. ATCC®. NCI-H1299 ATCC ® CRL-5803™ Homo sapiens lung. *American Type Culture Collection* https://www.lgcstandards-atcc.org/products/all/CRL-5803.aspx?geo_country=pt#characteristics (2012) (accessed:20 January 2021).

72. Shapiro, D. L., Nardone, L. L., Rooney, S. A., Motoyama, E. K. & Munoz, J. L. Phospholipid Biosynthesis and Secretion by a Cell Line (A549) which Resembles Type II Alveolar Epithelial Cells. *Biochim. Biophys. Acta (BBA)/Lipids Lipid Metab.* **530**, 197–207 (1978) DOI:10.1016/0005-2760(78)90005-X.

73. SRB Cytotoxicity Assay Kit, Colorimetric - Cepham Life Sciences Research Products. https://www.cephamls.com/srb-cytotoxicity-assay-kit-colorimetric/ (accessed:16 July 2021).

74. Terra, L., de L. Chazin, E., de S. Sanches, P., Saito, M., de Souza, M. V. N., Gomes, C. R. B., Wardell, J. L., Wardell, S. M. S. V., Sathler, P. C., Silva, G. C. C., Lione, V. O., Kalil, M., Joffily, A., Castro, H. C. & Vasconcelos, T. R. A. Evaluation of 1,3-benzoxathiol-2-one Derivatives as Potential Antifungal Agents. *Med. Chem. (Los. Angeles).* **14**, 304–310 (2018) DOI:10.2174/1573406413666170704095113.

75. Harvey Motulsky. *Intuitive Biostatistics: A Nonmathematical Guide to Statistical Thinking.* (Oxford University Press, 2014). ISBN:0199946647.

76. Liu, S., Li, D., Zhang, Z., Surya Prakash, G. K., Conti, P. S. & Li, Z. Efficient Synthesis of Fluorescent-PET Probes based on [18F]BODIPY Dye. *Chem. Commun.* **50**, 7371–7373 (2014) DOI: 10.1039/c4cc01411a.

77. Okutan, E., Tümay, S. O. & Yeşilot, S. Colorimetric Fluorescent Sensors for Hemoglobin Based on BODIPY Dyes. *J. Fluoresc.* **26**, 2333–2343 (2016) DOI:10.1007/s10895-016-1929-6.

78. Swedin, R. K., Zatsikha, Y. V., Healy, A. T., Didukh, N. O., Blesener, T. S., Fathi-Rasekh, M., Wang, T., King, A. J., Nemykin, V. N. & Blank, D. A. Rapid Excited-State Deactivation of BODIPY Derivatives by a Boron-Bound Catechol. *J. Phys. Chem. Lett.* **10**, 1828–1832 (2019) DOI:10.1021/acs.jpclett.9b00751.

79. Shaban Ragab, S., Swaminathan, S., Deniz, E., Captain, B. & Raymo, F. M. Fluorescence Photoactivation by Ligand Exchange around the Boron Center of a BODIPY Chromophore. *Org. Lett.* **15**, 3154–3157 (2013) DOI:10.1021/ol401380n.

80. Liu, L., Yuan, Y., Yang, Y., McMahon, M. T., Chen, S. & Zhou, X. A Fluorinated aza-BODIPY Derivative for NIR Fluorescence/PA/ 19 F MR Tri-modality in vivo Imaging. *Chem. Commun.* **55**, 5851–5854 (2019) DOI:10.1039/C9CC01253B.

81. ISO. ISO 10993-5:2009 Biological evaluation of medical devices - part 5: Tests for in vitro cytotoxicity. (2009).

82. ISO. ISO 10993-4:2002 Biological evaluation of medical devices — Part 4: Selection of

tests for interactions with blood.

83. Amin, K. & Dannenfelser, R.-M. In vitro Hemolysis: Guidance for the Pharmaceutical Scientist. *J. Pharm. Sci.* **95**, 1173–1176 (2006) DOI:10.1002/jps.20627.

84. Marima, R., Hull, R., Dlamini, Z. & Penny, C. Efavirenz Induces DNA Damage Response Pathway in Lung Cancer. *Oncotarget* **11**, 3737–3748 (2020) DOI:10.18632/oncotarget.27725.

85. Varbanov, H. P., Kuttler, F., Banfi, D., Turcatti, G. & Dyson, P. J. Screening-based Approach to Discover Effective Platinum-based Chemotherapies for Cancers with Poor Prognosis. *PLoS One* **14**, e0211268 (2019) DOI:10.1371/journal.pone.0211268.

86. Beer, A. J., Grosu, A.-L., Carlsen, J., Kolk, A., Sarbia, M., Stangier, I., Watzlowik, P., Wester, H.-J., Haubner, R. & Schwaiger, M. [18 F]Galacto-RGD Positron Emission Tomography for Imaging of αvβ3 Expression on the Neovasculature in Patients with Squamous Cell Carcinoma of the Head and Neck. *Clin. Cancer Res.* **13**, 6610–6616 (2007) DOI:10.1158/1078-0432.CCR-07-0528.

87. Li, L., Zhao, W., Sun, X., Liu, N., Zhou, Y., Luan, X., Gao, S., Zhao, S., Yu, J. & Yuan, S. 18F-RGD PET/CT Imaging Reveals Characteristics of Angiogenesis in Non-Small Cell Lung Cancer. *Transl. Lung Cancer Res.* **9**, 1324–1332 (2020) DOI:10.21037/tlcr-20-187.

88. Kang, F., Wang, Z., Li, G., Wang, S., Liu, D., Zhang, M., Zhao, M., Yang, W. & Wang, J. Inter-heterogeneity and Intra-heterogeneity of αvβ3 in Non-Small Cell Lung Cancer and Small Cell Lung Cancer Patients as Revealed by 68Ga-RGD2 PET Imaging. *Eur. J. Nucl. Med. Mol. Imaging* **44**, 1520–1528 (2017) DOI:10.1007/s00259-017-3696-2.

89. Kaira, K., Higuchi, T., Oriuchi, N., Sunaga, N., Hisada, T., Asao, T., Tsushima, Y. & Yamada, M. Usefulness of l-[3- 18 f]-α-methyl tyrosine (18 F-FAMT) PET as Therapeutic Monitoring for Patients with Advanced Lung Cancer. *J. Clin. Oncol.* **32**, 11096–11096 (2014) DOI:10.1200/jco.2014.32.15_suppl.11096.

APPENDIX I

APPENDIX I – Diagnostic Radiopharmaceuticals

Different radiopharmaceuticals, such as those described in table 7, are being investigated to assess different targets in tumours, some with the potential to be tested in clinical trials. Integrin αvβ3 (involved in neovascularization) is an appealing target, due to its high expression in activated endothelial cells during angiogenesis, and plays an essential role in the management of tumour growth, local invasiveness, and metastatic potential[86]. Protein, nucleotides, glutathione, and amino-sugars are synthetized from amino acids[54]; and aminoacid transporters are believed to play a key role in tumour formation and cell proliferation, which may be useful to assess in the tumour environment[54]. Hypoxia in tumours is related to resistance to radiation and chemotherapy, along with angiogenesis, metastasis, and tumour aggressiveness, all of which contribute to a poor prognosis; as a result, hypoxia is critical in the biology of several malignancies and is a target for tumour imaging[54]. As well as glucose metabolism, lipid metabolism is also essential for tumour growth, energy storage, and the production of signalling molecules; PET/CT scanning with ^{11}C-Choline or ^{18}F-Choline can be used to visualize fatty acid metabolism in malignant tumors[54].

The development of a theranostic substance that can be used for both therapy and diagnosis has been an area target of increasing investigation. ^{64}Cu-DOTA-RGD is one radiopharmaceutical under investigation for theranostic applications, as it seemed to be effective in monitoring αvβ3 at extremely low integrin levels. ^{64}Cu-DOTA-RGD peptides might be used in integrin-based imaging and radiotherapy (with targeting integrin αvβ3)[54]. Scientific investigation and progress are being done to get to personalized medicine through proper lung cancer staging, characterization, and response evaluation[54].

Table 7 - PET radiopharmaceuticals investigated for Lung Cancer diagnosis.

Radiopharmaceutical	Main Use	References
Integrin Marker/Angiogenesis Agent		
^{18}F-ALF-NOTA-PRGD2/ ^{18}F-RGD (^{18}F-Alfatide)	Allows the imaging of αvβ3 expression in NSCLC. It may be used to analyse the aberrant and varied tumour microenvironment. It can also help with the development and assessment of treatments that target αvβ3.	54,87
^{68}Ga-RGD$_2$ (^{68}Ga dimerized-RGD)	Its uptake is substantially lower in patients with SCLC than in those with NSCLC. Because of the inter-and intra-heterogeneity of αvβ3, current uses of αvβ3-targeted treatment and diagnostic imaging in lung cancer could be improved.	54,88
Amino-Acid Metabolism Agent		
^{18}F-FAMT (L-[3-^{18}F] (^{18}F-Fluorothymidine)	It may be beneficial to discern between malignant and benign lesions and is carried into tumour cells via the LAT1. There is no LAT1 expression in normal tissue or benign tumours. This radiopharmaceutical might be used to predict the prognosis of individuals with advanced lung cancer after chemotherapy.	54,89

Table 7 - PET radiopharmaceuticals investigated for Lung Cancer diagnosis (continuation).

Radiopharmaceutical	Main Use	References
Amino-Acid Metabolism Agent		
D-^{18}F-FMT (D-(^{18}F)-Fluoro-Methyl-Tyrosine)	It is a fluorine-labelled tyrosine derivative that is carried directly through the (LAT1) L-amino-acid transporter and clears the blood pool faster than the equivalent L-isomer. This radiopharmaceutical seems to have a lower sensitivity, but greater specificity than ^{18}F-FDG as there is no uptake of d-^{18}F-FMT in cases of inflammation.	54
Hypoxic Agent		
^{18}F-FETNIM (^{18}F-Fluoro Erytrho Nitro Imidazole)	This tracer seems to be better in predicting treatment outcomes than ^{18}F-MISO and has more selective uptake in hypoxic tumours. In comparison to ^{18}F-MISO though there is minimal data.	54
^{60}Cu-ASTM (^{60}Cu -4-(N)-methylthiosemicarbazone)	It seems to be a good radiotracer for those who do not respond to any therapy.	54
^{18}F-MISO (^{18}F-fluoromisonidazole)	FMISO accumulation within tumour cells facilitates the assessment of early treatment response and may serve as a predictive biomarker. The absence of a relation between FMISO and ^{18}F-FDG may suggested that enhanced hypoxia and glycolysis in NSCLC have a mismatch.	54
Brain Metastases		
^{18}F-FET (O-(2-[^{18}F]-fluoroethyl)-L-tyrosine)	^{18}F-FET PET in NSCLC patients treated with immunotherapy and radiotherapy for brain metastases evolution discrimination was evaluated in a small first study. ^{18}F-FET PET uptake ratios and dynamic uptake patterns may be able to distinguish between pseudoprogression and real progression of brain lesions, making it a potentially powerful diagnostic tool.	54,55
Bone Metastases		
^{18}F-NaF (^{18}F-sodium fluoride)	It is clinically approved used for diagnosis purposes and it is commonly used to compare bone metastases in individuals who have had previous NaF-PET scans.	54

APPENDIX II

APPENDIX II – Statistical Information

The concentrations uptaken in the form of average and CI are summarized in tables 8 and 9 for 1μM and 10μM, of each BODIPY in the study.

Table 8 - Uptake values in the form of average and CI for 1μM of BODIPYs 3 and 6.

	A549				H1299			
	BODIPY 3		BODIPY 6		BODIPY 3		BODIPY 6	
	μ	CI	μ	CI	μ	CI	μ	CI
1 hour	12.24	[-18.30, 42.78]	14.85	[0.32, 29.38]	14.01	[-6.19, 34.216]	12.64	[1.37, 23.92]
2 hours	26.12	[7.47, 44.76]	22.02	[13.10, 30.94]	24.09	[17.96, 30.22]	14.22	[-0.30, 28.74]
4 hours	37.05	[15.48, 58.61]	29.50	[13.19, 45.80]	30.68	[21.63, 39.72]	24.82	[6.69, 42.96]

Table 9 - Uptake values in the form of average and CI for 10μM of BODIPYs 3 and 6.

	A549				H1299			
	BODIPY 3		BODIPY 6		BODIPY 3		BODIPY 6	
	μ	CI	μ	CI	μ	CI	μ	CI
1 hour	46.78	[-22.54, 116.10]	33.64	[2.96, 64.31]	77.87	[-40.61, 196.35]	56.84	[-28.35, 142.02]
2 hours	93.72	[53.01, 134.44]	68.88	[12.10, 125.67]	97.56	[48.93, 146.19]	65.23	[49.77, 80.69]
4 hours	130.01	[-63.41, 323.44]	53.94	[5.80, 102.08]	126.86	[78.78, 174.94]	54.21	[1.50, 106.92]